INTERNATIONAL JOURNAL OF HYDROGEN ENERGY 52 (2024) 622–663

Available online at www.sciencedirect.com

ScienceDirect

journal homepage: www.elsevier.com/locate/he

A review on the design of nanostructure-based materials for photoelectrochemical hydrogen generation from wastewater: Bibliometric analysis, mechanisms, prospective, and challenges

Walid Nabgan [a,*], Hasan Alqaraghuli [b], A.H.K. Owgi [c], Muhammad Ikram [d,**], Dai-Viet N. Vo [e], Aishah Abdul Jalil [c], Ridha Djellabi [a], Abu Hassan Nordin [c,f], Francisco Medina [a]

[a] Department D'Enginyeria Química, Universitat Rovira I Virgili, Av Països Catalans 26, 43007, Tarragona, Spain
[b] Faculty Electrical Engineering Engineering, Universiti Teknologi Malaysia, 81310, Skudai, Johor, Malaysia
[c] Faculty of Chemical and Energy Engineering, Universiti Teknologi Malaysia, 81310, Skudai, Johor, Malaysia
[d] Solar Cell Applications Research Lab, Department of Physics, Government College University Lahore, 54000, Punjab, Pakistan
[e] Center of Excellence for Green Energy and Environmental Nanomaterials (CE@GrEEN), Nguyen Tat Thanh University, Ho Chi Minh City, Viet Nam
[f] Faculty of Applied Sciences, Universiti Teknologi MARA (UiTM), Arau, 02600, Perlis, Malaysia

HIGHLIGHTS

- This study conducted a bibliometric analysis to identify research trends and gaps.
- The design of photoelectrochemical devices was discussed and emphasized as necessary.
- A review of the most popular nanoporous materials for PEC systems was provided.
- The significant role of nanoporous materials in the PEC performance was emphasized.

GRAPHICAL ABSTRACT

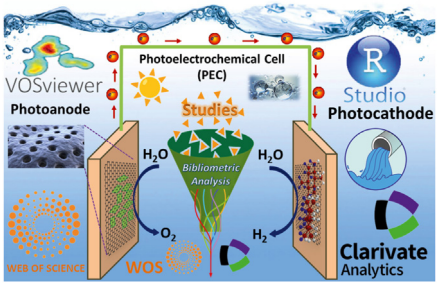

ARTICLE INFO

Article history:
Received 5 December 2022
Received in revised form

ABSTRACT

Years of study have shown that creating a commercial photoelectrode to solve particular bottlenecks, such as low charge separation and injection efficiency, short carrier diffusion length and lifespan, and poor stability, requires the employment of a variety of

* *Corresponding author*. Departament d'Enginyeria Química, Universitat Rovira i Virgili, Av Països Catalans 26, 43007, Tarragona, Spain.
** *Corresponding author*. Solar Cell Applications Research Lab, Department of Physics, Government College University Lahore, 54000, Punjab, Pakistan.
E-mail addresses: wnabgan@gmail.com (W. Nabgan), dr.muhammadikram@gcu.edu.pk (M. Ikram).
https://doi.org/10.1016/j.ijhydene.2023.05.152

8 May 2023
Accepted 14 May 2023
Available online 30 May 2023

Keywords:
Review
Bibliometric
Non-precious
Hydrogen
Water

components. Developing photovoltaic-electrolysis, photocatalytic, and photoelectrochemical approaches to accelerate hydrogen production from solar energy has been highly competitive. Photoelectrochemical water splitting utilizing nanoporous materials is one of the promising approaches to produce hydrogen more efficiently, cost-effectively, and on a long-term basis. Nanoporous materials have been highly used in photoelectrochemical water-splitting systems and are crucial in numerous applications. Those materials have a porous structure and excellent conductivity, enabling the deposition of transition metal atoms and electrochemically active chemicals on a large active surface area. However, there remains a dearth of review articles exploring the application of nanoporous materials in photoelectrochemical reactions. Therefore, this review provides bibliometric statistics and various perspectives on a range of nanoporous materials, including indium, nickel, gold, copper, lead, silver, aluminum, silicon, tin, iron, zinc, titanium, bismuth vanadate, cadmium sulfide, and zeolites. Additionally, this review offers a comprehensive assessment of worldwide studies on utilizing nanoporous materials in photoelectrochemical cells. We show how morphological modifications to materials may improve charge transfer and, as a consequence, overall power conversion efficiency.ke The superior catalytic performance of nanostructures with varying levels of complexity has been discovered in photoelectrochemical reactions. Finally, significant issues and future research directions in the domains are discussed.

Abbreviations

3D npNi/SPE	Three-dimensional nanoporous nickel on the screen-printed electrode
ATSC	Anodized titanium silicon carbide
$Au/TiN/TiO_2/Al_2O_3$	Gold/titanium nitride over titanium dioxide and aluminium oxide
$Au@A\text{-}B\text{-}TiO_2$	Gold over anatase-sodium borohydride-titanium
Au—ZnO NWs	Gold-zinc oxide nanowire
$Bi_4V_2O_{11}$	Aurivillius structural type of bismuth vanadium oxide
CdS QD	Cadmium sulfide quantum dots
CdS-QDs/SNWs@SNSs	Cadmium sulfide-quantum dots over single-crystalline tin oxide nanowires at screw-like tin oxide nanosheets
Co_3Mo/Cu	Molybdenum carbonate over copper
CODCr	Chemical oxygen demand based on potassium dichromate
COF-TRIPTA	Covalent organic frameworks of the 1,3,5-triformyl phloroglucinol and 1,3,5-Tris-(4-aminophenyl)triazine
$Co\text{-}Pi/H\text{—}BiVO_4$	Cobalt-phosphate over hydrogen-annealed bismuth vanadate
CPBL	Cotton pulp black liquor
CSZ-5-InBiSe	Indium selenide and bismuth-doped chalcogenide-based semiconductor zeolites
CSZ-5-InSe	Chalcogenide-based semiconductor zeolites doped with indium and selenium
$Cu(In, Ga)Se_2$	Copper indium gallium selenide
$Cu_8Co_3Mo_1Al_{88}$	Copper cobalt molybdenum alumina
$Fe_2O_3/NF\text{—}TiO_2$	Iron oxide supported on nitrogen and fluorine co-doped titanium-oxide
$HA\text{-}TiO_{2-x}$	Hydrogenated amorphous titanium oxide
HOMO	Highest occupied molecular orbital
HPLC	High-performance liquid chromatography
LUMO	Lowest unoccupied molecular orbital
N-CDs/Cu NRs	Nitrogen-doped carbon dots over copper nanorods
$Ni\text{—}Bi/H\text{—}BiVO_{4-x}$	Nickel—borate composite on the hydrogen-annealed bismuth vanadate
NiFe-LDHs	Nickel iron layered double hydroxides
$Pb(Zr_{0.2}Ti_{0.8})O_3/SrRuO_3$	Lead zirconium titanate over strontium ruthenate
PbO-ERGO	Lead oxide-electrochemically reduced graphene oxide nanocomposites
SNWs@SNSs	Single-crystalline tin oxide nanowires at screw-like tin oxide nanosheets
$TiN/TiO_2/Al_2O_3$	Titanium nitride over titanium dioxide and aluminum oxide
ZnO NT/Ag	Zinc oxide nanotube supported on silver
$ZnO\text{-}NR\text{-}Zn_{1-x}Cd_xS$	Zinc oxide nanorod over zinc cadmium sulfide
β-FeOOH	Titanium plasma implanted akaganeite

Introduction

Heavy oil production has become crucial for global energy security due to the depletion of conventional oil and gas reserves and growing global energy demand [1]. The new energy that can replace fossil fuels is urgently needed to attain the goal of carbon neutrality. Approximately 18% of the world's total energy consumption is derived from renewable sources such as biomass, hydropower, wind, and solar [2,3]. The predicted impact of climate change on the development and feasibility of renewable energy sources, such as solar, wind, geothermal, hydropower, and biomass, is expected to be significant [4]. Alterations in weather patterns, such as an increase in cloud cover and a higher frequency of extreme weather events like hurricanes and typhoons, are likely to pose challenges for solar energy, which relies on sunlight for power generation [5]. Consequently, the efficiency and predictability of solar power generation may be negatively affected. Similarly, changes in wind patterns resulting from climate change may have implications for wind power, which harnesses the kinetic energy of wind for electricity production. Shifts may influence the reliability and output of wind turbines in wind speed and direction. Compared to solar and wind energy, geothermal energy, which derives heat from the Earth's core, is expected to be less susceptible to the effects of climate change. However, changes in groundwater availability and temperature can still impact the efficiency of geothermal power plants. Furthermore, alterations in tectonic activity caused by climate change could affect the availability and stability of geothermal resources. Hydropower, which relies on the force of moving water, is particularly vulnerable to climate change [6]. Changes in precipitation patterns, including shifts in rainfall distribution and reduced snowpack, can affect water availability and overall hydropower capacity. Droughts and decreased river flow can result in reduced hydropower generation, thereby impacting the reliability and productivity of this renewable energy source [7]. Overall, climate change has complex and diverse impacts on renewable energy sources. While geothermal energy exhibits greater resilience, solar, wind, hydropower, and biomass are expected to face varying degrees of challenges due to weather patterns, water availability, and agricultural productivity shifts. It is imperative to prioritize the development of resilient renewable energy technologies and effective climate change adaptation and mitigation strategies to mitigate these impacts and ensure a sustainable energy future. Renewable energy sources such as solar and wind have an inherent variability that can be managed by hydrogen, which can serve not only as a fuel but also as an energy carrier and storage medium. Achieving net-zero CO_2 emissions by 2050 may require decarbonizing significant sectors of the economy [8]. As an energy source, hydrogen possesses numerous advantages. Primarily, it stands out as an environmentally friendly and pristine fuel. Hydrogen functions as a zero-emission energy source since water vapor is the sole byproduct generated during combustion or utilization in fuel cells [9,10]. Moreover, hydrogen exhibits a high energy density, signifying its capacity to store significant energy per unit of mass or volume. This attribute renders it a practical choice for applications requiring a portable or compact energy source, such as transportation. Additionally, hydrogen serves as a versatile energy carrier that can be derived from diverse sources, including fossil fuels with the application of carbon capture and storage technologies, as well as renewable sources like solar and wind energy [11]. Nonetheless, certain limitations must be considered. Hydrogen production necessitates energy, often obtained from non-renewable sources, potentially resulting in carbon emissions if not produced responsibly [12]. Furthermore, the low density of hydrogen poses challenges in storage and transportation, requiring specialized infrastructure. Additionally, the present cost associated with infrastructure construction and hydrogen generation renders it less economically competitive than alternative energy sources [13,14]. Nevertheless, ongoing research and technological advancements aim to address these drawbacks, aiming to fully unlock the potential of hydrogen as a sustainable and clean energy source.

Carbon-free hydrogen is increasingly recognized globally as a unique energy source and a potential fuel [15]. It is often viewed as a modern class of chemical energy carriers that can serve as an alternative to fossil fuels [16]. Hydrogen as an energy carrier on board for transportation has been acknowledged as a viable choice for long-term energy development because of its environmentally friendly characteristics. Traditionally, 60% of hydrogen production from fossil fuels occurs in specially designed facilities that create primary hydrogen. Natural gas-based hydrogen is costly in the Middle East, for example, where production predominantly relies on natural gas (71.27%) and coal (27.27%), while water electrolysis accounts for only 1.4% of the total hydrogen generated [17]. Hydrogen production from fossil sources results in significant greenhouse gas emissions, rendering it non-renewable and non-carbon-neutral [18]. Water splitting to produce hydrogen is appealing for storing the considerable flow of sunlight on earth. This clean energy carrier may be employed in fuel cells with high energy conversion efficiencies to create electricity on demand [19]. On the other hand, conventional hydrogen generation emits up to 830 million tonnes of carbon dioxide [20]. By 2050, about ten terawatts of energy must be collected from carbon-neutral-based sources to maintain the current carbon dioxide level in the atmosphere, posing a significant challenge to our civilization [21]. Regrettably, molecular hydrogen is not naturally present on Earth, meaning that, as Jules Verne's story implies, it is impossible to obtain hydrogen at no cost by extracting it from water [19]. To generate molecular hydrogen from hydrogen-rich substances, energy input is required [19]. However, a more cost-effective method and sustainable sources for producing renewable hydrogen are necessary in this scenario.

Suitable technologies can generate hydrogen from wastewater that contains a high percentage of carbohydrates. Wastewater may extract various essential resources, including water, multiple types of energy (e.g., hydrogen, electricity, and heat), and chemicals (e.g., inorganics and organics), making it a renewable supply in the water-energy relationship. Mine effluent, for example, has a considerable quantity of metal resources that may be recovered through the reduction process. Fortunately, microorganism-based technologies can extract up to 140 GW of energy from

biodegradable waste streams such as sewage sludge, municipal solid waste, and wastewater [22]. As sewage contains a significant amount of chemical energy, it makes a suitable candidate as a renewable energy source in this context. (e.g., hydrogen, electricity, and biogas) [23].

The conventional methods of metal recovery, such as ion exchange, chemical precipitation, and adsorption, are insufficient due to their inability to lower these oxidized metal ions, despite the volume of metal-laden wastewater. Others employed electrolytic [24], direct solar water splitting [25], and biological processes [26]. According to researchers, efficient use of solar energy can lower the overall energy consumption of water splitting. The most basic solar fuel is molecular hydrogen, formed when light energy splits water into its component portions. In electrolysis cells and photoelectrocatalytic cells, high-surface-area electrodes are required for the cost-effective synthesis of organic compounds and for converting photons into electricity. An electrochemical cell containing one or more photo-active electrodes executes reactions in which a direct semiconductor/liquid interface is employed for photoelectrochemical water splitting [27]. Fig. 1 depicts the several stages involved in photoelectrochemical water photolysis. Photoanode irradiated by light during water splitting is a photoactive semiconductor substantial-base electrode. Cathodes are sometimes known as counter electrodes since it is not bombarded by light.

Various stages are required to ensure the entire photoelectrochemical water photolysis process is smooth. These phases include the collection of visible-light photons, carrier separation, charge transfer transportation of separated electron/hole pairs, which must be catalytically active, and surface reactions. The possibility of the excited charge carters and appropriate water oxidation kinetics is required for successful water photoelectrolysis processes. Because this process occurs at room temperature and pressure and produces harmless byproducts, it is less energy-intensive and ecologically friendly

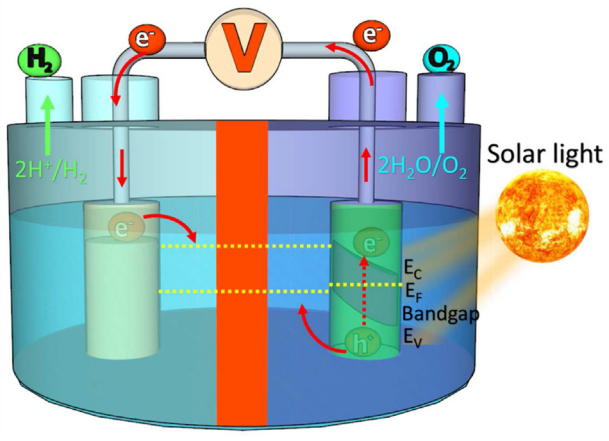

Fig. 1 – A schematic illustration for a photoanodes (n-type semiconductor) for solar water splitting photoelectrochemical cells where oxygen develops and a cathode where hydrogen develops. (H_2: hydrogen; O_2:oxygen; H_2O:water; O_2: Oxygen; e^-: electron; H^+: hydrogen ion; E_C: conduction-band-edge; E_F: valence-band-edge; E_V: fermi-level energy).

than alternative methods. Although photoelectrochemical water splitting appears promising, solar-to-hydrogen conversion capabilities are insufficient for practical use [28,29]. Intensive efforts are required to build more active photocatalysts, low-cost, durable, high-performance semiconductor materials, and sophisticated systems [30–32] to allow practical photoelectrochemical solar fuel generation.

Some of the significant features of the process and material selection include the ability to absorb incoming photons and catch the light to efficiently generate electron-hole pairs, the separation, and migration of charge at the semiconductor-electrolyte interface, as well as improved corrosion capability [33]. Chemical stability and photocatalytic properties make semiconducting metal oxide nanostructures extremely interesting. Due to their unusual photophysical activities, semiconductor quantum dots are also being investigated extensively. Carbon-based nanomaterials and metal nanoparticles are frequently employed as recognition components in biosensors due to their excellent electrocatalytic activity and biocompatibility, increasing sensitivity and selectivity. A large number of photoactive semiconductor materials based on double or ternary oxides [34], sulfides [35], and phosphides [36] of transition metals exhibiting high activity in various photoelectrochemical reactions have been studied and proposed.

Some photocatalytic compounds, such as cadmium selenide [37], graphitic carbon nitride [38], and titania [39], have shown considerable promise. Strontium titanate, a typical photocatalyst with suitable valence (+2.10 eV) and conduction bands (−1.02 eV) and a high dielectric constant, has been demonstrated to destroy dye contaminants [40,41]. It has been reported that a variety of materials and systems have been investigated, namely silicon–germanium [42], indium oxide [43], tungsten trioxide over bismuth vanadate [44], iron oxide [45], cobalt oxide [46], copper oxide [47], zinc tungstate over zinc oxide [48], zinc oxide [49], bismuth oxide [50], bismuth vanadate [51], silicon [52], and a variety of other compounds [53–55]. Due to restrictions such as wide band gap energy, a high recombination rate, and cost, their performance is not yet suitable for practical deployment. Researchers are investigating band gap science of semiconductor photocatalysts by co-catalyst addition, preparation of diverse morphologies, heterojunction, and Z-scheme creation to address these issues. For example, Patil et al. [56] studied photoelectrochemical hydrogen generation by double nanoporous architecture zinc cadmium sulfide nanosheets and zinc oxide nanorods (Fig. 2). In porous zinc oxide nanorod over zinc cadmium sulfide (ZnO-NR-$Zn_{1-x}Cd_xS$) nanosheets photoanodes, the visible surfaces of straight-up oriented hexagonal zinc oxide nanorod and porous zinc cadmium sulfide nanosheets photoanodes cause to the proper shape, effective charge separation, and outstanding light-harvesting. Numerous established semiconductor photocatalysts' performance is inadequate to fulfill the needs of their feasible uses due to their tiny specific surface area. Nanostructured silicon is a promising element that may be utilized to build several sorts of heterojunction structures with semiconductors, and when lit, the porous silica might create photocurrent [57]. However, this photocurrent is unsteady in a liquefied electrolyte [58]. When the electrolyte contains no fluoric anion, oxidations form on the porous silicon surface, blocking the

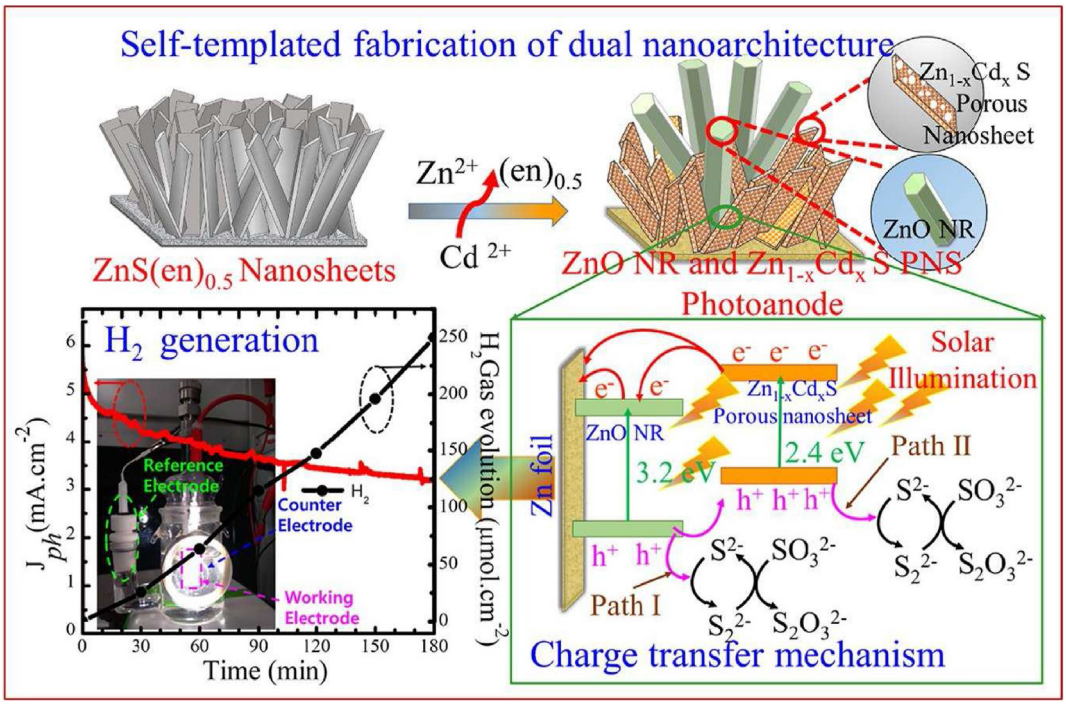

Fig. 2 – Self-templated creation of double nanoporous architecture zinc cadmium sulfide ($Zn_{1-x}Cd_xS$) nanosheets and zinc oxide nanorods (ZnO NR) for photoelectrochemical hydrogen generation. (Zn^{2+}:cationic form of zinc; Cd^{2+}: cationic form of cadmium; H^+: hydrogen ion; e^-: electron; $ZnS(en)_{0.5}$: zinc sulphide-ethylenediamine hybrid; SO_3^{2-}: sulfite ion, S^{2-}: sulfide; H_2: hydrogen). Reuse with permission from Ref. [56].

flow of photocurrent [59]. As a result, titania nanowires can keep porous Si from oxidation in electrolytes by acting as a shield. Porous composites have received the greatest attention among the numerous materials described above, owing to their pore volume, high surface area, great conductivity, porous structure, and strong adsorption capacity in endeavors to solve the issues related with photoelectrochemical water splitting. Fabricating porous composites, on the other hand, has presented some difficulties due to the fact that it is a composite and costly preparation process concerning high temperatures and high-cost facilities. Finding a modest and cost-effective way for generating porous carbon is of paramount importance. The creation of nanometrically sized materials will aid in the study of reaction processes as well as the development of new catalytic systems. Despite various advancements in the invention of new technologies for obtaining repeatable materials, there are still a number of challenges to solve. Photocatalysts, from the standpoint of materials, require a variety of characteristics depending on their uses, such as particle size, specific surface area, or distance between the electrical levels, among others.

In this study, an assessment was made of the latest advancements in photoactive materials produced through electrochemistry to improve their photoelectrochemical activity. Using a title search for "photoelectrochemical" and "hydrogen" combined with a topic search for "nanoporous" in the Web of Science database, only 11 items were identified as of March 12th, 2022, and presented in Table 1. However, when we replaced the "nanoporous" keyword with terms such as "overview" or "review" in the same merged search, no results were found. We also developed a word cloud (RStudio; RStudio, Boston, USA) diagram using big-sized words to signify words' growing occurrence employing "photoelectrochemical" and "hydrogen" in the title search of the Web of Science database from 1970 to 2022. This technique helps researchers gain a quick overview of the textual quantity and visualizations of a specific area of research; the top frequent words were set on 80 out of 994 words, and the result is depicted in Fig. 3. The data presented in Table 1 and Fig. 3 indicates a noticeable insufficiency in the all-encompassing examination and discourse of studies that address the generation of hydrogen in nanoporous materials using photoelectrochemical water splitting. This review focuses on methods that utilize sunlight to break water molecules into oxygen and hydrogen to give readers a fundamental understanding of photoelectrochemical technology while concentrating on light-harvesting nanoporous materials.

First, a bibliometric analysis was conducted and described in section Theoretical, Technical, and Economic Assessment of Hydrogen Generation to find the research highlights and trends based on the Web of Science. The fundamental principles and mechanisms of photoelectrochemical have been discussed in section Bibliometric Analysis. Section Photoelectrochemical cells explains the fundamental principles behind the generation of photoanodes through various techniques, including anodic electrodeposition, potential pulsed/cycling electrodeposition, cathodic electrodeposition, and metal anodization approaches for photoelectrochemical water splitting. Using nanoporous

Table 1 – Instant of issued articles (1970–March 12, 2022) in the Web of Science database by merging the title examines to keywords such as "photoelectrochemical" and "hydrogen" and topic analysis to keywords such as "nanoporous".

No.	Year	Main focus	Ref.
1	2014	"CdSe quantum dots sensitized nanoporous hematite for photoelectrochemical generation of hydrogen" • For photoelectrochemical hydrogen production, cadmium selenide quantum dot sensitization on hematite is being investigated. • The photoelectrochemical characteristics are determined by the sensitizer loading time on hematite films. • Sensitization enhanced the films' apparent absorbance and conductivity.	[60]
2	2015	"Photoelectrochemical oxidation of azo dye and generation of hydrogen via C–N co-doped TiO_2 nanotube arrays" • In a photoelectrochemical system, carbon, nitrogen co-doped titania nanotube array is a photoanode. • Photo-generated holes and electron recombination were considerably minimized. • In the degradation of photoelectrochemical, the synergetic impact was measured.	[61]
3	2015	"Efficient photoelectrochemical water oxidation over hydrogen-reduced nanoporous $BiVO_4$ with Ni–B-i electrocatalyst" • Bismuth vanadate's photochemical activity has been hampered by its low charge-separation yield. • They get around this problem by creating a nanoporous shape that efficiently prevents bulk carrier recombination. • To increase the water oxidation kinetics, they use a layer of nickel–borate composite on the hydrogen-annealed bismuth vanadate (Ni–Bi/H–$BiVO_{4-x}$) surface as an oxygen development catalyst. • At pH 9, the Ni–Bi/H–$BiVO_{4-x}$ photoanodes cause a considerable cathodic change (350 mV) in the water oxidation onset perspective.	[62]
4	2015	"Novel photoelectrochemical hydrogen peroxide sensor based on hemin sensitized nanoporous NiO based photocathode" • Under visible light, the photocathode showed increased cathodic photocurrent. • The cathodic photocurrent reacted to hydrogen peroxide sensitively and selectively. • The photoelectrochemical sensors were also used to sense hydrogen peroxide in actual high-performance samples.	[63]
5	2016	"InP nanopore arrays for photoelectrochemical hydrogen generation" • It was demonstrated in a large-scale and straightforward manner how to fabricate one-dimensional indium phosphide nanopore arrays that can be used as photoelectrodes to generate hydrogen electrochemically. • Indium phosphide nanopore arrays exhibit exceptional photoelectrochemical performance due to their light-trapping solid properties, high-quality one-dimensional conducting channels, and vast surface areas.	[64]
6	2016	"Nanoporous black silicon as a platform for photoelectrochemical hydrogen production: Exciting catalysts and nailing down the flatband potential"	[65]
7	2016	"Enhanced photoelectrochemical performance of nanoporous $BiVO_4$ photoanode by combining surface deposited cobalt-phosphate with hydrogenation treatment" • A combination of hydrogenation treatment and cobalt-phosphate deposition created a nanoporous cobalt-phosphate over hydrogen-annealed bismuth vanadate (Co-Pi/H–$BiVO_4$) photoanode. • The cobalt-phosphate surface modification reduced unwanted recombination caused by hydrogenation, improving the photoelectrochemical performance of the nanoporous H–$BiVO_4$ photoanode even further.	[66]
8	2016	"Unique three-dimensional InP nanopore arrays for improved photoelectrochemical hydrogen production" • The authors describe the high capabilities of trapping the light properties and with significant surface areas by fabricating indium phosphide nanopore arrays in three-dimensional designs, and this yields remarkably active photoelectrodes in photoelectrochemical hydrogen evolution instruments. • They showed that using sodium chloride as the neutral electrolyte in anodic etching of indium phosphide instead of other solutions like hydrochloric acid may considerably passivate the surface states of three-dimensional nanopore arrays.	[67]
9	2017	"A non-enzymatic hydrogen peroxide photoelectrochemical sensor based on a $BiVO_4$ electrode" • Researchers have developed a sensor with a hydrogen peroxide non-enzymatic photoelectrochemical based on a nanoporous bismuth vanadate film electrode. • In visible light, the electrode becomes photoelectrochemically active, yielding a hole scavenger operation with hydrogen peroxide, producing a reaction on the valence band for the light-induced electron holes.	[68]

(*continued on next page*)

Table 1 – (continued)

No.	Year	Main focus	Ref.
10	2017	"Photoelectrochemistry by design: tailoring the nanoscale structure of Pt/NiO composites leads to enhanced photoelectrochemical hydrogen evolution performance" • A concurrent optimization was adapted by employing both the semiconductor light absorber's morphological properties (nickel oxide) and the cocatalyst (platinum). • Wet chemical procedures were used to make monodisperse Pt nanoparticles, whereas electrochemical anodization was used to make nanoporous nickel oxide sheets. • The proportionate augmentation of photocurrents as nanoparticle size and loading functions was observed.	[69]
11	2021	"Nanoporous TiN/TiO_2/Alumina Membrane for Photoelectrochemical Hydrogen Production from Sewage Water" • In order to generate hydrogen from sewage water, titanium nitride is used over titanium dioxide and aluminium oxide nanotubes (TiN/TiO_2/Al_2O_3). • A unique nickel imprinting process is used to create an alumina template with great hexagonal pore precision and order.	[70]
12	2022	"An overview of the application of the porous nano-composites for photoelectrochemical hydrogen generation from wastewater" • Investigation the publication trend and bibliometric analysis. • Subject category distribution for the literature. • Review the typical nanoporous materials used in photoelectrochemical systems. • Challenges and perspectives	Current research

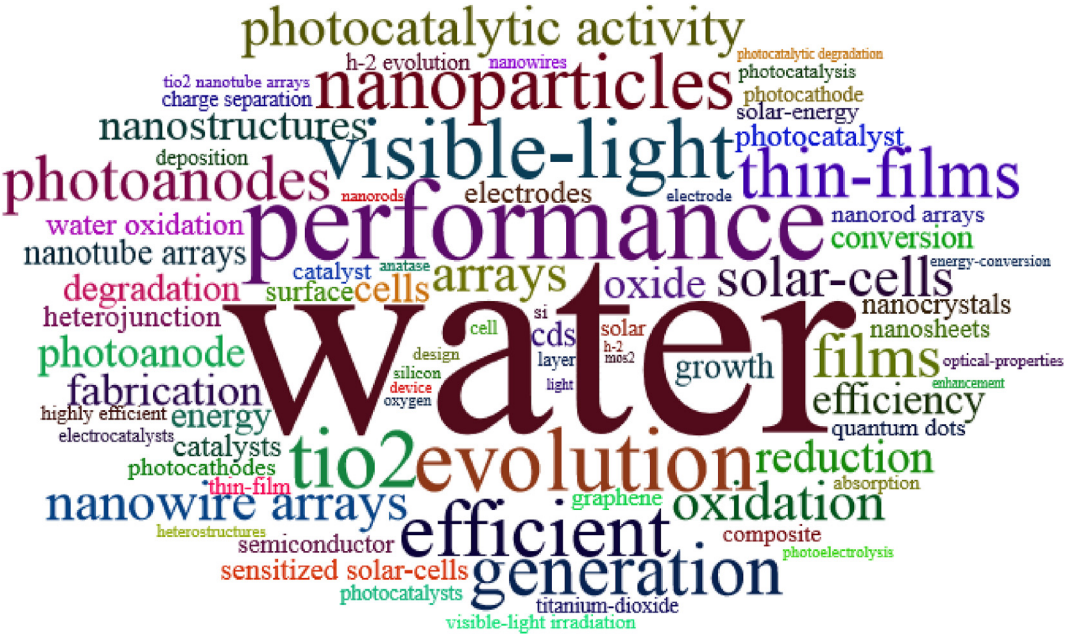

Fig. 3 – Word cloud diagram of most frequent keywords using biblioshiny source of the Web of Science dataset; title search: "photoelectrochemical" and "hydrogen".

materials, such as indium, nickel, gold, copper, lead, silver, aluminum, silicon, tin, iron, zinc, titanium, bismuth vanadate, cadmium sulfide, and zeolites, for the photoelectrochemical reaction is reviewed in this section. Moreover, this study discusses various types of photocatalysts and their applications in photochemical processes, starting from binary and ternary semiconductors and advancing to more advanced characteristics of nanocomposite photocatalysts. Section Nanoporous Materials outlines the challenges of prior research and future perspectives on the utilization of nanoporous materials in photoelectrochemical systems. A summary of the work and future perspective is given at the end of section Challenges and Future Prospects. This review is anticipated to provide new perspectives on utilizing nanoporous materials for photoelectrochemical techniques to produce hydrogen from wastewater.

Theoretical, technical, and economic assessment of hydrogen generation

Understanding the potential advantages and disadvantages of hydrogen production as a renewable energy source necessitates theoretical analyses. The transition towards a sustainable

energy future could greatly benefit from using renewable energy sources for hydrogen production. One of the main advantages of hydrogen lies in its ability to efficiently store and distribute energy. The intermittent challenges associated with renewable energy generation can be addressed by electrolyzing surplus power from sources such as solar or wind. The resulting hydrogen can be stored and utilized during periods of power shortage, enabling grid balancing and ensuring a consistent energy supply. Moreover, hydrogen possesses diverse applications in the industrial, heating, and transportation sectors, offering a versatile solution for decarbonizing these industries and reducing dependence on fossil fuels [71]. In theory, hydrogen production from photoelectrochemical wastewater holds promise as an environmentally responsible and sustainable approach [72]. Wastewater treatment plants generate substantial volumes of organic waste, which can be used as a renewable hydrogen production feedstock. The photoelectrochemical process harnesses solar energy and converts it into chemical energy in hydrogen by employing specialized semiconductor materials. This method reduces the environmental impact of wastewater discharge by utilizing wastewater as a valuable resource and provides a solution for wastewater treatment [73].

The theoretical assessment of this technique considers various factors, including the effectiveness of the photoelectrochemical system, the selection of suitable semiconductor materials, and the optimization of operating parameters [74]. It is crucial to ensure that the system achieves high hydrogen production rates while maintaining an acceptable level of wastewater treatment effectiveness. Additionally, the overall energy balance, environmental benefits, and potential reduction in greenhouse gas emissions are evaluated compared to conventional wastewater treatment methods [75]. This assessment involves accounting for the energy input required for hydrogen production and wastewater treatment. Further research and development efforts are necessary to explore the theoretical potential of hydrogen generation from photoelectrochemical wastewater and to address practical challenges for its large-scale implementation.

A comprehensive examination of the technical features and engineering aspects is integral to the technical assessment of hydrogen synthesis from photoelectrochemical effluent. The initial step entails selecting suitable photoelectrochemical cells and materials. Specifically, specialized semiconductor materials capable of effectively absorbing solar energy and facilitating the water-splitting process are required. Extensive experimental testing and characterization are conducted to thoroughly assess the performance of these materials in terms of photoconversion efficiency, stability, and catalytic activity. The design and optimization of the photoelectrochemical system significantly impact the technical evaluation. Factors such as cell structure, electrode arrangement, and light management strategies are carefully considered to maximize solar energy utilization and enhance hydrogen production. Crucial technological considerations include the incorporation of efficient catalysts and electrolytes, as well as the development of appropriate membrane systems. The assessment also encompasses important technical parameters such as hydrogen generation rate and overall system efficiency.

To maximize the hydrogen generation rate while minimizing energy losses, a precise adjustment of variables such as the intensity and spectral characteristics of the incident light, the flow rate and composition of the wastewater, and the operating parameters (including temperature, pressure, and pH) is carried out. Cost-effectiveness and scalability are also taken into account in the technical assessment. Key considerations include evaluating the potential for large-scale implementation, determining the feasibility of integrating the photoelectrochemical system with existing wastewater treatment infrastructure and estimating capital and operational expenses. To fully harness the potential of this method for sustainable hydrogen generation, the technical assessment of hydrogen production from photoelectrochemical wastewater aims to study and optimize the multitude of technological factors involved comprehensively.

The economic analysis of hydrogen generation from photoelectrochemical wastewater focuses on evaluating commercializing this technology's financial viability and cost-effectiveness [76]. This assessment considers various criteria to understand the economic aspects involved comprehensively. Initially, the analysis considers the capital expenditure required to establish the photoelectrochemical wastewater treatment and hydrogen generation system. This includes the costs of acquiring and installing essential equipment such as photoelectrochemical cells, electrodes, catalysts, membranes, and auxiliary components. Additionally, expenses related to modifying or integrating the system into existing wastewater treatment facilities are considered. The economic analysis aims to determine the initial investment needed and evaluates the payback period for the technology.

Furthermore, the assessment examines the operational expenses associated with the hydrogen production process. This includes the cost of energy input, typically electricity, required for the photoelectrochemical reaction and the costs associated with wastewater treatment and system maintenance. The efficiency of the photoelectrochemical process and the availability and cost of renewable energy sources for powering the system play a significant role in determining the operational expenses [77]. The economic analysis also considers potential revenue sources associated with hydrogen generation. This involves calculating the market price of hydrogen and identifying potential customers or applications, such as fuel cell vehicles, industrial operations, or energy storage [78]. The analysis considers the demand for hydrogen, pricing trends, and potential government incentives or subsidies to assess the revenue generation potential. Moreover, the economic evaluation compares the cost competitiveness of hydrogen production from photoelectrochemical wastewater with alternative technologies. This can involve evaluating the costs of conventional hydrogen generation methods, such as steam methane reforming or electrolysis using grid power. Factors such as the cost of raw materials, system efficiency, operational scale, and environmental benefits are considered in this analysis. Overall, the economic analysis of hydrogen generation from photoelectrochemical wastewater aims to provide insights into the financial viability and potential return on investment of implementing this technology [79]. It assists stakeholders in making informed decisions regarding the economic feasibility of large-scale

implementation and guides further research and development efforts to maximize the cost-effectiveness of the technology.

Bibliometric analysis

Bibliometric analysis is a standard method for determining state of the art in a given research area. The technique may describe publication trends over time or across literature by analyzing quantitative data and statistics. Consequently, data on the number of papers issued by an institute, nation, research teams, or authors with the highest technical generation could be detected. We apply the bibliometric approach, which analyzes bibliometric and bibliographic data using quantitative techniques [80]. Unlike systematic literature reviews, bibliometric reviews can provide information on any research area using various bibliometric and bibliographic data [81–83]. The Web of Science Core Collection is the most reliable citation database globally due to its thorough evaluation and curation of data. It emphasizes more recent sources and encompasses a broader range of scientific citations than other databases, such as Scopus [84]. One of the advantages of WoS is its focus on more current sources due to its recent establishment compared to specific other databases like Scopus [85]. In addition, WoS provides more comprehensive citation analysis and better visual representations than Scopus [86]. The broad usage, high-quality data, user-friendly interface, comprehensive coverage, and cited reference searches make the Web of Science a valuable resource for scholars and researchers [87,88]. In this study, we have chosen the WoS database as the primary source for our bibliometric analysis. This section examines the growth and publishing patterns of photoelectrochemical and hydrogen literature research using bibliometric analysis. We could get a basic idea of study subjects in this domain by analyzing keywords found in all collected items. We used the Web of Science database to extract as a text file bibliometric records covering the period 1970–2022 (March 12th). We found 994 items encompassing 690 publications covering review papers, books, conference articles, and research articles relating to the paper's research area. Fig. 4 shows that the number of documents connected to photoelectrochemical and hydrogen research is steadily increasing, with an exceptionally high level of interest in the previous decades. The first article was published in 1976, and most articles (number = 106) were published in 2019. The citations began in 2005, and the year with the most citations (number = 5162) was 2020. Year after year, the data revealed variable growth. To develop the area of photoelectrochemical in hydrogen generation in this age of fast-evolving technology, it is critical to base new work on previously published research.

Fig. 4 similarly depicts nations' collaboration efforts using a chord-linked visualization diagram with a minimum number of documents 13 and a minimum number of zero citations. The chord diagram is a visualization method of displaying the relationship or *trans*-flows among different countries and was developed by OriginPro 2021 version 9.8.0.200. Additionally, the chord diagram is a clever interactive tool for illustrating the relationship between category and function, which may

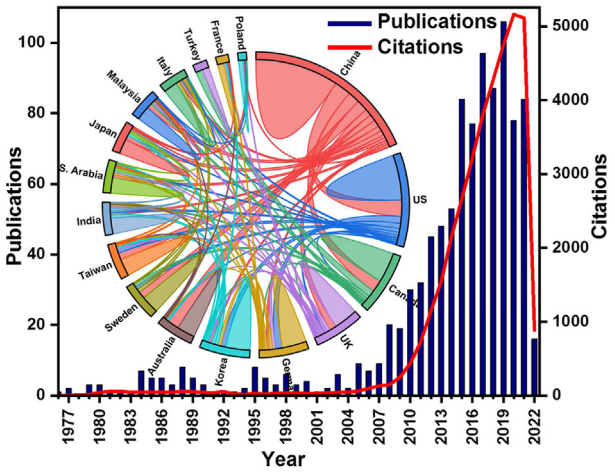

Fig. 4 – Total publications and the sum of times cited by year from 1970 to 2022. Retrieved from Web of Science for title search of "photoelectrochemical" and "hydrogen", along with chord-linked visualization of a country co-authorship network, dated March 12, 2021.

be used for primary data exploration or to generate interactive data visualizations for publications. It allows adding arcs between nodes (countries) to show flows displayed around a circle and connected with curves (links). The tight connections between two nodes relate to the line's thickness; the thicker the relation between two countries, the closer the association. Each node signifies a country, and the dimension shows the number of publications added by the country. As Fig. 4 shows, the research on photoelectrochemical and hydrogen is the most popular in China, the US, Canada, the UK, Germany, South Korea, and Australia, with total link strengths of 111, 60, 40, 32, 32, 32, and 24, respectively. China is the most productive in photoelectrochemical and hydrogen research. This is not unexpected because China's publication output is top for most research fields. Some countries such as Italy, Turkey, France, and Poland are showing much fewer publications; however, anticipating the growing importance of photoelectrochemical and hydrogen, further research can be expected in this region. China is a virtual and central node between the US, Canada, the UK, Australia, Sweden, Taiwan, and India. Meanwhile, the US and Canada, in turn, play the role of a center node among many European countries.

Sankey diagrams are commonly used to depict energy or material movement in various networks and operations. They use quantitative features to illustrate flows, relationships, and transitions. Sankey diagrams are directed and weighted graphs with weighted elements that keep the flow going. The quantity of inflow weights at each node is the same as the outgoing consequences. A three-field Plot (Sankey diagram) of Country, Keyword plus, and journals were created by biblioshiny command of bibliometrics using Rstudio software. As shown in Fig. 5, the main interests of photoelectrochemical and hydrogen research in China are water, performance, evolution, titania, efficiency, and visible light. The dominant topic of research in the US and Korea is water. Keywords such as reduction, fabrication, nanostructures, and arrays are less frequent in almost all countries. The top dominant journals

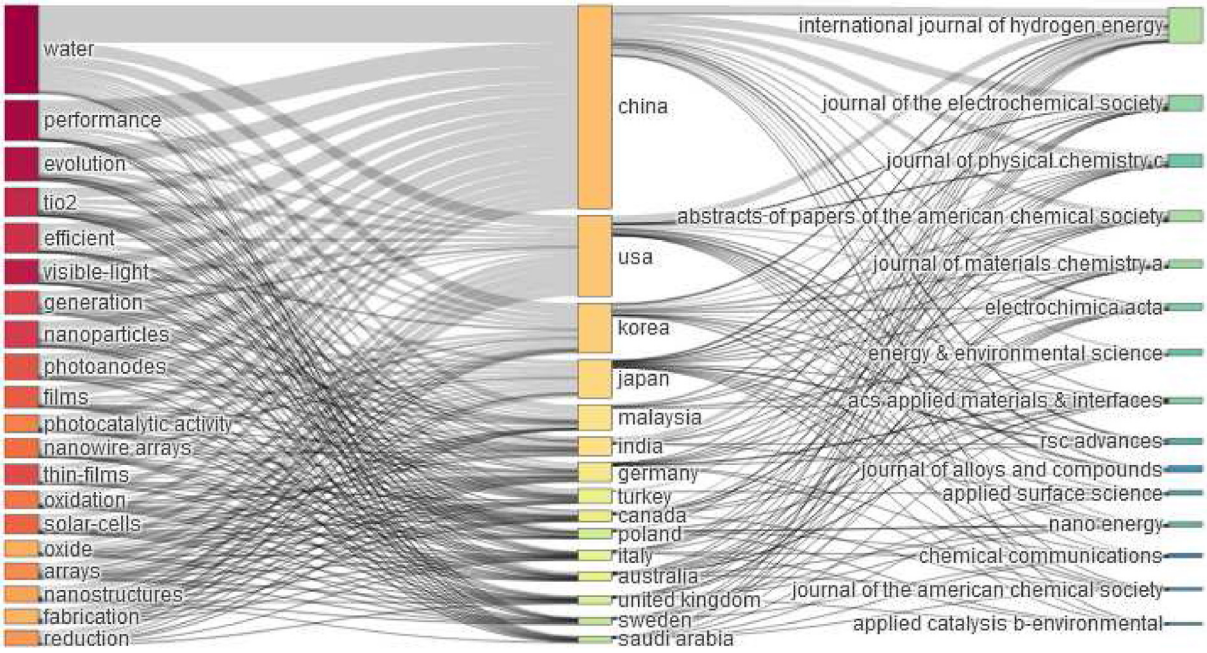

Fig. 5 – A three-field Plot (Sankey diagram) of middle: country (number of keywords: 15), left: keywords plus (number of keywords: 20), and right: publication sources (number of keywords: 20) for the most researched topics using title search of "photoelectrochemical" and "hydrogen".

that published papers in photoelectrochemical and hydrogen in nearly all countries are the *International Journal of Hydrogen Energy*, the *Journal of Electroanalytical Chemistry*, and *The Journal of Physical Chemistry C*. On the other hand, *Applied Catalysis B: Environmental*, *Journal of the American Chemical Society*, and *Chemical Communications* have published fewer articles than other journals in this area of research. In summary, Sankey Diagram is practical to explain complex processes with the spotlight on a single aspect we want to focus on, but it is hard to analyze each keyword. Therefore, we conduct the co-occurrence visualization plot in Fig. 6 because the Sankey diagram cannot highlight an actionable insight into this area of research.

This section will show how to utilize term co-occurrence maps, visual representations of the associations between frequently occurring terms in a group of texts. For example, coconut, co-word, and co-link matrices supply us with essential data for mapping and comprehending the structures in the underlying document sets. Text mining and visualization are rapidly being used in various academic areas to discover, show, and evaluate the thematic coverage of massive text volumes. This procedure, known as bibliometric

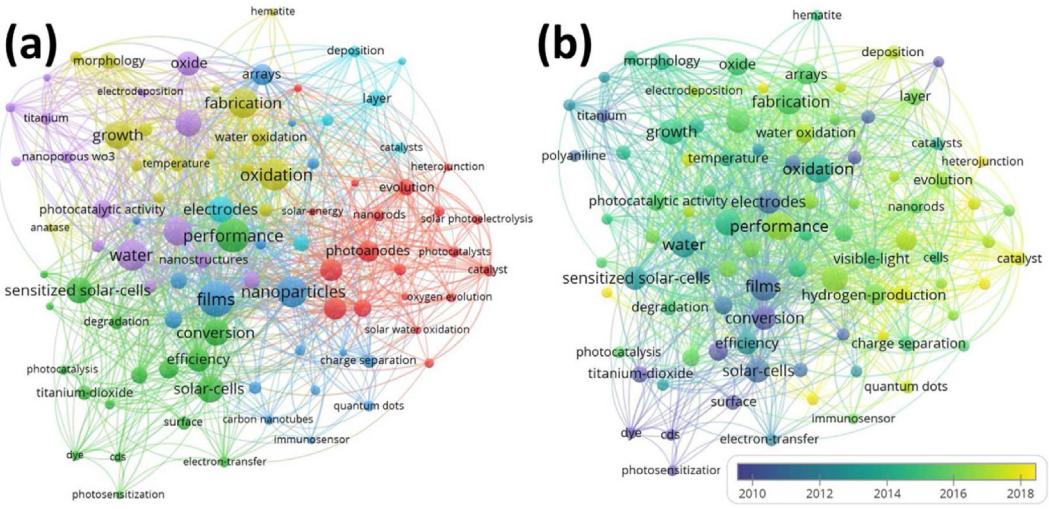

Fig. 6 – (a) co-occurrence visualization map and (b) co-occurrence chronology view of authors keyword plus using title search of "photoelectrochemical" merged with the topic search of "nanoporous"; 273 items detected on March 12, 2021, (minimum number of keyword occurrence = 5; 92 out of 793 met the threshold).

mapping, is relatively prevalent in research and information science. While its practical implementation in academic libraries is still in its early stages, scholars may find these approaches useful for several objectives. As seen in Fig. 6, the phrase map visualization is used for this purpose. We combined the title search "photoelectrochemical" with the subject search "nanoporous" to produce this graphic. Based on these criteria, the Web of Science database could detect 273 published items we extracted as a plain text file and analyzed them by VOSviewer (version 1.6.11). 92 terms were retained, organized in 6 clusters with 2096 total links and 1389 links, eliminating generic terms related to the research process. Each node represents one keyword, and the node's size corresponds to the number of occurrences, i.e., in how many authors' comments a given keyword was found (the more significant node's size, the greater the number of occurrences). The distance between nodes indicates their relatedness according to their co-occurrences in the literature. The thickness of the line connecting two nodes reflects how often they are mentioned together (actual overlap/concurrence); the thicker the line, the more frequently they appear together in a publication. With 19 keywords, the red cluster (1) is the largest one, followed by green (clusters 2 and 18 items), blue (clusters 3 and 17 items), yellow (clusters 4 and 16 items), purple (clusters 5 and 15 items), and light blue (cluster 6 and 7 items) (Fig. 6 (a)). The largest size of the nodes belongs to the key terms "performance" (cluster 2), "oxidation" (cluster 4), "nanoparticles" (cluster 3), and "films" (cluster 3), representing the keywords that have the highest frequency of occurrence. These clusters are connected with the others through these keywords. Other keywords in large nodes related to performance were a fabrication, growth, visible light, titania, photoanodes, electrodes, and nanoparticles. This indicated that photoelectrochemical research was mainly concerned with photoactive nanomaterials design for electrodes. However, there are some least mentioned keywords with a deficient total link strength, such as cadmium sulfide (16), photosensitization (11), polyaniline (14), immunosensor (17), layers (18), photocatalyst (20), anodic growth (20), hematite (20), and graphene oxide (22). Nanoporous terms appeared twice only in the entire graph with nanoporous titania (cluster 3 and total link strength of 29) and nanoporous tungsten trioxide (cluster 5 and total link strength of 40). The lowest frequent keywords, cadmium sulfide, photosensitization, layers, photocatalyst, anodic growth, hematite, graphene oxide, nanoporous titania, and tungsten trioxide, illustrated a lack of research in those areas. Additionally, we could not detect terms with wastewater in the analysis. To further confirm this phenomenon, we merged the title search of "photoelectrochemical" and "wastewater" with the topic search of nanoporous, but we could not detect any publication in the Web of Science database.

To further analyze and categorize the most common research areas in photoelectrochemical and nanoporous studies and identify the changing trends in keywords over time, an overlay (chronology) visualization is selected as a useful tool using VOSviewer. This tool allows us to classify the items using a timescale. We use this function of bibliometric analysis (Fig. 6 (b)) to help researchers determine potential future research directions. Fig. 6 (b) displayed keywords with dark purple colors, such as conversion, light, surface, cadmium sulfide, dye, titanium dioxide, mechanism, and spectroscopy, which have appeared over the last decades. Although keywords such as catalyst, oxygen evolution, efficient, graphene oxide, carbon nanotubes, layer, and titania nanotubes have occurred since 2018, this field has conducted novel research. Even though the dark purple color idea was introduced late, it has developed a unique interaction with various scientific domains due to its quick growth. The field of nanoporous materials is relatively new to photoelectrochemical research, and researchers are drawn to many of its aspects. These findings provide insights for further investigation, and advanced searches can be conducted using the keywords mentioned above to discover new results in the field of photoelectrochemical and nanoporous research.

Photoelectrochemical cells

Photoelectrochemical cells were first discovered in the early 1970s and may convert solar energy into useable fuels or electricity [89]. Since then, significant advancements in cell design and material selection for the photoelectrode, electrolyte, and auxiliary electrode have been made. Photoelectrochemical cells are a new technology that has shown promise in offering a solution for hydrogen generation, with more uses as the technology evolves. Photoelectrochemical cells are still in the research phases, but they can efficiently exploit a more extensive range of visible radiation. The combination of electrolytic and photocatalytic processes allows the photoelectrochemical process to leverage the advantages of both approaches, while also increasing the efficiency of radical synthesis. The main components of photoelectrochemical water splitting systems are the separation membrane, electrolyte, and semiconductor light-absorbing photoelectrodes. However, more study is needed before photoelectrochemical cells may be viable. To remain competitive, it is essential to consider both efficiency and material costs. The advantages of success are desirable and persuasive since fully developed photoelectrochemical technology provides a practically infinite energy source with little environmental effect.

Solar energy is converted directly into chemical energy in the form of hydrogen through semiconductor constituents in the photoelectrochemical water-splitting process. Photoelectrochemical cells consist of semiconductors, or photosensitizers, as a crucial component of the working electrode. It is similar to the semiconductor constituents used in photovoltaic solar power production that is used in photoelectrochemical systems, but for photoelectrochemical applications, the semiconductors are immersed in water-based electrolytes, in which sunlight is used to activate water-splitting systems. An n-type and p-type semiconductor electrode is shown in Fig. 7 (a and b) as the basic design of a photoelectrochemical cell. Electrons are stimulated to a higher energy level when light is absorbed by the semiconductor electrode (left). At the semiconductor/liquid interface, these electrons (and their corresponding absence, the "hole") may carry out redox processes. At the semiconductor/liquid junction, holes oxidize the "water" anion to produce the

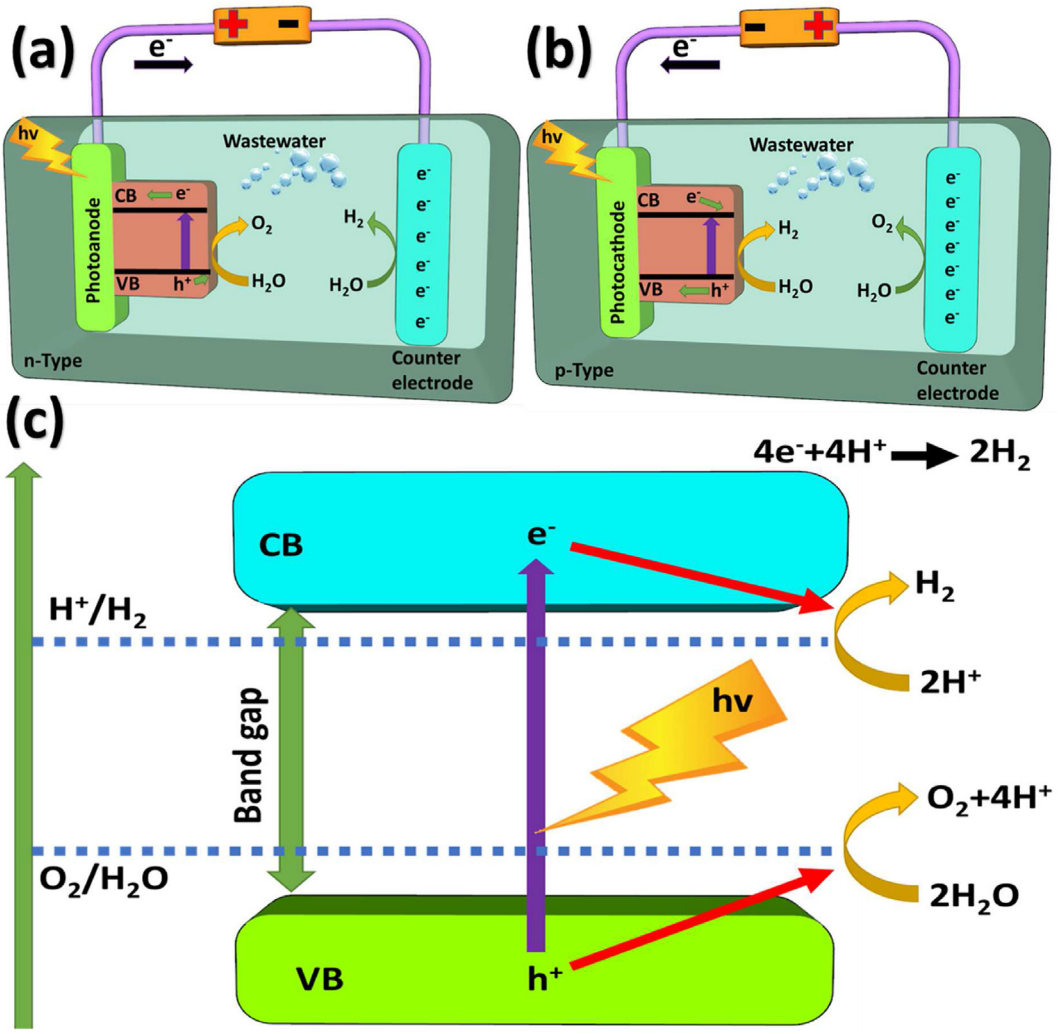

Fig. 7 – Photoelectrochemical system (a) n-type semiconductor photoanodes, (b) p-type semiconductor photocathodes, and (c) band edge and band gap situation for solar water splitting systems. (H_2: hydrogen; O_2:oxygen; H_2O:water; CB:conduction band; VB: valence band; hv:high voltage; e^- = electron; H^+ = hydrogen ion).

"oxygen" molecule. As shown here, a reduction process happens at the counter electrode by reducing the "water" molecule to the "hydrogen" anion. This is similar to a traditional electrochemical cell, except that light provides energy for the redox processes. Due to this occurrence, there will be many free electrons, yet there will still be covalent bond breaks in the crystal owing to thermal stimulation at ambient temperature. As a result of the breakdown of covalent bonds between semiconductors and impurities, a crystal's total number of free electrons is determined. Although a vacancy is generated in the broken link at any time, a free electron is created when analyzing a semiconductor-to-semiconductor covalent connection. Holes are the term for these voids. As a result of the loss of one electron, each of these holes is regarded a positive equal of a negative electron. Electrons are the primary mobile charge carriers in this system. There will be free electrons and holes in an n-type semiconductor (Fig. 7 (a)).

An essential semiconductor fixed with antimony, arsenic, or phosphorus as an impurity is an n-type semiconductor. A p-type semiconductor has been loaded with electron acceptor atoms (positive charge carriers) since electron holes account for the majority of charge transfer in the structure. In its usual crystal structure, silicon is a tetravalent material with four crosslinks created by four electron pairs. The most common dopants in silicon are cluster V and III elements. The cluster III components (trivalent) contains three valence electrons, making them acceptors when used to dope silicon. An empty state (an electron-hole) is generated when an acceptor atom substitutes a tetravalent silicon particle in the structure (Fig. 7 (b)). A band gap is a space between the conduction and valence bands of electrons. An electron must be excited by a minimum amount of energy to conduct in the conduction band, thus defining the band gap. The reduced energy amount is the valence band, and if there is a space between it and the higher energy conduction band, energy must be provided to enable electrons to become loose. This band gap's presence and magnitude help differentiate insulators, semiconductors, and conductors. These gaps could be seen in band illustrations, such as the one exemplified in Fig. 7 (c). Efficiently replicating and executing the process can have significant implications

for the utilization of low-cost nanoporous materials. Such an understanding is an effective conceptual motivator for our study and many others.

Nanoporous materials

Nanopores, a type of nanomaterial, are characterized by tiny holes ranging from 1 nm to 100 nm in size that selectively allow the passage of certain materials based on pore size. These nanoporous materials are commonly found in nature and may also be produced. Because of their superior porosity qualities, nanoporous materials have piqued curiosity, and their organized nano space structures are predicted to lead to several uses. Porous nanomaterials possess several characteristics that render them suitable for use as electrode materials in photoelectrochemical water-splitting systems. Thermal stability, chemical resistance, hardness, huge surface area, electron transport, conductance, and impedance are just a few of nanoporous materials' physical and chemical features due to an interaction between the surface and the analyte. Porous nanomaterials are crucial in purification, biological molecule isolation, sensors, catalysis, separation, ion exchange, and the removal of harmful heavy metals from wastewater (see Fig. 8). This section aims to highlight the use of a photoelectrochemical biosensor based on nanoporous materials for detecting heavy metal ions and organic contaminants in wastewater.

Indium

German scientist Ferdinand Reich discovered indium in 1863 at the Freiberg School of Mines. Indium is a malleable metallic element with a face-centered tetragonal structure, a silvery-white appearance, and remarkable flexibility. Indium enhances the corrosion resistance, hardness, and strength of alloys, and it is employed as a covering plate for bearings and other metal surfaces, as well as in low-melting combustible alloys. Indium is a reasonably unique element found at modest levels in the Earth's layer, with 0.05 ppm in the interior film of the earth and 0.072 ppm in the ocean crust, respectively [90]. Indium mining as a stand-alone commodity is unprofitable; hence it's a common byproduct of mining a significant industrial metal like zinc [91]. However, traces of indium can also be found in minerals such as galena, cassiterite, chalcopyrite, and sphalerite [92], which enables indium to be extracted from by-products produced during the generation of tin, copper, and zinc [93]. Due to its low melting point (156.6 °C or 429.8 K) and high boiling point (2353.2 K), indium becomes superconducting at 3.37 K [92]. Optoelectronic and electronic systems, transparent conducting materials, alkaline batteries, solar cells, and other uses make indium a valuable metal [94]. The presence of indium in semiconductors and alloys has led many researchers to focus on developing indium-containing semiconductors and alloy compounds. Other studies focused on indium ions and indium metal reduction and oxidation. The indium's (+3) cathodic decline and the indium's metal anodic dissolution are known to happen in two charge-transfer phases, with indium (1+) serving as an intermediary species in the In^{3+}/In^{0} electron transfer developments. Yi et al. [95] have developed a method to enhance the efficiency of photoelectrochemical water splitting by depositing an indium oxide layer on hematite, as shown in Fig. 9 (a). The hematite nanoarray photoanode was modified with indium oxide nanolayers to minimize surface recombination of charge carriers and extend the lifetime of the photoanode. As a result of surface passivation and enhanced electric interface field effects of indium oxide, the iron oxide photoanode exhibits significantly improved photoelectrochemical activity for water oxidation. The current density of the treated iron oxide of 3.4 mA cm−2 at 1.23 V versus a reversible hydrogen electrode can achieve a significant high-efficiency photon to current with 80% at 400 nm.

Many attempts have been made to synthesize chalcopyrite materials using a one-step electrodeposition process, like copper indium gallium selenide (Cu(In, Ga)Se_2) and copper indium selenide [94]. Kim and co-authors [96] carried out Pulse-driven photoelectrochemical water splitting using a p-type and n-type blended copper indium selenide photoelectrode. Upon application of the bias, minority carriers generated by photons may be carried into interleaved reduction regions and move efficiently through an exteriorly generated built-in field, as illustrated in Fig. 9 (b). Choosing the charge transport path parallel to the formation of the interleaved inner-depletion zone significantly increased the efficiency of charge transport from the bulk to the surface of the photoelectrode. With no further intermediary stages, Kim et al. [97] adopted a straightforward one-step annealing preparation technique employing electrochemically produced copper/indium bilayer precursors and a source of copious Se vapor (Fig. 9 (c)). A photoanode consisting of p-copper indium selenide nano-sized particles implanted in the n-copper indium selenide matrix exhibited significantly improved photocurrent and high stability when equipped with an ultrathin alumina protective layer. The enhanced photoelectrochemical capabilities were attributed to the ineffective nano-sized particles and matrix and the generated internal charges that efficiently separated the electron-hole pairs generated by photoelectrochemistry, as indicated by current-voltage and transmission electron microscopy measurements. Acid was often added to the electrolyte to prevent hydrolysis, and the formation of coatings on the indium electrodes. There were, however, some instances in which the additional acid posed difficulties. For potential equilibrium

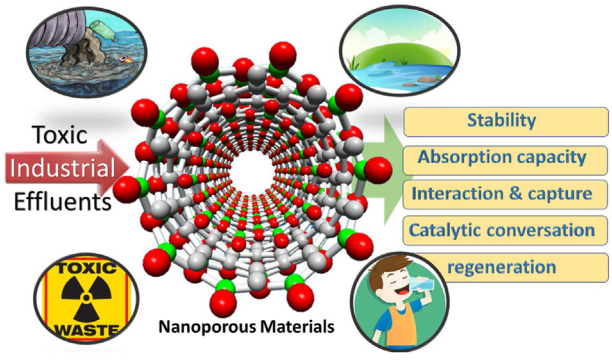

Fig. 8 – Nanoporous materials to remove pollutants from wastewater.

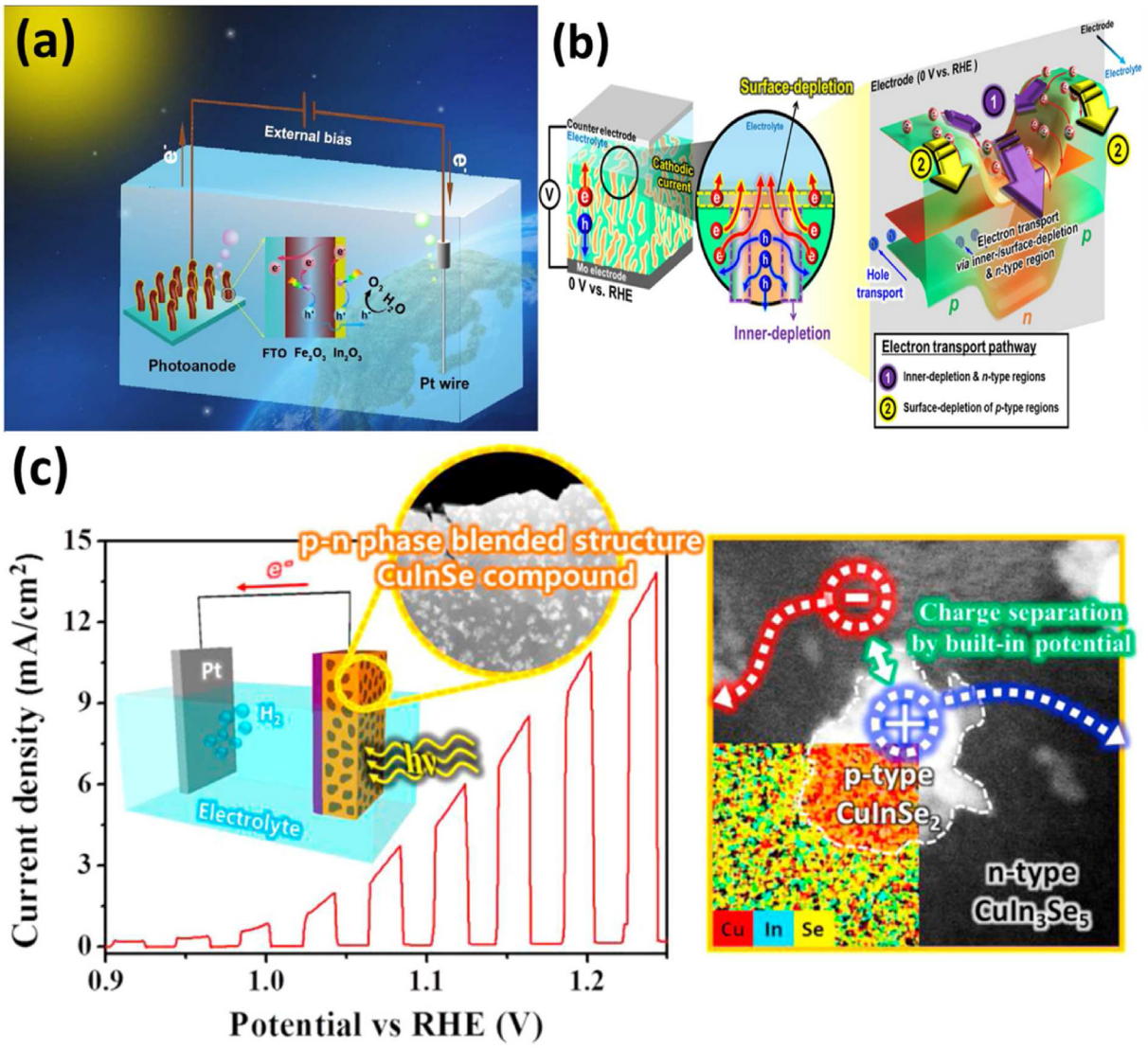

Fig. 9 – Coupling influence of indium oxide layer on hematite assisting effective photoelectrochemical water splitting, reuse with permission of [95]; (b) minority carriers created by photons flow into included reduction areas and travel beside the visibly encouraged built-in field at zero volts of reversible hydrogen electrode (0 V_{RHE}), reuse with permission of [96]; (c) copper indium selenide water splitting photoanodes with for photoelectrochemical performances, reuse with permission of [97]. (n-type: there is an excess of negatively charged carriers; p-type: there is an excess of positively charged carriers; $CuIn_3Se_5$: copper indium selenide; CIGS).

measurements with indium trichloride solutions, the addition of acid made it difficult to process data due to the lack of an adequate theory of activity coefficients for mixed electrolytes of different valency types.

There is the possibility that indium's cationic form, which is involved in the anodic process, can be oxidized by hydrogen ions in the solution, adversely affecting the dissolution process's kinetics [98]. The anodic reaction mechanism in perchlorate media depended on the equilibrium between the rates of indium oxidation achieved through electrochemical means and the rates achieved through hydrogen ion reactivity via chemical means [99]. A similar occurrence was seen in chloride media; however, due to the accelerated influence of chloride ions on the electrochemical reaction, an additional difficulty occurred, which was the oxidation of indium(I)/indium (III) [100]. A sulfate solution was the most used electrolyte for indium electrodeposition [94]. Current transient analysis may systematically investigate electrochemical nucleation and growth during indium electrodeposition. Thus, indium oxide is a viable alternative electron transport layer material for Photoelectrochemical cells.

Nickel

Nickel Oxide is a ferromagnetic solid with a green crystalline structure (Néel temperature is 523 K); because of its remarkable electrical, magnetic, and optical characteristics, nickel oxide has been the topic of several scholarly articles [101]. Nickel is engaged in a variety of electrochemical processes with practical applications. Nickel deposition in acidic

conditions to generate protective coatings such as amorphous phosphorus–nickel alloys [102,103] has a large body of knowledge. Besides nickel deposition research, nickel's surface oxidation characteristics are a primary and practical concern in electrochemistry. Furthermore, because the (charge/discharge) storage mechanism based on pseudo-capacitor materials emerges from reversible redox processes on the surface of electro-active electrodes, the nanoporous shape of nickel with the increased surface area can boost the pseudo-capacitance. Using nanoporous nickel-iron oxy-hydroxide-borate as the electrocatalyst, Huang and co-authors [104] synthesized formic acid by photo-electrochemical methanol-reforming. Electrocatalytic methanol reformation at near-neutral pH is enhanced by adding a sufficient iron concentration to nanoporous nickel-iron oxy-hydroxide. The apparent heterogeneous electron transfer rate steady was also found to increase the production of innovative nickel (3+) species and methanol oxidation rate constant with nickel (3+) species. A screen-printed electrode was electrochemically produced by Beluomini et al. [105] with three-dimensional nanoporous nickel (3D np Ni/SPE) to detect narirutin in citrus wastewater. Nanoporous nickel-modified screen-printed electrodes significantly improved the electrode's electrochemical activity in narirutin oxidation compared with bare screen-printed electrodes. The outcomes acquired utilizing the suggested 3DnpNi/SPE-based electro-analytical technique were correlated with those obtained following the highly efficient liquid chromatography (HPLC) methodology, and excellent agreement was observed between the two approaches., Bachmeier et al. [106] used a dye-sensitized nickel oxide photocathode to reduce carbon dioxide selectively with visible light. Fig. 10 (a) shows a photo-electrocatalytic cathode made from a donor–π–bridge–acceptor molecule (P1)-the sensitized skeleton of nanostructured nickel oxide. The injection of a hole into nickel oxide's valence band can restore the P1 ground state. However, the organic dye donor-π-bridge-acceptor molecule absorbs light and transfers electrons to the carboxydothermus hydrogenoformans (CODH), which binds to the nickel oxide surface and reduces the amount of carbon dioxide. In this configuration, the enzyme carbon monoxide dehydrogenase I adsorb impulsively on the nickel oxide surface and acts as a catalytic unit in the conversion of carbon dioxide to carbon monoxide. In addition to organic semiconductor-based photoelectrodes for photoelectrochemical water splitting, nickel oxide's fermi level and valence band potentials have been investigated due to their limited water stability [107]. According to Fig. 10 (b), nickel-iron double hydroxides (NiFe-LDHs), gallium-indium eutectic, and nickel foils are combined to passivate organic-photoactive-layer-based photoanodes to enhance their performance and stability.

Nickel metal foils enclose an organic photoactive layer, preventing water from entering. Gallium-indium eutectic is a medium between the organic photoactive layer and nickel foils to facilitate charge transfer. As a final step, NiFe-LDHs with surface-reaching pores were created to prevent photo corrosion of organic photoactive layers and improve charge separation efficiency. A reversible hydrogen electrode at 1.23 V and a photocurrent density of 15.1 mA cm^{-2} was attained by producing and utilizing highly photostable organic photoactive layers, resulting in an onset potential of 0.55 V. It is anticipated that high-performance organic photoanodes will be developed that have an advantage over inorganic photoanodes in terms of stability. Fig. 10 (c) illustrates the schematic diagram of the wastewater-resourcezation process, which utilized a three-compartment electrocatalytic cell system to generate hydrochloric acid from electroless nickel plating effluents Zhang et al. [108]. According to in situ Raman spectroscopy, nickel cation first interacted with the hydroxide to generate inner layer nickel (II) hydroxide, which was then progressively reduced to metallic nickel. The cathode cell of the three-compartment arrangement benefited from a minor pH decrease, thus reducing nickel cations to metallic nickel. Chemical precipitation was used to extract the obtained phosphate (3−). Moreover, the cathode cell of this method exhibits excellent pH control, which increases the efficiency of nickel recovery. The accumulation of charge carriers in the anode and cathode cells can also transport hydrogen and chloride (with positively charged ions) to the intermediate cell via cationic form, resulting in hydrochloric acid formation. Hence, employing three-compartment electrocatalytic cell systems and 3D-linked NiO hetero-structured nanosheets and NiO with surface-reaching pores is a viable technique to increase electrolyzer performance in hydrogen production.

Gold

Nanoporous gold is a gold sponge with nanometer-sized holes that may be found all over the body. The characteristics of compact gold with a filled body within are considerably different. Nanopores are generally 20–50 nm in size in nanoporous gold structures, although they can be as tiny as 5 nm. In aqueous conditions, gold is usually regarded as the ideal metal for studying solid electrode behavior, which is commonly thought of in significantly simplified terms as a metal resistant to dissolution. Young's modulus of nanoporous metals is associated with the sample's porosity. Consider a metal sponge for an easy method to understand the connection. Nanoporous gold, an open-cell structure material with nanoscale pores and ligaments, has sparked a lot of consideration due to its novel properties and simplicity of manufacture. A high surface-to-volume ratio of ligaments and pores results from gold's chemical properties. This enables them to be used for various applications, including catalysis [109], anodes [110], cathodes [111], sensors Kim, 2018; Ruffino and Grimaldi, 2020; Downs et al., 2021), heat sinks, energy absorption devices, lightweight structural panels, and laser beam shaping. It has been demonstrated that the incorporation of isolated gold nanoparticles in A-B-TiO_2 nanoporous film, Shi et al. [112] have demonstrated efficient photoelectrochemical water splitting over gold over anatase-sodium borohydride-titanium (Au@A-B-TiO_2). Due to A-B-TiO2's intermediate energy levels, hot electrons from gold nanoparticles are captured and transmitted with greater efficiency, leading to a significant increase in the separation performance of the pair of hot electrons and holes. A comparison was made with raw amorphous black titania and gold nanoparticle-deposited titania, which significantly increased photoelectrochemical water-splitting capabilities. There may be new approaches to developing innovative, high-efficiency

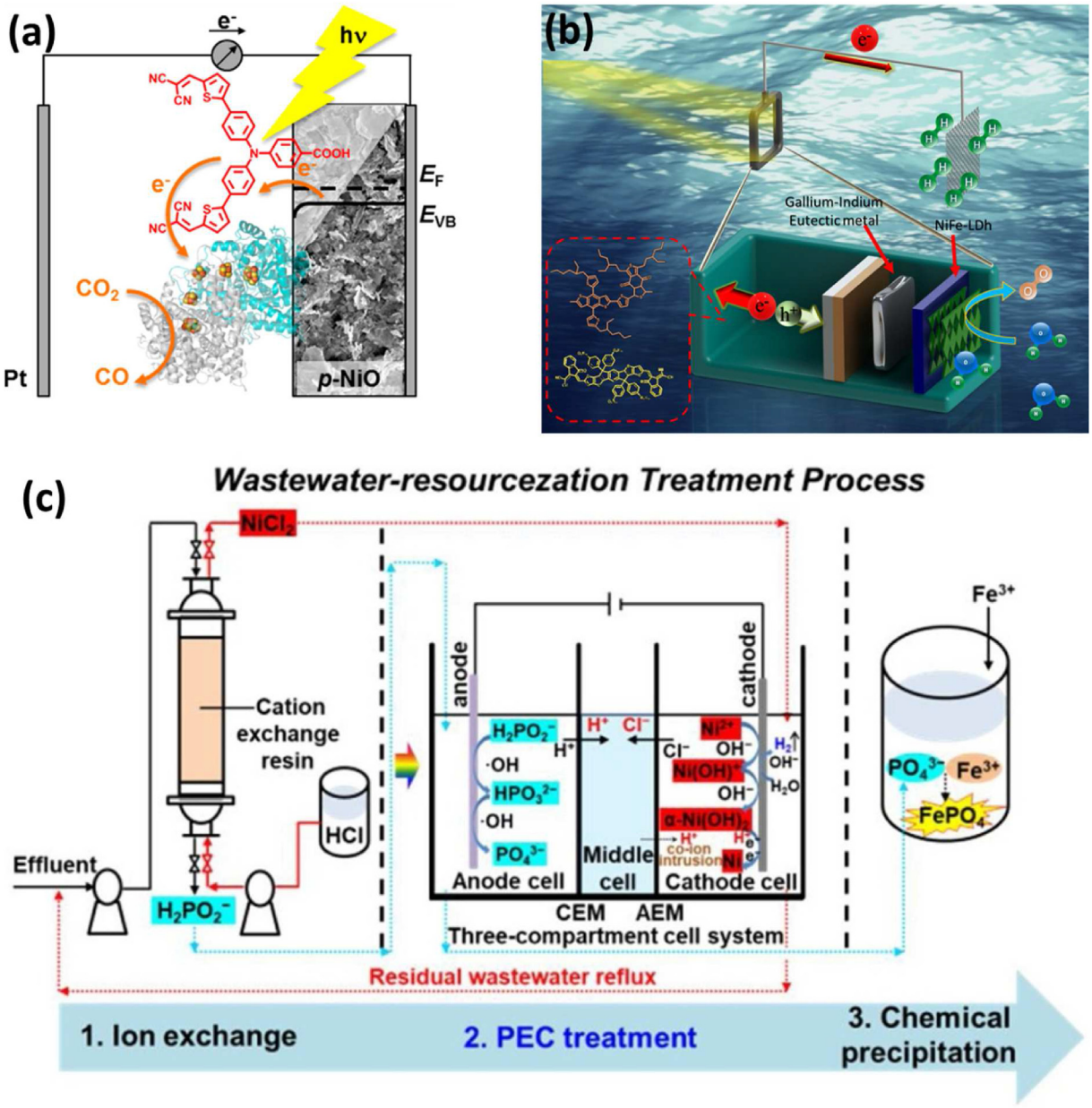

Fig. 10 – (a) A photoelectrochemical cell for selective carbon dioxide reduction to carbon monoxide at p-type nickel oxide (NiO) is depicted in this diagram, adapted with permission from Ref. [106]. (b) Gallium Indium eutectic, nickel foils, and nickel-iron layered double hydroxides (NiFe-LDHs) secure the organic-photoactive-layer from not only water but also aid separation and charge transport for high-performance photoelectrochemical water splitting (reproduced from Ref. [107] under a Creative Commons Attribution 4.0 International License); (c) schematic diagram of wastewater-resourcezation treatment (WRT) process. The continuous flow is represented by solid arrows, whereas the step process is characterized by dotted arrows, adapted with permission from Ref. [108]. (E_f: fermi level electrochemical potential; E_{VB}: valence band electrochemical potential; hv: high voltage; e^- = electron; H^+ = hydrogen ion; $NiCl_2$: nickel chloride; $H_2PO_2^-$: hypophosphite; and Ni^{2+}: a cationic form of nickel; PO_4^{3-}: phosphate; Fe^{3+}: a cationic form of ferric; $FePO_4$: ferric phosphate; α-$Ni(OH)_2$: inner layer nickel (II) hydroxide).

plasmonic photocatalysts based on synergistic interactions between localized surface plasmon resonance and impurity energy levels. In a specifically built photocatalytic reactor, hydrothermally produced gold-loaded hydroxyapatite nanocomposites with mesoporous architectures and substantial surface area were shown to be efficient for the degradation and removal of modeled methylene blue dye [113], and a mechanism of this research is shown in Fig. 11 (a and b). Research utilizing Fourier transform infrared spectroscopy demonstrated that plasmonic gold nanoparticles increased hydroxyapatite's photoabsorption capacity and photostability. The gold-loaded hydroxyapatite nanocomposite is well-suited for removing waste dyes due to the surface plasmon resonance of the gold nanoparticles and hydroxyapatite's

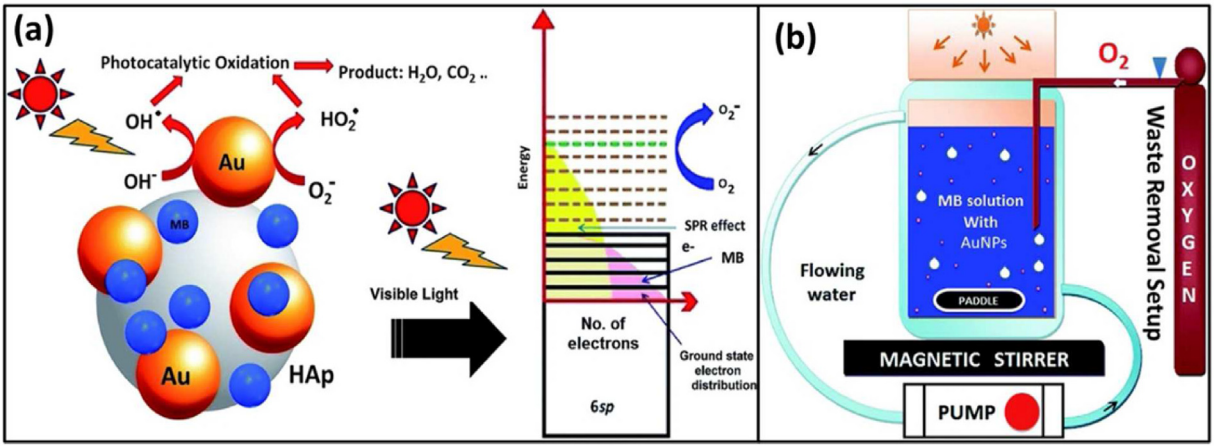

Fig. 11 – Contaminent elimination employing plasmonic gold nanoparticles based photocatalysts: (a) a mechanism of photocatalytic waste elimination, (b) water waste removal reactor, adapted with permission from Ref. [113]. (For interpretation of the references to color in this figure legend, the reader is referred to the Web version of this article.)

excellent dye adsorption capability in the visible range of solar light.

By sputtering a gold coating followed by annealing at various temperatures, Ajay and Mohammed [114] showed the functionalization of zinc oxide nanowires by size-controlled gold nanoparticles. Raising the annealing temperature to 400 °C produces more significant gold nanoparticles (10–20 nm), and increasing the annealing temperature to 600 °C produces the most prominent size particles (10–30 nm). The introduction of 'multifunctional' gold nanoparticles in the photoanode might explain the greater efficiency and stability. First, the localized electric field of gold nanoparticles interacts with the zinc oxide surface (owing to surface plasmon resonance), increasing visible light absorption and forming additional electron-hole pairs at the nanowire surface. The second step is to reduce the hole trapping by employing passivation of the zinc oxide surface defects/traps, which enhances the water-splitting capabilities for indium tin oxide over the free tin oxide anodes doped with fluorine. Consequently, this method is a synthetic, straightforward, and cost-effective way to produce photoactive materials that can be scaled up. It may be used to develop and fabricate improved photoactive materials for catalysis and other applications.

Copper

Copper oxide, a desirable noble metal oxide from the monoclinic crystal family, has been widely employed in various sectors [115]. Lithium-ion batteries, catalysis, high-temperature semiconductors, gas sensors, photoelectrochemical sensors, supercapacitors, and the innovative manufacturing of antimicrobial agents and memristors are just a few of the advanced uses for this transition metal oxide [116]. Due to its high theoretical capacity, cheap cost, and benign nature, there has been considerable interest in copper oxide as an anode material [117,118]. The low conductivity of copper oxide and the significant volume variation that occurs during the conversion process of lithium ions have made it difficult for copper oxide anodes to achieve high capacity and rate capabilities. Nanostructures have recently improved the performance of electrochemical systems and the incorporation of carbon materials developed to avoid copper oxide's weak conductivity [119]. Despite their potential to extend cycle lives and enhance the ability to operate at high rates, copper oxide anode materials have not yet achieved significant success. One of the solutions is that the fabrication of copper materials in the size range of 1–100 nm can produce a more desirable property than their conventional counterparts. There is also the possibility of copper nanowires and nanorods being considered promising candidates for several potential applications, for example, the interconnect of nanoelectronic devices.

It has been discovered that nanoporous copper can also be used for electrochemical catalysis and sensors, as well as for energy utilization and preservation. As a subcategory of nanoporous products with a significantly organized porous network, slight pore size variation, and high conductive properties, copper nanoporous is particularly desirable for various applications. The surface wettability of the nanoporous copper is considerably superior to that of the plain copper surface primarily because of the increase in surface roughness associated with the nanoporous structure [120]. Fig. 12 (a) shows the bottom-up gradient filling of copper within porous silicon surfaces by utilizing a contactless electrochemical approach [121]. The modified cell design was employed to generate a radiating symmetrical current that altered radially along the sample area's radius, resulting in gradient filling of the vias (hole depth to hole diameter). Studying the impact of copper sulfate concentrations demonstrated the necessity of mass transfer constraints in the procedure, as shown by the data acquired at lower copper sulfate concentrations (0.1 M), where the bottom-up deposition was not acquired. The gradient in deposition was less owing to mass transport restrictions at the sample area's boundary, even though the copper sulfate concentration was raised from 0.1 to 0.25 M. Through in-situ hydroxylation and electro-oxidation, Shi et al. [122] discovered that intermetallic molybdenum carbonate spontaneously dissociated from a hierarchical nanoporous copper substrate; thus, it is an ideal candidate for use as a very reliable electrocatalyst for alkaline

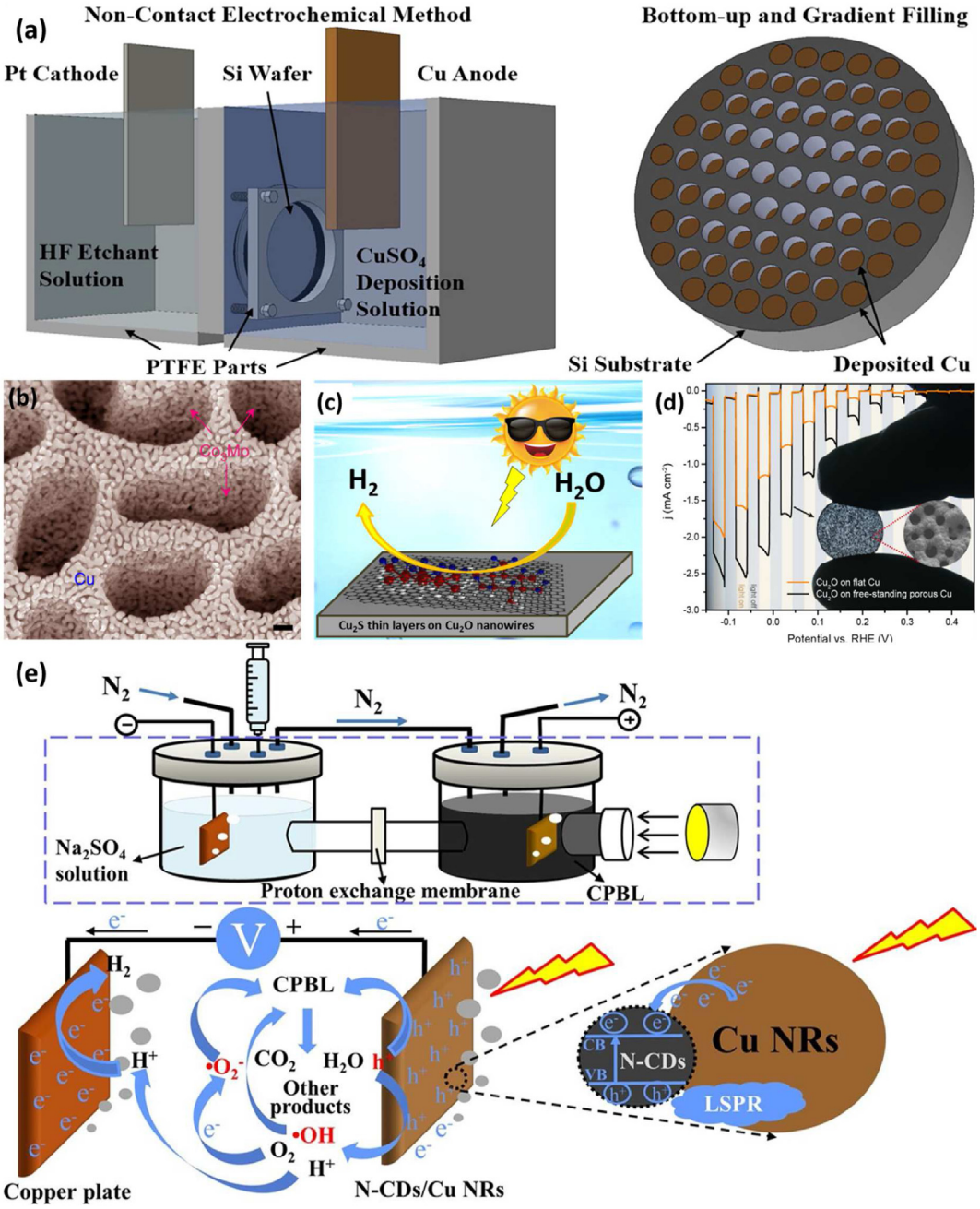

Fig. 12 – (a) demonstration of bottom-up gradient filling of Cu in porous silicon substrates by a non-contact electrochemical technique, adapted with permission from Ref. [121]; (b) conventional cross-sectional scanning electron microscope (SEM) illustration of molybdenum carbonate over copper (Co_3Mo/Cu) electrode synthesized by chemically dealloying copper cobalt molybdenum alumina ($Cu_8Co_3Mo_1Al_{88}$) alloy precursor, showing a three-dimensional bicontinuous and bimodal nanoporous design. Scale bar, 200 nm, adapted with permission from Ref. [122]; (c) tetrafunctional copper sulfide (Cu_2S) thin layers on copper oxide (Cu_2O) nanowires for effective photoelectrochemical water splitting [123]; (d) cuprous oxide electrodeposition on a porous copper framework for better photoelectrochemical activity, adapted with permission from Ref. [124]; (e) copper nanorod-supported coal-based N-carbon dot complex nanocatalysts for hydrogen production from photoelectrocatalytic degradation of wastewater, reused with permission from Ref. [125]. ($CuSO_4$: copper sulfate; HF etchant: Etching with hydrofluoric acid; Na_2SO_4: Sodium sulfate; CPBL: cotton pulp black liquor; N-CDs/Cu NRs: nitrogen-doped carbon dots over copper nanorods). (For interpretation of the references to color in this figure legend, the reader is referred to the Web version of this article.)

hydrogen/oxygen development processes. A nanoporous molybdenum carbonate over a copper electrode prepared by chemical dealloying the copper cobalt molybdenum alumina ($Cu_8Co_3Mo_1Al_{88}$) alloy in potassium hydroxide electrolyte is shown in Fig. 12 (b). Nanopores of 25 nm and large 300 nm channels are present in a hierarchical nanoporous copper skeleton. Despite the natural solid behavior of molybdenum carbonate and the rapid electron transfer and mass-transport pathways of the hierarchical nanoporous copper skeleton, nanoporous molybdenum carbonate over copper electrodes exhibits a low Tafel slope of 40 mV dec−1 and minimal onset overpotential. These materials are promising as economical anodes and cathodes for various water-splitting utilizations due to their remarkable electrochemical performance. The innovative photocathode presented by Zhenzhen and Zhonghai [123] is composed of copper sulfide-coated copper oxide nanowires reinforced on a three-dimensional porous copper foam, as illustrated in Fig. 12(c)'s schematic design. The photoelectrochemical performance and long-term photostability of copper oxide nanowires were increased by a tetrafunctional copper sulfide layer on their surface. They demonstrate a simple way to fabricate highly efficient and stable photoelectrochemical devices without a time-consuming and expensive fabrication procedure.

Kurniawan et al. [124] created a dendritic porous copper structure with a large surface area using hydrogen-evolution-assisted copper electrodeposition (Fig. 12 (d)). According to photoelectrochemical water splitting studies, a copper oxide film produced on an even surface copper substrate exhibits a photocurrent intensity of 1.25 mA cm^{-2} at zero volts. In the Mott-Schottky analysis, the highest photocurrents are produced by thin and homogeneous copper oxide layers formed during a brief deposition period (5 min). Copper nanorod-supported coal-based N-carbon dot composite nanocatalysts were also used to generate hydrogen from photoelectrocatalytic wastewater degradation [125]. The research's schematic flow diagram is shown in Fig. 12 (e). The findings demonstrated that nitrogen-doped carbon dots over copper nanorods (N-CDs/Cu NRs) performed brilliantly degrading cotton pulp black liquor and hydrogen generation as a simple, efficient, and stable catalytic material. Furthermore, the oxidation process for degrading high-chemical oxygen demand based on potassium dichromate (COD_{Cr}) wastewater and the reduction reaction for creating hydrogen is carried out simultaneously.

Lead

Lead is a soft, malleable, ductile metallic element with thick, bluish-grey color. It was one of the first metals discovered. Car batteries, pigments, ammunition, cable sheathing, lifting weights, diving weight belts, lead crystal glass, radiation protection, and specific links still utilize lead. Lead is a rare metal in the earth's crust at concentrations of 1.410^{-3}% (w/w). Due to its non-biodegradability, it is a poisonous heavy metal that only exists in a cubic close-packed metallic state [126]. When the lead oxide over the lead metal pair is oxidized or reduced, the lead oxide can develop as a transient phase. In alkaline solutions, it's exceptionally stable. Lead oxide has two crystallographic forms – orthorhombic inner layer lead oxide and tetragonal outer layer lead oxide. When lead metal is anodically oxidized, the outer layer of lead oxide will be formed, which may be converted to the inner layer of lead oxide [126]. The internal layer-lead oxide has a more compact structure and excellent mechanical stability and can be synthesized electrochemically in alkaline solutions. In contrast, the outer layer-lead of oxide is more porous and is synthesized in acidic solutions. Temperature, solution composition, and applied current density all influence the morphology of lead oxide [127].

Elementary lead has a wide range of uses due to its adaptability in welding, low melting point, high density, and capacity to absorb gamma and X-rays, among other attributes. Despite its limited tensile and fatigue strengths and propensity to flow under light loads, lead is not suitable for structural applications due to its limited tensile and fatigue strengths. The electrochemical manufacturing of lead oxide-electrochemically reduced graphene oxide nanocomposites (PbO-ERGO), and their photoelectrochemical characteristics were explored by Bingül and colleagues [128]. The production of the (PbO-ERGO) material is shown schematically in Fig. 13 (a). In an aqueous solution comprising 1.0 mM lead nitrate, 0.1 M perchloric acids, 0.1 M potassium nitrate, and graphene oxide suspension, cathodic electrodeposition for 60 min, the study was conducted at a constant potential of −0.6 V (vs. silver chloride electrode). Fig. 13 (b and c) shows examining electron microscope illustrations of an indium tin oxide electrode changed with a lead oxide-electrochemically reduced graphene oxide nanocomposite. There are often ripples, crumples, and layers of single or fragile graphene oxide sheets in electrochemically condensed graphene oxide sheets. It is shown in Fig. 13 (b) that a lead oxide composite with electrochemically reduced graphene oxide has been studied on a large scale through scanning electron microscopy. Lead oxide nanoparticles were evenly distributed across the electrochemically reduced graphene oxide surface without aggregating. The top white region of the lead oxide layer and the dark bottom section of the electrochemically reduced graphene oxide structures were readily visible. Furthermore, the lead oxide-electrochemically reduced graphene oxide nanocomposite electrode surface was evenly coated. The intermixed lead oxide particles were encased in a wrinkled graphene lattice.

A scanning electron microscope picture in Fig. 13 (c) shows platelets on the surface of lead oxide particles in the top layer. Photoluminescence experiments conducted on lead oxide-electrochemically reduced graphene oxide nanostructures demonstrated a decrease in fault concentration and enhanced optical performance. The lead oxide-electrochemically reduced graphene oxide nanostructures also displayed stable and reproducible photocurrent across multiple cycles, indicating that the electrode is not susceptible to photo corrosion, likely due to the synergistic effects of the lead oxide nanostructure and electrochemically reduced graphene oxide. According to the research, lead oxide-electrochemically reduced graphene oxide nanocomposites might be suitable candidates for next-generation solar systems. Negishi and co-authors [129] combined gold (core)–lead (shell) nanoporous-loaded titania and unmodified gold-titanium oxide on a fluorine-doped tin oxide electrode to serve as the photoanode

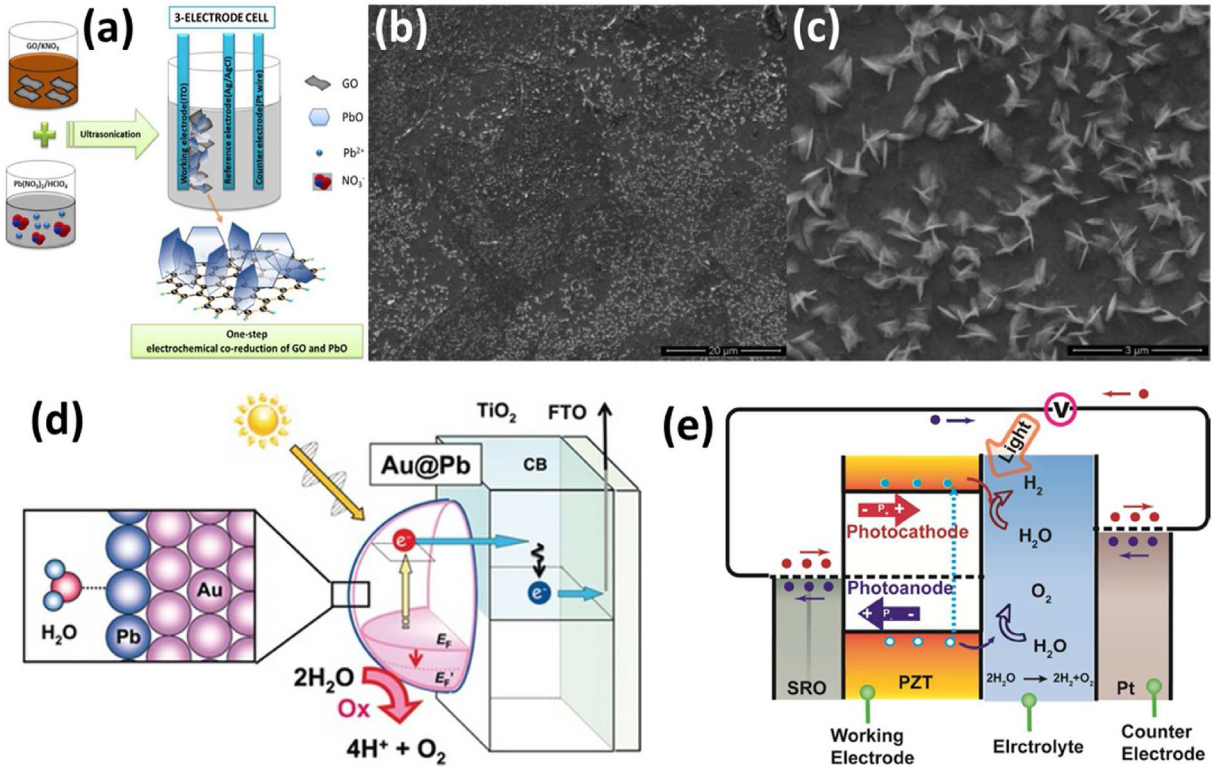

Fig. 13 – (a) Diagram image of the preparation of the lead oxide-electrochemically reduced graphene oxide nanocomposites (PbO-ERGO) material for photovoltaic cells, adapted with permission from Ref. [128]; (b,c) The scanning electron microscope pictures of PbO- electrochemically reduced graphene oxide nanocomposites on indium tin oxide electrode ((b) large-scale image and (c) top-layer image), adapted with permission from Ref. [128]; (d) schematic diagram of gold (Core)–lead (Shell) nanoparticle-loaded titanium (IV) oxide, reused with permission from Ref. [129]; (e) illustration of the switchable photoelectrochemical response measured by ferroelectric polarization in (101)-oriented lead zirconium titanate ($Pb(Zr_{0.2}Ti_{0.8})O_3$ (PZT)) epitaxial films synthesized on the (110) Strontium titanate ($SrTiO_3$) substrate with strontium ruthenate ($SrRuO_3$) as bottom electrodes, adapted with permission from Ref. [130]. (H_2: hydrogen; O_2:oxygen; H_2O: water; CB: conduction band; VB: valence band; hv: high voltage; e^-: electron; GO: graphene oxide, PbO: lead oxide; Pb^{2+}: a cationic form of lead; NO_3^-: nitrate; Au@Pb: gold supported on lead; SRO: strontium ruthenate). (For interpretation of the references to color in this figure legend, the reader is referred to the Web version of this article.)

in photoelectrochemical cells, as shown in Fig. 13 (d). Underpotential photo deposition forms a monolayer level of lead shell on the gold (111) surface of gold-titanium oxide, resulting in Au@Pb/TiO_2 with heteroepitaxial nanojunction, according to findings. In addition to providing water oxidation resistance, the lead shell on gold nanoparticles increases the visibility of gold-titanium oxide. For the photoelectrochemical response under illumination, Tan et al. [130] developed 100 nm (101)-oriented lead zirconium titanate epitaxial films on strontium titanate substrate with strontium ruthenate as bottom electrodes (Fig. 13 (e)). An external electric field may be used to pol the lead zirconium titanate electrode over the strontium ruthenate electrode ($Pb(Zr0.2Ti0.8)O_3/SrRuO_3$) to operate it as a photoanode or photocathode. Several theories have been proposed to explain the switchable photoelectrochemical response. These include the electric field induced by ferroelectric polarization and the depletion area caused by ferroelectric polarization at the lead zirconium titanate material. Hence, it becomes clear that lead oxide controls the electro-chemical characteristics of the electrode in the PbO potential zone. Last but not least, despite the fact that PbO materials applications PEC systems have generated a lot of attention and an increasing number of studies and publications, the commercialization of these prospective applications is required.

Silver

Silver nanoparticles are among the most researched and commercially exploited nanomaterials in recent years, and they're often seen in nano-functionalized consumer goods [131]. The antimicrobial properties of silver nanoparticles are well established. Due to its eco-friendly and cost-effective synthesis processes, green synthesis of silver nanoparticles is becoming more popular as an alternative to chemical and physical approaches. Because of its many advantages, including cheap material cost, strong catalytic activity, and stability, silver, and its composites have been extensively employed. However, the system's flaws include its moisture sensitivity and the expensive cost of ionic liquids, both of which would limit the catalysts' scalability [132]. Silver is noted for its strong oxygen solubility and rapid diffusion rates.

In other words, silver can function as reversible electrode material in photoelectrochemical cells. Silver is a good contender for photoelectrochemical cathodes because of these features. Wang et al. [133] made a porous silicon composite using a one-step lithium aluminum hydride reduction process. In addition, the authors then connected nano-silver and lithium carbonate molecules to the porous silicon substrate. The experimental findings demonstrate that porous silicon compounds enriched with silver nanoparticles (silica-silver) have a greater specific capacity (476.0195 mA h.g−1) and reduced interfacial resistance (~0.8 Ω), and two apparent reduction potentials of ~0.3 V and ~−0.1 V in those composites materials. Under moderate overpotentials of <0.50 V, Lu and co-authors [132] reported a nanoporous silver electrocatalyst capable of electrochemically reducing carbon dioxide to carbon monoxide with nearly 92% selectivity at a frequency (that is, current) over 3000 times greater than its polycrystalline alternative. The authors demonstrate that electrochemically active nanoporous silver catalysts can effectively and selectively reduce carbon dioxide to carbon monoxide. In addition to creating a large surface area for catalytic reactions (ca. 150 times greater than polycrystalline silver), the porous structure also results in a large number of highly active carbon dioxide conversion step sites (at least 20 times more active than polycrystalline silver). At a moderate overturn rate, its activity is approximately three orders of magnitude greater than that of its polycrystalline competitor. This carbon dioxide electroreduction operation was accomplished with a carbon monoxide Faradaic efficiency of 92%. In addition, Zhao et al. [134] developed nanoporous silver structures composed of nano-sized particles using a one-step pulsed laser deposition method under a regulated background gas pressure.

The porous pulsed laser deposition-silver for hydrogen peroxide detection demonstrated excellent oxygen reduction reaction performance, sensitivity, and selectivity. Furthermore, porous pulsed laser deposition-silver may be deposited on flexible substrates for flexible hydrogen peroxide sensing applications. Ali et al. [135] discovered that co-modifying tin oxide and silver for carbon dioxide reduction and 2,4-dichlorophenol degradation improves the visible-light characteristics of graphitic carbon nitride, and the schematic diagram of their results is shown in Fig. 14 (a). The improved photoactivity was observed through transient-state surface photovoltage responses, transient-state photoluminescence spectra, and electrochemical analyses, which indicated that the extended charge lifetime and provided catalytic function could be attributed to the enhanced photoactivity by adjusting the tin oxide and silver compositions. It is possible to obtain the catalytic function from reprocessed silver, which can act as a co-catalyst, and to provide the charge lifetime from modified tin oxide, which can accept electrons from pure graphitic carbon nitride. Other noble metals may also benefit from the synergistic effect. Direct ammonia-borane electrooxidation by bimodal nanoporous silver produced from a dual-phase silver-zinc (10/90) precursor was also studied by Luo and co-authors [136] (see Fig. 14 (b)). Wide holes were generated by dissolving zinc-rich phases while selectively dissolving silver/zinc (1/3) with intermetallics formed ultrafine nanopores. The electrocatalytic activity of ammonia-borane oxidation is enhanced by bimodal nanoporous silver with its initial potential of 195 mV compared with the monomodal nanoporous silver. Hierarchical nanoarchitectures produce an increased catalytic activity for ammonia-borane oxidation, in which the nanoporosity delivers a high active surface area, while broad channels facilitate the rapid mass transfer.

Aluminium

The first effort at porous metals was in 1943 when pores were purposely created into molten aluminum by adding mercury [137]. Aluminum is often chosen as the material to be eliminated (less noble) in many applications, and it is still one of the most common options [138]. It was chosen because of its high activity, ease of alloying with a wide range of metals, availability, and inexpensive cost. Aluminum nanomaterials have

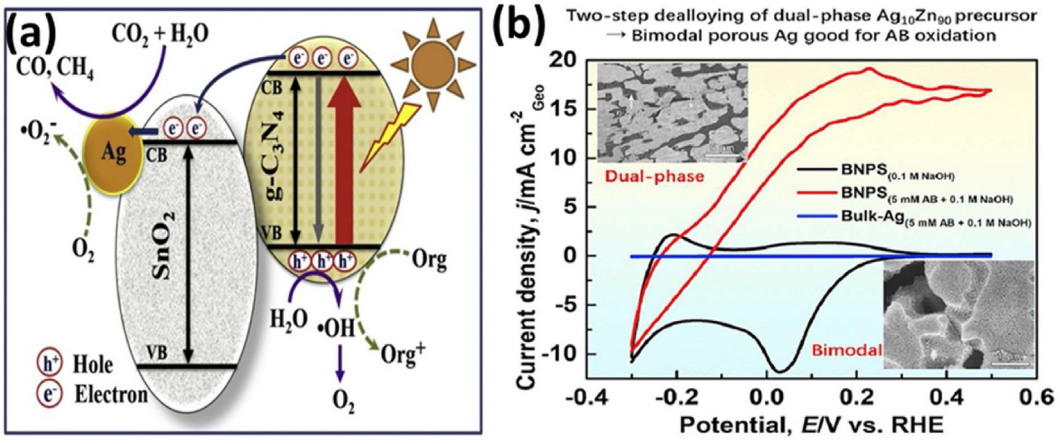

Fig. 14 – (a) the synergistic impact of co-modifying tin oxide to extend charge lifetime and silver (Ag) to offer catalytic function for carbon dioxide reduction and 2,4-Dichlorophenol (2,4-DCP) degradation improves the visible-light activities of graphitic carbon nitride, adapted with permission from Ref. [135]; (b) direct ammonia-borane electrooxidation by bimodal nanoporous silver produced from a dual-phase silver-zinc ($Ag_{10}Zn_{90}$) precursor, adapted with permission from Ref. [136]. (BNPS: Bimodal nanoporous silver).

demonstrated unique controlled capabilities to suit the demands of tissue engineering cell growth and proliferation. It is possible, however, that aluminum may become a more noble metal in the future due to such high activity. It has been long anticipated that nanoporous metals could be successfully synthesized through the galvanic replacement reaction or dealloying [139] in a binary system where aluminum is the nobler element [140]. Nanoporous anodic aluminum oxide has garnered significant attention as a potential structure for photoelectrochemical water splitting owing to its exceptional chemical and mechanical properties. Porous anodic aluminum oxide may be manufactured by electrochemical anodizing aluminum. With proper anodization processing parameters (e.g., voltage, electrolyte concentration, etc.), it can be possible to control the location of pores, the spacing between pores, the thickness of porous layers, and the overall aspect ratio of the pores [141]. Anodic aluminum oxide comprises a hexagonally arranged array of cylindrical nanopores extending perpendicularly from the surface of the underlying aluminum substrate [142]. As part of a photoelectrochemical hydrogen production process for sewage water, Almohammedi and co-authors [70] used a nanoporous titanium nitride over a titanium dioxide/alumina membrane in Fig. 15 (a). The aluminum oxide template was morphologically characterized after pore widening at 60 °C (Fig. 15 (a)). As in Fig. 15 (b), a top-view scanning electron microscope image of gold/titanium nitride over titanium dioxide and aluminum oxide ($Au/TiN/TiO_2/Al_2O_3$) reveals agglomerated gold nanoparticles covering the top surface and template pores, with average diameters of 285 nm. Using $TiN/TiO_2/Al_2O_3$ materials as photocathodes with and without gold nanoparticles, sewage water can be split using gold materials.

As a function of nanoporous anodic alumina porosity and gold thickness, Hernández-Eguía and co-authors [143] studied the reflection spectrum of nanoporous anodic alumina films sputtered with gold overlayers. A first layer is constructed using nanoporous anodic alumina film with a small quantity of gold placed on the pores' inner walls to allow for gold penetration during sputtering. Essentially, the first coat is defined by the effective medium's thickness, porosity, and volume percentage of gold. Furthermore, the second layer comprises a porous gold film similar to what nanoporous anodic alumina sputtered on its gold layer. The nanoporous anodic alumina layer and deposited gold thin film have been modeled based on the active medium approximation and depict excellent agreement with experimental observations. The model can determine the structure of the steep reflection troughs in the near-IR for varying gold thicknesses and nanoporous anodic alumina porosities. Fig. 15 (c) depicts a production procedure for nanoporous anodic alumina using basic electrochemical anodization of aluminum, which results in densely packed hexagonal arrays of nanopores from top to bottom. Despite several study efforts in recent years, a thorough description of self-organization development has

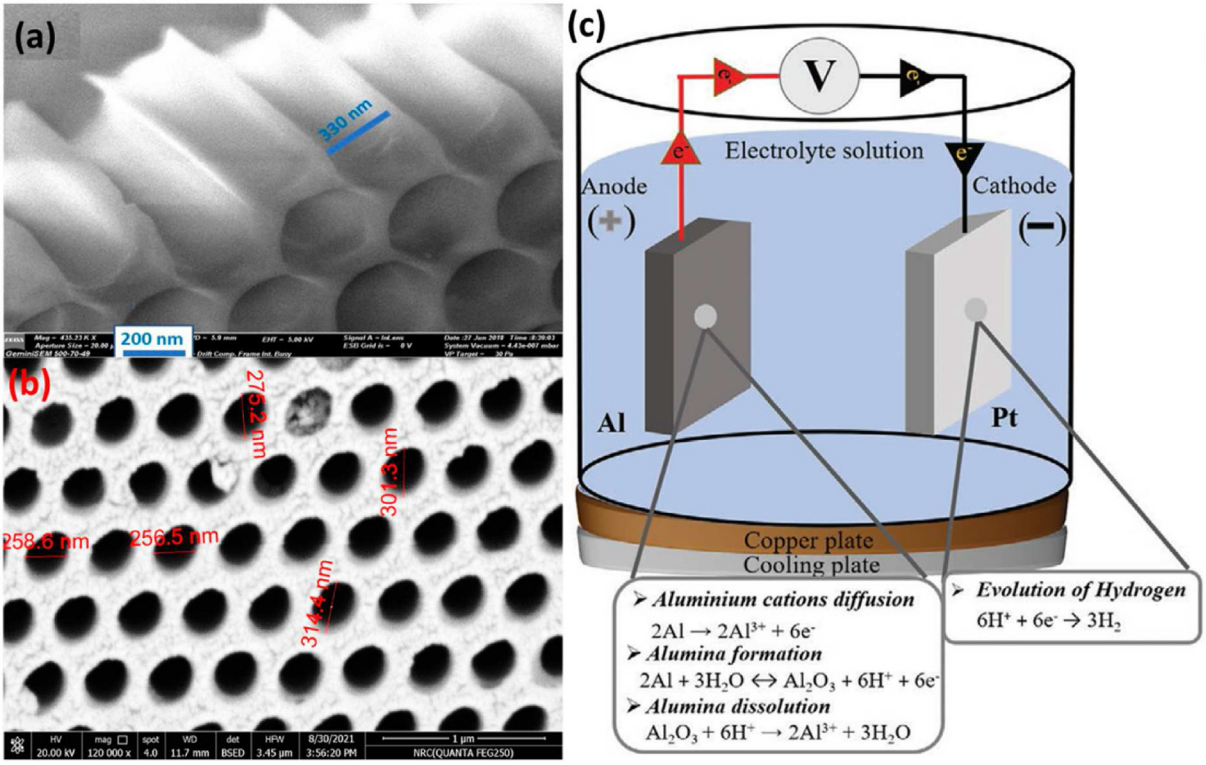

Fig. 15 – (a) scanning electron microscope pictures of Al_2O_3 shape after pore widening; (b) scanning electron microscope image of gold/titanium nitride over titanium dioxide and aluminium oxide ($Au/TiN/TiO_2/Al_2O_3$) (no permission is required) [70]; (c) fabrication method of NAA employing an electrochemical system, reuse with permission from Ref. [144]. (d_1: thickness; P_1: out of a donor–π–bridge–acceptor molecule, and f_{Au}: volume percentage of gold in the effective medium). (For interpretation of the references to color in this figure legend, the reader is referred to the Web version of this article.)

yet to be established. Innovative materials are likely to be integrated into current systems in the future, sometimes as quick and inexpensive methods to improve the capabilities of existing materials, but also as carefully manufactured alternatives that can compete with and replace more expensive options.

Silicon

Silicon is now the most frequently used material in microelectronics; however, it is not widely utilized in photoelectrochemical cells. This is because of the intrinsic nature of the indirect transition in band-edge emission. In 1990, electrochemically etched porous silicon exhibited visible photoluminescence [145]. The material has since been widely investigated to elucidate the luminescence process and study its potential usage as a novel material for optical device applications. Nanoporous silicon is a monocrystalline silicon structure with a sponge-like morphology that, despite its accidental discovery, has quickly become one of the most extensively investigated silicon structures. Several books and over a dozen review articles have focused on its features and uses. To create a compound that shows macroscopic electro strains in an electrolyte, Brinker et al. [146] combined wafer-scale nanoporosity in single-crystalline silicon with polymerization of an artificial strength substance inside pore volume (Fig. 16 (a)). The length (I_0), width (w), and thickness (t) of the as-fabricated membrane are depicted on the left. The sample compresses when a 0.4-V voltage is applied, and the perchlorate anions are released from the polypyrrole, as seen in the central area. A voltage of 0.9 V is used in the right portion, and the anions are absorbed, followed by the sample's subsequent expansion. Upon inspection of the single pores, they found pressures of up to 150 atm generated by the coordinated action of 100 billion nanopores per square centimeter cross-section. Zhao et al. [147] used nanoporous "black silicon" photoelectrodes with electroless deposited platinum nanoparticle samples for photoelectrochemical proton reduction, and the schematic diagram of the synthesis is shown in Fig. 16 (b). In step one, the platinum-silicon

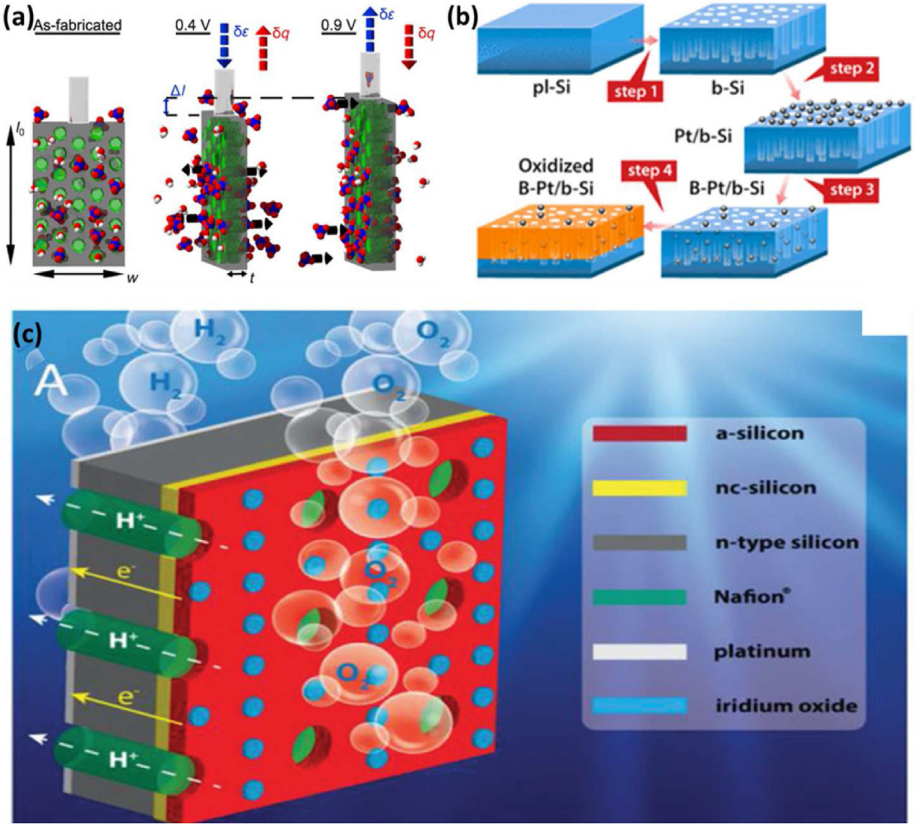

Fig. 16 – (a) Diagrams of the electroactuation experiments on the porous silicon membrane (grey) occupied with polypyrrole (green) dipped in an aqueous electrolyte [perchloric acid (blue and red) and water (red and white) molecules] (no permission is required) [146]; (b) diagram of the synthesis steps for air-stable high-performance nanoporous black silica electrode with platinum-deposited black silica (B–Pt/b-Si) photocathodes and the region of surface oxidation following air aging, reprinted with permission from Ref. [147]; (c) Schematic illustration stand-alone photoelectrochemical cell, based on amorphous silicon (a-Si) membrane with micron-sized pores with surrounded ion exchange substantial, highlighting the diverse constituents, adapted with permission from Ref. [148]. (nc-Si:H: nanocrystalline silicon; SHJ: silicon heterojunction; b-Si: black silicon; pl-Si: planar silicon wafer; B–Pt/b-Si: platinum-deposited black silica; pSi: porous silicon; InP NCs: indium phosphide nanocrystals). (For interpretation of the references to color in this figure legend, the reader is referred to the Web version of this article.)

photoelectrode is transformed into a nanoporous black silicon photoelectrode using a metal-assisted etching technique.

During the second step, platinum nanoparticle catalysts are deposited via electroless deposition. The platinum/black silicon electrode is a black silicon electrode with platinum. In the third step of the process, hydrogen peroxide is utilized to oxidize the nanoporous silicon photoelectrodes with platinum nanoparticles adsorbed on the surface, which is followed by a second metal-assisted etching process that employs the surface-adsorbed platinum nanoparticles as an etching catalyst to embed them deep within the nanopores of the black silicon electrodes. Based on scanning and transmission electron micrographs, it was found that the platinum nanoparticle catalysts were deeply embedded in the photoelectrodes by the second etch, hiding behind a matrix of primarily amorphous silicon dioxide with a small amount of crystalline silicon. Based on electrochemical impedance measurements, it is demonstrated that covering the platinum nanoparticles enhances interfacial interaction, suggesting that the second etch significantly reduces interfacial charge-transfer resistance compared to materials without it. It was shown in another study that a silicon membrane-based photoelectrochemical cell architecture embedding ion exchange materials with micron-sized holes could be fabricated [148]. According to Fig. 16 (c), a photoelectrochemical cell consists of a silicon membrane with micropores surrounded by a substantial cation exchange. A triple photovoltaic cell built entirely of silicon in the early stages of research supplied enough current for both hydrogen and oxygen evolution processes. An amorphous silicon absorbent was present in the top cell (red), a nanocrystalline silicon absorber was present in the medium cell (yellow), and a monocrystalline silicon wafer with a silicon heterojunction crystal was present in the bottom cell (dark grey) [149]. In steady-state operation, the solar-to-hydrogen effectiveness of 7% is achieved due to the absorption losses caused by the micropores and catalyst microdots, compared to 10.8% for an unpatterned percentage of photovoltaic panel efficiency. All losses have been reduced and kept below the 250 mV limit by adding micropores to a triple silicon cell. Chandrasekaran et al. [150] employed porous silicon nanoparticles as a photocathode for photoelectrochemical water splitting, and the system provided a photocurrent density of -2.2 μA cm^{-2} while producing hydrogen gas. This method is a significant step in establishing low-cost photoelectrochemical renewable energy systems. Attempts are underway to improve the stability of the porous silicon nanoparticle photocathode system by employing different surface passivation processes such as thermal hydrocarbonization and electrografting.

Tin

Tin is a malleable, flexible silvery-white metal. Tin does not oxidize fast and is corrosion-resistant because an oxide layer protects it. While tin is not as well-known as copper, it is a commonly utilized metal in industrial applications and is insoluble in water and oxygen resistance. Tin is often employed in electroplating, which involves coating other base metals with the metal to protect them from other variables, such as corrosion. Tin may be extracted from cassiterite by reducing it with carbon due to poor electropositivity. Tin oxide, a wide-band-gap semiconductor, has long piqued the curiosity of both practical and pure researchers. Tin dioxide has been used as a transparent conductor, mainly using both accidental conductivity and high transparency [151]. While tin oxide is technically *n*-type, current research suggests that it is more readily doped *p*-type than several other regularly used oxides, such as zinc oxide, indicating that it might be a superior candidate for light emitters and other optoelectronic devices [152]. The oxidation states of tin compounds are +2 and + 4, with +4 being the most stable. Due to their electronic, optical, and exceptional semiconducting properties, tin oxides have gained much attention in the scientific community [153,154]. These characteristics make them ideal candidates for photovoltaic [155] and photoelectrochemical [156] applications. Moreover, they have been touted as promising materials for many energy storage devices, such as Li-ion and Na-ion batteries [157,158]. It is widely recognized that appropriately constructed nanomorphologies of such oxides may show improved properties (e.g., surface area, electron mobility), making them even more suitable for the above applications [159]. According to Cao et al. [160], self-passivated electrochemically generated nanoporous tin foams demonstrate hydrophobic or superhydrophobic behavior without additional surface alteration. Water-oil separation, microfluidic devices, and other applications might benefit from conductive superhydrophobic metal surfaces [161,162]. Gurgul et al. [163] proposed a simple two-step electrochemical technique for synthesizing nanoporous tin/tin oxide systems; the field emission scanning electron microscopy illustrations of as acquired nanostructured layers are displayed in Fig. 17 (a and b). The metal foam structure did not change considerably for samples anodized for 600 and 1200 s, and an open-porous structure was kept; similarly, these surfaces are entirely covered with a porous anodic oxide layer.

Nanoporous tin/tin oxides were shown to be superhydrophilic even after additional thermal treatment, in contrast to thermally oxidized foams, which are hydrophobic. In this regard, it is possible to modify the wetting behavior of porous materials through anodic oxidation. Fig. 17 (c) shows the creation of a screw-like tin oxide nanostructure and its use as a photoanode for photoelectrochemical water splitting by Zhang et al. [156]. The screw-like tin oxide nanosheets were grown over rod-like single-crystalline tin oxide nanowires (SNWs@SNSs). Light absorption is efficient, electron movement is fast, and the surface-to-volume ratio is big in such a structure. The superb photoelectrochemical water splitting performance of cadmium sulfide-quantum dots over single-crystalline tin oxide nanowires and screw-like tin oxide nanosheets (CdS-QDs/SNWs@SNSs) photoanode is ascribed to the combination of fast electron transport in one-dimensional single-crystalline tin oxide nanowires, the larger surface area and improved light absorption of two-dimensional screw-like tin oxide nanosheets, the intense visible-light absorption of cadmium sulfide, and their corresponded energy level position. They plan to apply the screw-like nanostructure seen here with tin oxide to other semiconductors in photoelectrochemical cells, greatly enhancing their performance. Liu et al. [164] prepared nanoporous tin oxides by a scalable and facile electrochemical anodic oxidation technique. The

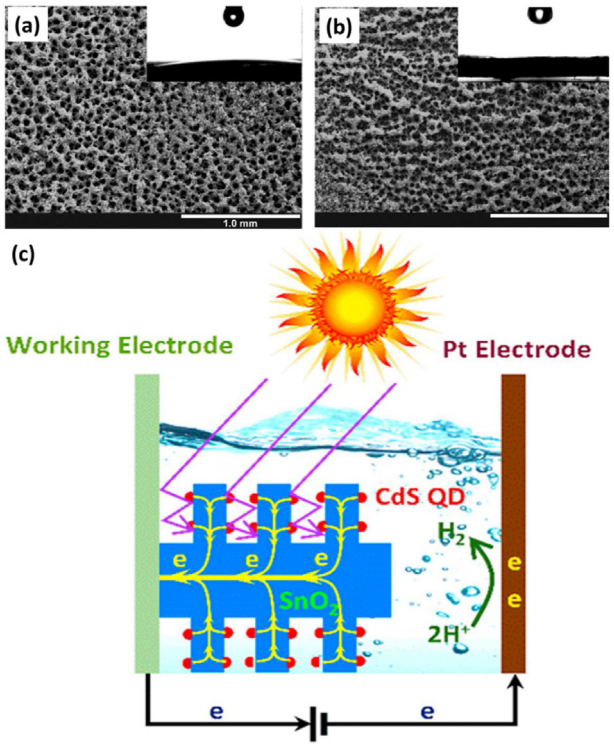

Fig. 17 – Field emission scanning electron microscopy illustrations of anodic tin/tin oxide (Sn/SnO_x) foams gained by anodic oxidation of metallic foams in 1 M NaOH electrolyte at the potential of 4 V during 600 s (a) and 1200 s (b) (no permission is required) [163]; (c) Screw-like tin oxide nanostructure that assists as a model design for effective photoelectrochemical water splitting devices, adapted with permission from Ref. [156]. (CdS QD: cadmium sulfide quantum dots; H^+: hydrogen ion; e^-: electron; SnO_2: tin oxide).

elevated local pH inside the porous structure led to the enhancement of formate production, according to Operando Raman's characterization. Consequently, these findings could open the way for designing porous composites for energy conversion and storage applications.

Iron

Iron is a transition metal that may be found in quantities ranging from nanogram/liter in marine settings to milligram/liter in freshwater receiving acid mine drainage. Depending on external variables, it can be found in various oxidation states in water. Ferrous iron is more soluble than ferric iron, shapes weaker links with complexing agents, and is generally more accessible to eukaryotes [165]. High strength-to-weight ratios, high surface area, and ultralow density are only advantages of porous nanostructured iron composites. As a result, they are appealing items for use in photoelectrochemical cells. Guoxia and colleagues [166] created nanoporous iron-doped bismuth vanadate modified with the iron-based metal-organic framework to improve photoelectrochemical stability and water-splitting performance. During photoelectrochemical experiments, it was observed that doping bismuth vanadate with iron ions improved its stability and photoelectrochemical performance. This enhancement could be attributed to iron ion doping improving the crystalline structure of bismuth vanadate and reducing crystal defects. Furthermore, iron doping can synergize with co-catalysts to further enhance the photoelectrochemical performance of bismuth vanadate. Peerakiatkhajohn et al. [167] used a simple anodization method to make hematite films for increased photoelectrochemical water splitting (Fig. 18 (a)). Adding silver nanoparticles to iron oxide nanosheet surfaces increases light harvesting and charge transfer across a wide wavelength range, eliminating pure iron oxide's short diffusion length problem. Because silver nanoparticles' surface plasmon state has a higher energy position than iron oxide's conduction band, charge transfer from silver nanoparticles to iron oxide is likely to be quiet. Using a cobalt-phosphate cocatalyst is crucial for trapping photogenerated holes and encouraging charge separation, which leads to successful water oxidation for oxygen production while stabilizing the iron oxide photoanode's surface, according to the researchers. Wang and coworkers [168] fabricated visible-light active iron oxide-quantum dots over nitrogen and fluorine co-doped titanium-oxide composite films via electro-oxidation and sequential electro-deposition procedures for the highly enhanced photoelectrocatalytic performance (Fig. 18 (b and c)). Nanostructured hematite and graphene quantum dots were deposited on nitrogen and fluorine co-doped titanium-oxide surfaces using successive electro-deposition and electro-oxidation procedures, as illustrated in Fig. 18 (b). A significantly increased use of iron oxide-quantum dots supported on nitrogen and fluorine co-doped titanium-oxide (Fe_2O_3-GQDs/NF–TiO_2) as photoanode and a titanium sheet as cathode photoelectrochemical performance was accomplished due to the joined impact of visible-light-active constituents (nanostructured hematite and nitrogen and fluorine co-doped titanium-oxide) and good electron conductors.

Fig. 18 (c) depicts possible processes for reducing hexavalent chromium and separating/transferring photogenerated electron-hole pairs on iron oxide-graphene quantum dots supported on nitrogen and fluorine co-doped titanium-oxide. The X-ray diffraction investigation found anatase and rutile phases in nitrogen and fluorine co-doped titanium oxide. Because of the diverse band gaps and conduction band situations, the essential band difference among rutile and anatase titania will favor electron-hole splitting [169,170]. Furthermore, it was observed that despite hematite having a lower conduction band position than titania, the Fermi level of hematite was similar to that of nitrogen and fluorine co-doped titanium oxide when they were in contact. The combined impact of visible-light active constituents (nitrogen and fluorine co-doped titanium-oxide and hematite) and suitable electron accelerators made generating, separating, and transporting electron–cationic form hydrogen pairs easier. Using Fe_2O_3-GQDs/NF–TiO_2 as an anode and a titanium sheet as a cathode resulted in higher photoelectrochemical activity and stability for hexavalent chromium reduction. Therefore, iron is thought to collect photogenerated holes, improving charge separation effectiveness and photoelectrochemical performances. As a result, it could be considered an alternative candidate for future

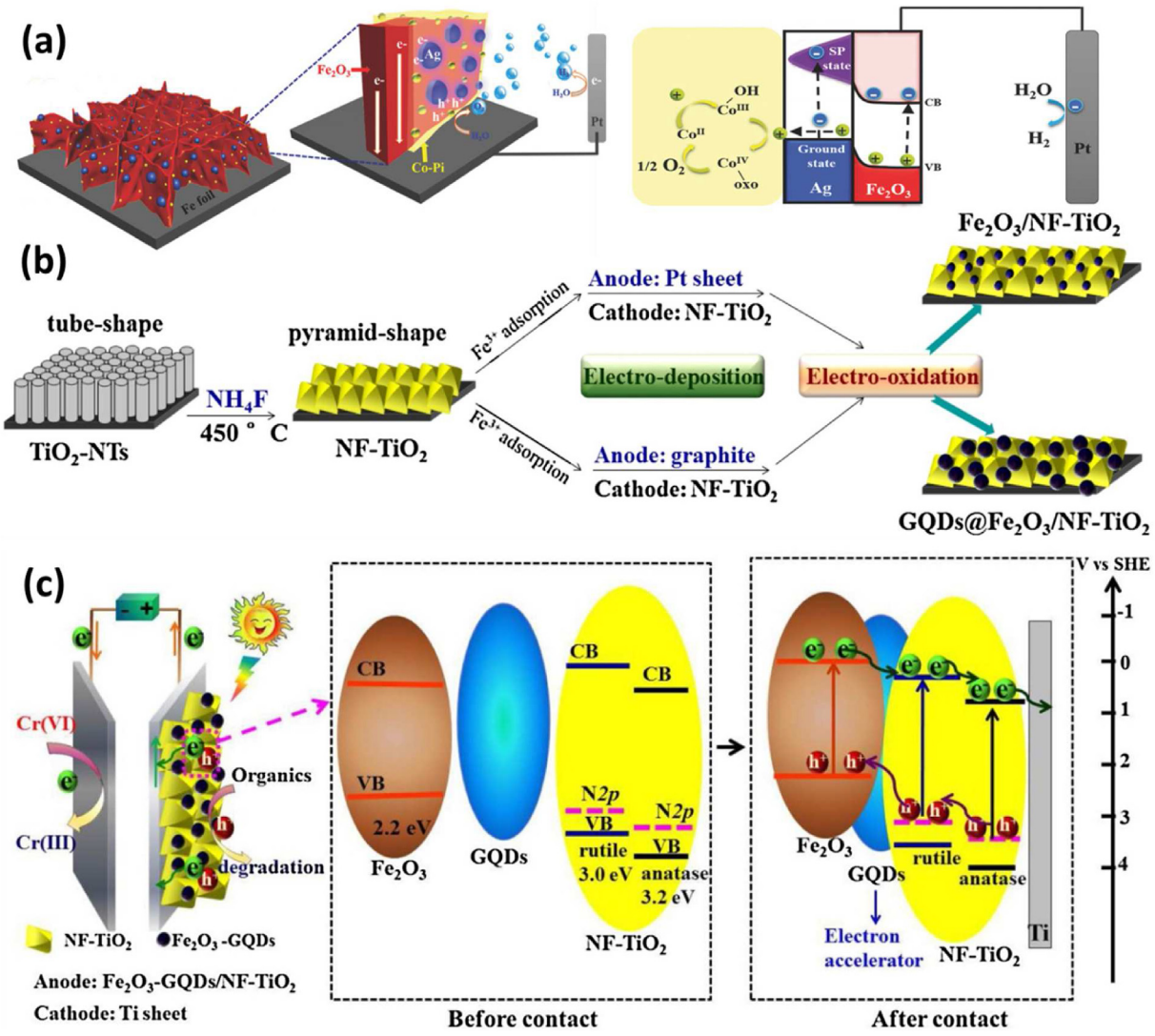

Fig. 18 – (a) diagram of hematite (α-Fe_2O_3) improved with plasmonic silver nanoparticles (Ag NPs) and cobalt-phosphate (Co-Pi) for effective photoelectrochemical water splitting, adapted with permission from Ref. [167]; (b) diagram showing the synthesis of iron oxide supported on nitrogen and fluorine co-doped titanium-oxide (Fe_2O_3/NF−TiO_2) and iron oxide-graphene quantum dots supported on nitrogen and fluorine co-doped titanium-oxide (Fe_2O_3-GQDs/NF−TiO_2) films, reprinted with permission from Ref. [168]; (c) graphic depiction for the photoelectrochemical reduction of hexavalent chromium (Cr(VI)) (left) and the separation/transfer of photogenerated electron-hole pairs on Fe_2O_3-GQDs/NF−TiO_2 during the photoelectrochemical process (right), reprinted with permission from Ref. [168]. (MIL-53(Fe): iron-based metal-organic framework; FTO: Fluorine-doped tin oxide; HOMO: highest occupied molecular orbital; LUMO: lowest unoccupied molecular orbital; GQDs: graphene quantum dots).

heterostructure design and co-catalyst utilization in photoelectrochemical applications.

Zinc

Zinc oxide has been categorized as one of the most capable constituents for gas sensors that work under ultraviolet irradiation due to its large band gap of 3.37 eV [171]. With its high capacity, worldwide abundance, and compatibility with aqueous electrolytes, zinc oxide continues to pique the interest of researchers and developers [172]. Surface morphologies substantially impact zinc oxide-based devices' sensing capabilities and optical characteristics. Many studies have focused on creating diverse morphologies of zinc oxide thin films using single-step physical deposition processes such as vacuum evaporation and sputtering [173,174]. Compared to other metal oxides such as tungsten trioxide and titania, zinc oxide nanowires have high electron mobility and are easy to manufacture, making them attractive for photoelectrochemical water splitting [175,176]. Some of the significant hurdles to the practical deployment of zinc oxide nanowire films as photoanodes are photo-corrosion of zinc oxide in the electrolyte solution, rapid recombination of photo-generated charge carriers (high concentration of surface traps), and poor visible light absorption. Rasouli et al. [177] employed a low-cost electrodeposition method to

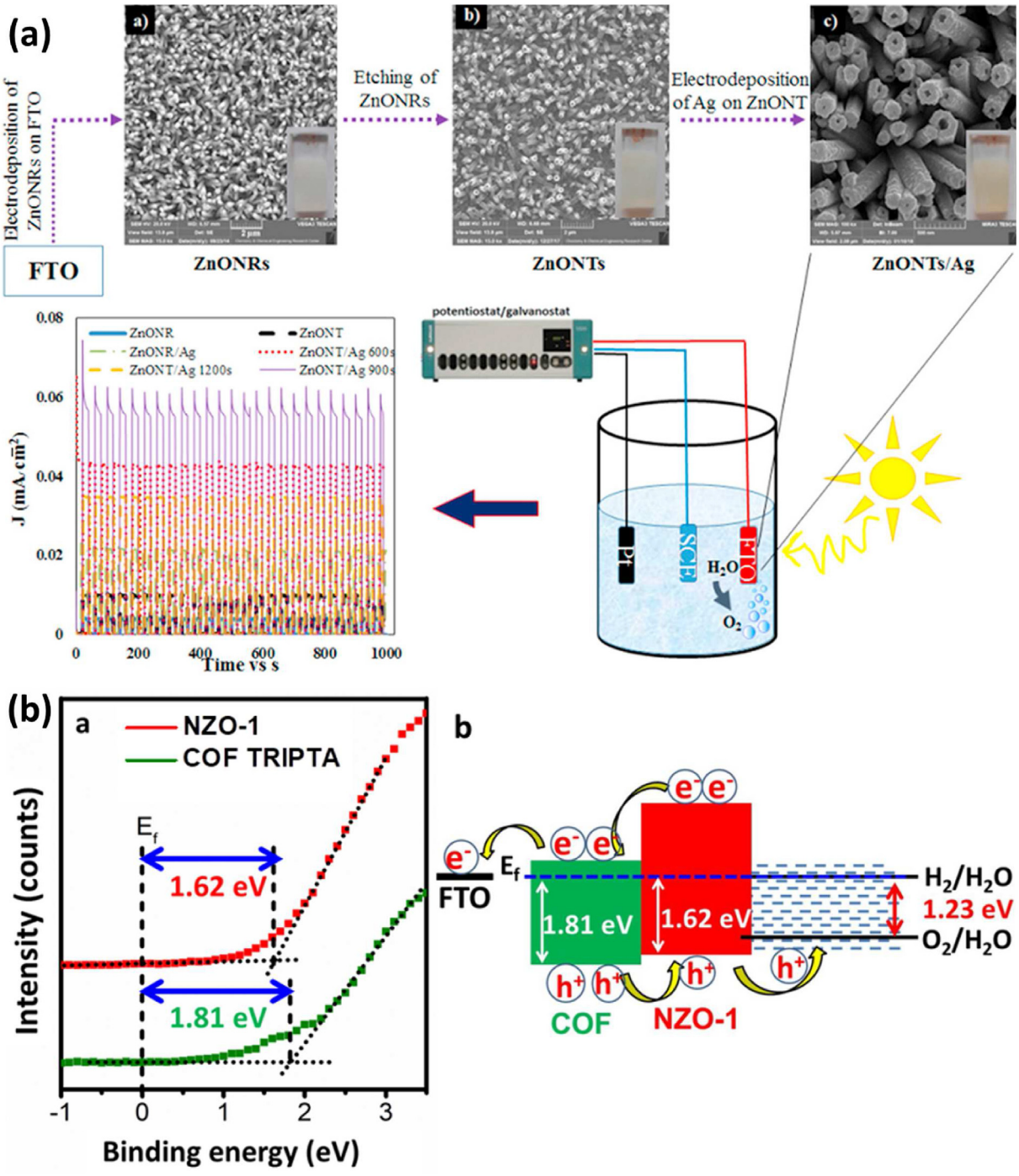

Fig. 19 – (a) Silver nanoparticles decorated zinc oxide nanotubes for photoelectrochemical water splitting, adapted with permission from Ref. [177] (FTO: Fluorine-doped Tin Oxide; SCE: saturated calomel electrode); (b) XPS valence band spectra of nanoporous zinc oxide (NZO-1) and covalent organic frameworks (COF) among the graphic mechanism photoanode for the effective charge transfer, reused with permission from Ref. [178]. (FTO: Fluorine-doped tin oxide; ZnONRs: zinc oxide nanorods; ZnONTs: zinc oxide nanotubes; ZnONTs/Ag: zinc oxide nanotubes over silver; SCE: saturated calomel electrode; COF-TRIPTA: covalent organic frameworks of the 1,3,5-triformyl phloroglucinol and 1,3,5-Tris-(4-aminophenyl)triazine).

synthesize silver nanoparticles decorated with zinc oxide nanotubes for photoelectrochemical water splitting, and the schematic flow diagram is shown in Fig. 19 (a). The etching method of zinc oxide nanorod arrays yielded well-aligned zinc oxide nanotube arrays. The results show that zinc oxide nanotube supported on silver (ZnO NT/Ag) arrays perform better under visible light irradiation than other arrays due to a reduction in charge recombination caused by the reduced band gap caused by the surface plasmon resonance impact of decorated silver nanoparticles on zinc oxide nanotube. Chatterjee et al. [178] used the N-rich antidiabetic medicine metformin as a template to create a new crystalline triclinic phase

of zinc oxide nanotube by hydrothermal synthesis with a self-assembled nanorod-like particle shape.

Fig. 19 (b) shows the effective charge transfer mechanism for increased photoelectrochemical activity. They were willing to formulate an effective load carrier photoanode with greater photocurrent density in photoelectrochemical oxygen evolution reactions through water splitting and outstanding photon-to-current conversion efficiency at nearly neutral pH combining porous zinc oxide with a covalent organic framework material. According to the valence band spectra, the edge of maximum energy for nanoporous zinc oxide is 1.62 eV, and for covalent organic frameworks of the 1,3,5-triformyl phloroglucinol and 1,3,5-Tris-(4-aminophenyl)triazine (COF-TRIPTA) is 1.81 eV. These two materials have bandgaps of 2.91 and 2.0 eV, respectively. They are projected to have conduction bands of −1.29 and −0.19 eV. The new crystalline phase of nanoporous zinc oxide with nanoscale pores, a low optical band gap, and a high specific surface area has been found to have high efficiency in heterojunction photoanodes with covalent organic frameworks in photoelectrochemical oxygen evolution reactions. These properties could lead to the development of novel devices for various applications.

Titanium

Titanium is an appealing contender due to its low toxicity, redox activity, natural abundance, and suitability for imbuing photoactivity into porous materials. Due to practical concerns like light-assisted hydrogen generation, self-cleaning of surfaces, environmental purification, wastewater treatment, and air and water remediation, titania has been intensively explored. Titanium incorporation in porous materials was confined to silicate substitution in zeolites or manufacturing titanium phosphates, diphosphonates, or dialcoholates with limited porosity [179,180]. Nanoporous titanium refers to titanium materials with many pores, such as titanium foam and cellular titanium. Dense titanium materials exhibit excellent properties such as high specific strength, stiffness, superior corrosion resistance, and biocompatibility, which can be compared to nanoporous titanium. Developing new and more effective titania photoactive layers is crucial for enhancing the conversion efficiency of photoelectrochemical water splitting. The titania-based photoelectrochemical signal is significantly attenuated by quick electron-hole recombination in titania, limiting its use. Composite materials consisting of conducting carbon materials, noble metal surface loading, and multicomponent heterojunctions have been found to enhance cationic form hydrogen/electron charge separation and photoactivity compared to titanium [181,182]. Using a narrow band gap semiconductor alone or combined with varied morphologies of titania can result in an adjustable absorption band edge, single-photon-generated multiple electrons, long-lasting electron-hole pairs, and overall good photoelectrode performance [183]. Wang et al. [184] investigated the photoelectrochemical properties of nanostructural silica-coated titanium carbide integrated on conductive titanium silicon carbide, and the morphologies of anodized titanium and anodized titanium silicon carbide (ATSC) oxidized for 12 h at 30 V in a fluoride ion based electrolyte is shown in Fig. 20 (a, b, c). After annealing, anodized titanium silicon carbide effectively produces silica-coated titanium carbide with a uniform scattered nanoporous structure. On the titanium basal plane, scanning electron microscope images of anodized titanium indicate a highly organized vertically oriented nanotubular structure, implying controlled production of an oxide layer with a typical thickness of 5.17 μm (Fig. 20 (a)) and an inner (outer) diameter of 48.40 nm (128.17 nm), as shown in Fig. 20 (b). Under the scanning electron microscope, the layered ATSC with a porous morphology that expands in the direction of the electric field and the rough and organized independent nanopore structure is apparent (Fig. 20 (c)). The ATSC electrode's close interfacial contacts facilitate electron migration, considerably improving high-area capacitance and excellent cycle stability. Feng et al. [185] used a new liquid plasma hydrogenation approach to synthesize hydrogenated amorphous titanium oxide (HA-TiO_{2-x}) and established its strong visible-light photoactivity. Fig. 20 (d) shows a schematic representation of HA-TiO_{2-x} photodegradation. The quantity of oxygen vacancy in the solution affects photocatalytic efficiency significantly. The greater the oxygen vacancy concentration, the lower the bandgap received by the HA-TiO_{2-x} and the better the photocatalytic efficiency. Excellent photodegradation and stability in visible light. In theophylline, methyl blue, and rhodamine B dyes, HA-TiO_{2-x} showed improved visible-light photodegradation. Furthermore, surface oxygen vacancy in HA-TiO_{2-x} was quite stable and could be stored in an ambient environment for up to a year.

Peng et al. [186] employed a simple hydrothermal process to manufacture nanoporous titanium-doped hematite thin films, then improved hematite's photoelectrochemical water oxidation performance using strong plasma ion implantation and a post-annealing method. A graphical depiction of the findings is shown in Fig. 20 (e). After the post-annealing process, the titanium plasma-implanted akaganeite film was changed to titanium ion-implanted hematite with lowered charge transfer resistance and enhanced charge carrier density. Well-distributed titanium doping improves photoelectrochemical water oxidation performance by increasing charge carrier transport while minimizing photogenerated charge carrier recombination. Therefore, titanium-implanted hematite nanoporous material exhibits higher photoelectrochemical water oxidation capability than bare hematite. Highly ordered titania nanopore/nanotube arrays fabricated through anodization, rather than a random network of nanocrystalline particles, are particularly attractive for photoelectrochemical cells because they provide a clear one-dimensional electrical pathway and a large internal surface area. For conventional planar photoelectrochemical cells, the use of titania nanopore/nanotube arrays is suggested to enhance charge collection efficiency.

Bismuth vanadate

Despite the promising examples above, more work must be done to improve photoelectrochemical sensing performance by inventing new and more efficient optoelectronic materials and improving electron transmission between the aptamer and the photoelectrode. Because of its great optical stability, low cost, and environmentally friendly properties, bismuth

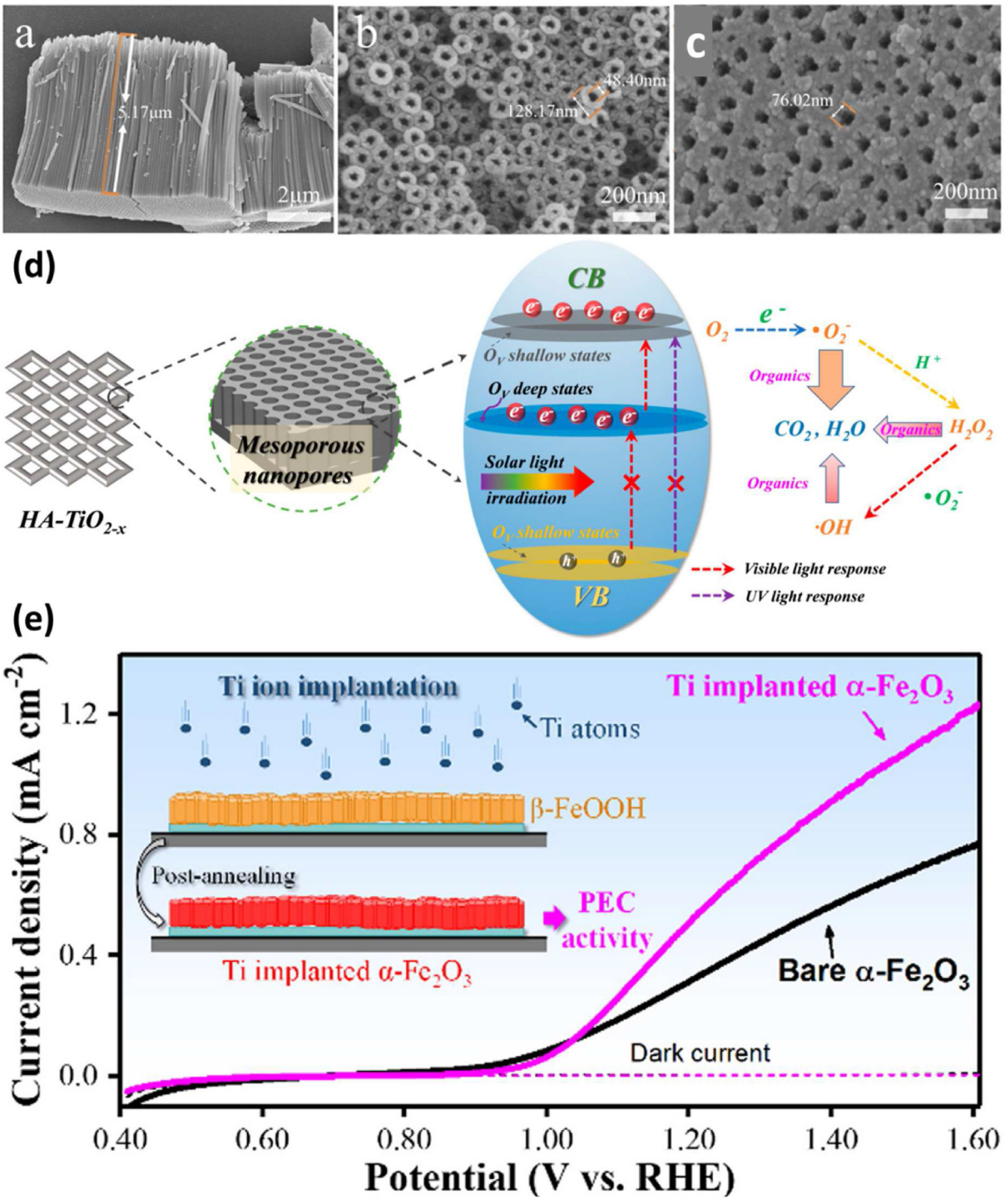

Fig. 20 – (a) Scanning electron microscope (SEM) cross-section images and (b) top sight of anodized titanium (AT), and (c) scanning electron microscope top visions of anodized titanium silicon carbide (Ti_3SiC_2) (ATSC), reprinted with permission from Ref. [184]; (d) Proposed graphic illustration of visible–light photoactivity for hydrogenated amorphous titanium oxide (HA-TiO_{2-x}) (no permission is required) [185]; (e) using energetic titanium plasma ion implantation method to modify hematite (α-Fe_2O_3) [186]. (β-FeOOH: titanium plasma implanted akaganeite; O_V: oxygen vacancy; RHE: reversible hydrogen electrode; PEC: photoelectrochemical; CB: conduction band; VB: valence band; e^- = electron; H^+ = hydrogen ion). (For interpretation of the references to color in this figure legend, the reader is referred to the Web version of this article.)

vanadate has been investigated as a visible-light-driven photoelectrode option for photocatalytic and photoelectrochemical applications [187]. Bismuth vanadate, a visible-light photocatalyst with a bandgap of roughly 2.4 eV, has also been identified as a potential visible-light-driven photocatalyst for degrading colorants [188,189]. However, because of the material's weak electron-hole separation yield ($\varphi_{separation}$), the solar-to-hydrogen conversion efficiency obtained with bismuth vanadate has been much below predicted [187]. The photocatalytic properties are influenced by the materials' morphology, particle size, and crystal structure [190]. The band gap (~2.5 eV), which restricts photon absorption, is one of bismuth vanadate's significant restrictions for further enhancing solar energy conversion efficiency [191]. Many endeavors have been made to increase the photoelectrochemical performance of bismuth vanadate photoelectrodes, such as noble metal modification [192], formation of heterojunction [193], and doping [194]. Given many photons in the solar spectrum's 2.0–2.5 eV area, even a 0.1–0.3 eV drop in bandgap can result in a considerable gain in efficiency [195]. For example, it has been observed that coating with titania can provide a tunneling barrier for photogenerated holes, so consistently preventing pinholes in films and suppressing active corrosion over macroscopic regions, effectively overcoming bismuth vanadate's fundamental flaw [196–198]. For example, Rassoolkhani et al. [199] described the creation of earth-abundant, nanostructured bismuth vanadate/tungsten trioxide photoanode assemblies that create chlorine while creating hydrogen at the dark cathode in an acidic sodium chloride solution. Fig. 23 (a) shows the bare bismuth vanadate electrode in top sight and cross-sectional scanning electron microscope images. Scanning electron microscope scans revealed a nanoporous architecture for bismuth vanadate with about 90 nm in diameter linked particles. Using a peroxytungstic acid solution, the tungsten trioxide layer (~20 nm thick) was electrodeposited on bismuth vanadate (Fig. 21 (b)). To avoid photooxidative corrosion of bismuth vanadate, the tungsten trioxide deposition was carried out in the dark at pH of 2 under cathodic conditions. High-resolution transmission electron micrograph was used further to analyze the nanostructured bismuth vanadate/tungsten trioxide films, as illustrated in Fig. 21 (c, d). High-resolution transmission electron micrograph pictures and fast Fourier transform patterns (Fig. 21 (c, d), inset) of bare bismuth vanadate particles and bismuth vanadate coated with tungsten trioxide are shown in those two figures. The photoelectrooxidation of chloride ions using a bismuth vanadate/tungsten trioxide photoanode assembly may be conceptualized using the following diagram (Fig. 21 e, f). Photogenerated holes in bismuth vanadate are transported away to the surface by amorphous tungsten trioxide sheets, where chloride ions are oxidized to chlorine (Fig. 21 f). The electrons from the oxidation stage are delivered to a dark platinum cathode for hydrogen generation through an external connection. The multi-shell hollow spheres of the heterostructured bismuth vanadium oxide were built up using a modified carbonaceous sphere sacrificial template growing approach described by Zong et al. [200]; related morphologies are shown in Fig. 21 (a and b). A randomly chosen sphere's transmission electron microscopy picture shows that multi-shell hollow spheres comprise linked grains, confirmed by the magnified view of double-shell structured hollow spheres (Fig. 21 (b)). Figure 22 illustrates distinct lattice fringes observed in the high-resolution transmission electron micrograph (HRTEM) image of the double-shell hollow spheres. These lattice fringes can be attributed to the crystallographic planes of the monoclinic bismuth vanadate (121), orthorhombic $Bi_4V_2O_{11}$ (040), and monoclinic bismuth vanadate (113) particles, respectively.

The proposed mechanism of photocatalytic reactions on heterostructured bismuth vanadium oxide multi-shell hollow spheres is illustrated in Fig. 21 (c). The higher concentration of aurivillius structural type of bismuth vanadium oxide ($Bi_4V_2O_{11}$) and the creation of heterostructured structures between bismuth vanadate and $Bi_4V_2O_{11}$, which result in an effective separation of photogenerated electrons and holes, are thought to be responsible for the substantial performance improvement of bismuth vanadium oxide double-shell hollow spheres. The increased photocatalytic capability might be due to the efficient use of visible light caused by repeated reflections of their multi-shell open structures. Orimolade et al. [201] examined the use of bismuth vanadate in photoelectrocatalytic water treatment applications, and Fig. 21 (d) shows a schematic model for photoelectrocatalytic organic degradation utilizing a bismuth vanadate anode. Several forms of heterostructures based on bismuth vanadate have been studied to enhance hydroxyl radical generation, including n-type and p-type, n-type and n-type, or p-type and p-type semiconductors. However, heterostructures of n-type and p-type semiconductors have shown superior results. This is because pairing n-type bismuth vanadate with a p-type semiconductor typically leads to a type II heterojunction, which promotes efficient charge separation and makes more holes available, facilitating hydroxyl radical generation. The bismuth vanadate-based photoanode in actual wastewater samples allows additional exploration to assess the semiconductor's durability. Furthermore, since bismuth vanadate has a high absorption of visible light, it would be exciting and advantageous if future research focused on employing direct sunlight as a source of irradiation rather than commercially simulated solar light. Most investigations on the use of bismuth vanadate for photoelectrocatalytic degradation of organics have shown that little is known about how the manufacture and structural characteristics of bismuth vanadate impact the effectiveness of the process. As a result, future research should pay close attention to how these parameters impact photoanode effectiveness.

Cadmium sulfide

Cadmium sulfide is one of the most popular photoactive semiconductor materials. Light-emitting diodes, field-effect transistors, photo and gas sensors, optical waveguides, transducers, laser devices, and photo-conducting cells are a few specialized sectors and applications where cadmium sulfide nanocomposite is used. Cadmium sulfide is a semiconductor with a band gap of 2.42 eV and a maximum absorption peak of 514 nm, indicating that it can absorb visible and ultraviolet light with less than 514 nm. As a result, cadmium sulfide is an effective photocatalyst. Due to its small energy gap, cadmium sulfide is the most often used in solar

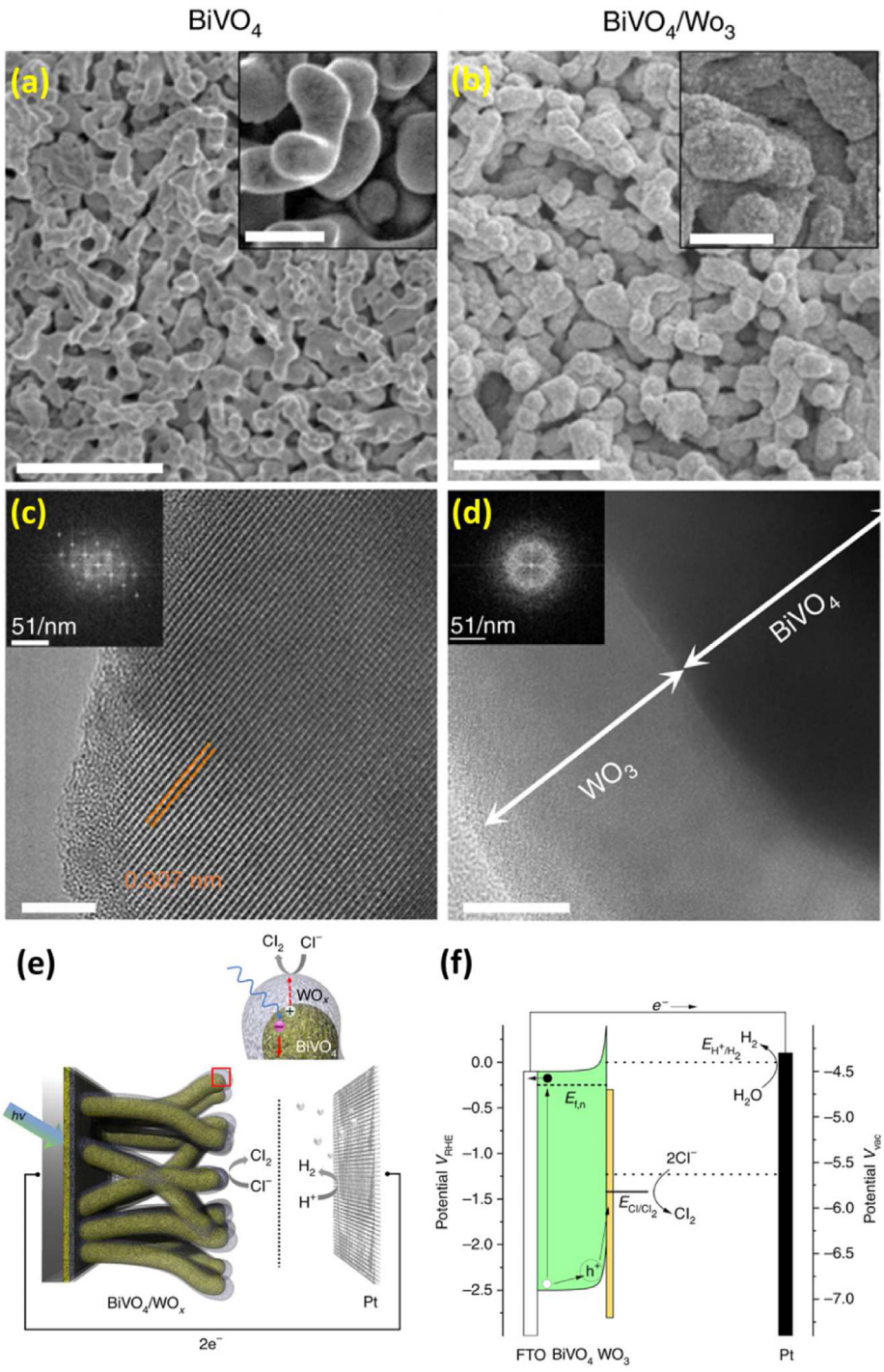

Fig. 21 – Scanning electron microscope photo of (a) bare bismuth vanadate ($BiVO_4$) and (b) bismuth vanadate electrode coated with 20 nm thick tungsten trioxide (WO_3) (scale bar - 1 μm) with inset displaying high magnification scanning electron microscope pictures (scale bar - 200 nm), high-resolution transmission electron micrograph pictures of (c) bare bismuth vanadate (scale bar – 5 nm) and (d) bismuth vanadate/tungsten trioxide (scale bar - 10 nm) with inset presentation fast Fourier transform (FFT) design, (e) Schematic illustration the general reaction system and (f) charge transfer process at the photoanode (no permission is required) [199].

photocatalysis. However, it shows a significant degree of photo-corrosion, releasing vast quantities of the poisonous cationic form of cadmium. Nonetheless, unless paired with another, more stable catalyst, it is seldom employed in photocatalysis [202] or as a suitable method to synthesize nanoporous cadmium sulfide. Hu et al. [203] employed an economical and straightforward flame approach to creating a porous carbon black film, which was then used as a template to produce three-dimensional nanoporous tin oxide using the atomic layer deposition method, followed by cadmium sulfide

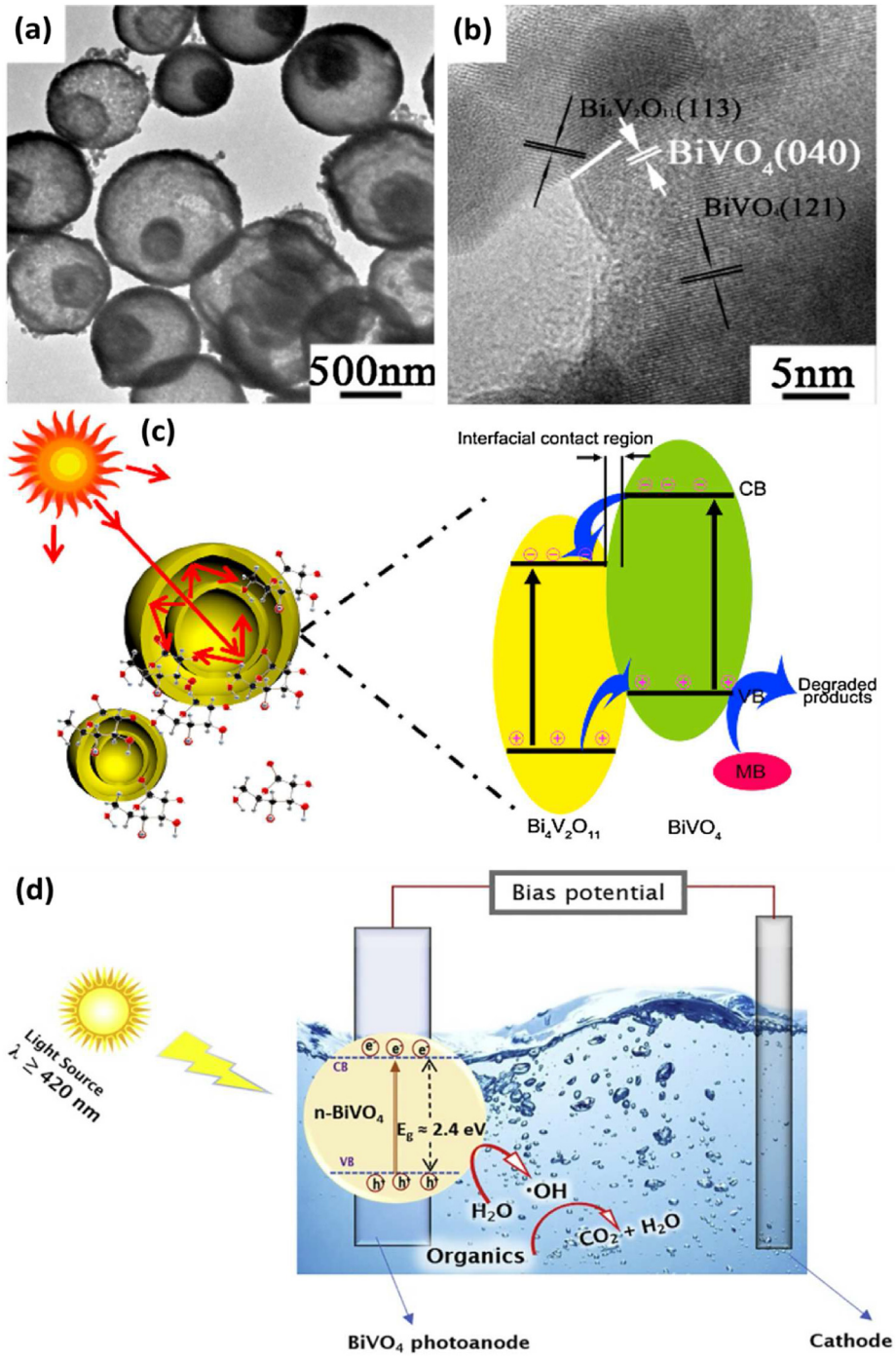

Fig. 22 – (a) Transmission electron microscopy (TEM) illustration of bismuth vanadium oxide (Bi–V–O) dual-shell hollow spheres, (b) high-resolution transmission electron micrograph illustration of a single Bi–V–O double-shell hollow spheres, (c) basic diagram figure of the heterostructured Bi–V–O multi-shell hollow spheres and the photocatalytic mechanism, reprinted with permission from Ref. [200]; (d) illustration image for photoelectrocatalytic degradation of organic employing bismuth vanadate ($BiVO_4$) photoanode, reprinted with permission from Ref. [201].

thin film coating and the schematic diagram of the synthesis process is shown in Fig. 23. The optimized nanoporous tin oxide (conduction band: 105)/cadmium sulfide electrode has a photocurrent density 9.7 times greater than the planar tin oxide/cadmium sulfide electrode. Under comparable testing settings, the photocurrent stability was also enhanced by 2.2 times. According to the findings, a three-dimensional nanoporous tin oxide/cadmium sulfide heterojunction constructed using a black carbon template is a promising option for high catalytic photoelectrochemical water splitting.

Shaban and co-authors [204] used two-step anodization followed by a sol-gel spin coating process to create a cadmium sulfide/anodic alumina nanoporous bi-layer film. The suggested technique offers advantages such as low-cost handling,

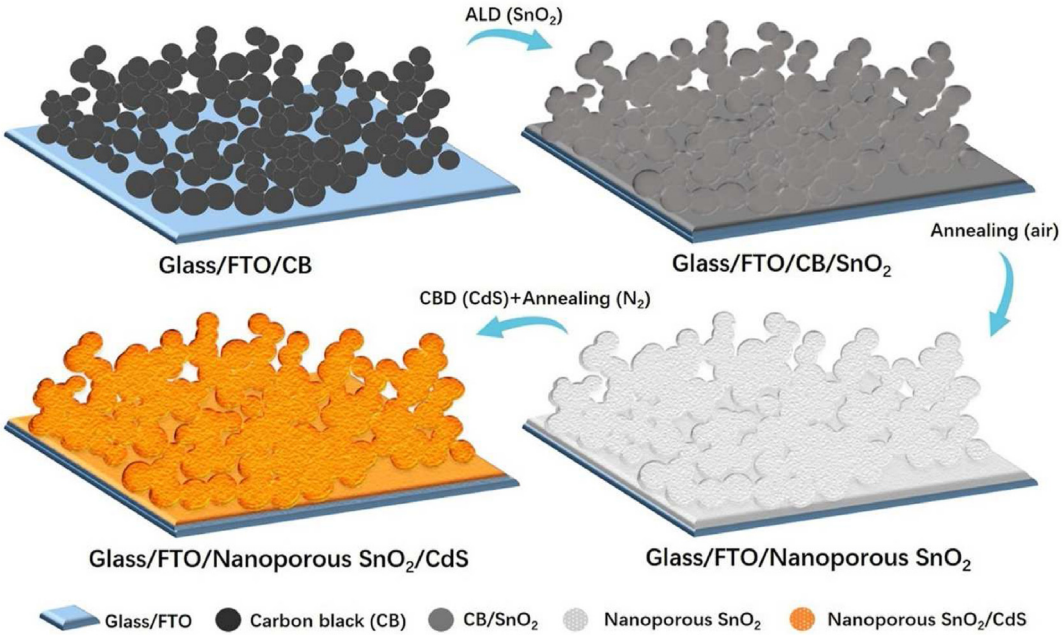

Fig. 23 – Graphic design of the three-dimensional nanoporous tin oxide over cadmium sulfide (3D NP SnO_2/CdS) heterostructure, reprinted with permission from Ref. [203]. (ALD: atomic layer deposition; Cd^{2+}: a cationic form of cadmium; FTO: Fluorine-doped tin oxide; SnO_2: tin oxide; CB: carbon black; CBD: chemical bath deposition).

straightforward technology, and reasonably basic equipment with excellent controllability. These elements facilitate the use of the produced films in sensing device applications. Kandy and Gaikar [205] studied the anodization of aluminum foil at room temperature for sufficient time to fabricate self-standing porous anodic alumina as the support for the graphene as cadmium sulfide photo-catalyst for continuous photocatalytic reduction of carbon dioxide. Porous anodic alumina is made by anodizing aluminum for a brief period at room temperature, which results in the manufacture of porous anodic alumina on two sides of a very thin layer of aluminum in the center. The novel one-dimensional nanostructure on graphene looks to be a superior light-collecting structure with less electron-hole recombination in porous anodic alumina. Using the compound parabola as a sunlight reflector, superior photo-catalytic carbon dioxide reduction was reported. Shen et al. [206] developed nanoporous cadmium sulfide hollow microrods for photocatalytic hydrogen generation. Introducing unique nanoporous hollow structures resulting from the effective kinetic separation of photo-generated carriers significantly increased photoconversion efficiency. The simple synthesis approach may be used to create various sulfides and core-shell nanostructures, possibly further improving photoconversion efficiency. Controlled creation of semiconductor nanorod antennas using *E. coli* pili as templates in the energy collection process provides another path to enhance efficiency [206]. The usage of chalcogenide hollow nanostructures with varying stoichiometry might improve photoconversion efficiency even further.

Zeolites

Zeolites are aluminosilicate oxides in nanoporous crystal form that are frequently employed in catalysis and adsorption [207], and there are about 40 known natural zeolites and over 150 zeolites synthesized [208]. The use of zeolitic materials for environmental protection is encouraged by their excellent physicochemical properties, such as cheap cost, availability, non-toxic nature, and selective sorption. Clinoptilolite, mordenite, and chabazite, the most common natural zeolites, have been very interesting recently. Zeolites are especially beneficial for photoelectrochemical water splitting because they contain various compounds in their cavities and channels, including organics. Such inclusions have been proven to alter a species' usual solution photochemistry. Because of their capabilities to deliver cation exchange, zeolites are effective as industrial water softeners in eliminating hazardous cationic form cesium and cationic form of strontium cations from liquid nuclear waste and removing toxic heavy metal cations from underground water and run-off waters. Surfactant-modified zeolites are particularly useful for simultaneously removing harmful anions and organic contaminants. The first discovery of an intermittent chalcogenide-based zeolite-analog semiconductor with a wholly unique boracite-related framework and specific sites at the interrupted region was reported by Lin et al. [209]. An interrupted chalcogenide-based zeolite-analog semiconductor with a novel boracite-related framework and particular locations at the interrupted area has been reported. The specific indium sites that function as effective electrocatalytic active centers for the oxygen removal process are doped with trivalent bismuth ions. In comparison to the marketed indium selenide and bismuth-doped chalcogenide-based semiconductor zeolites (CSZ-5-InBiSe), chalcogenide-based semiconductor zeolites doped with indium and selenium (CSZ-5-InSe) exhibit superior electrocatalytic activity for the oxygen reduction reaction. Atomically precise doping with

intentionally disrupted sites in zeolitic semiconductor materials can offer a new approach to fine-tune semiconductor materials' electronic structure and photoelectrical properties. The ability to make highly structured quantum dot materials opens up a new universe of possibilities for assembling highly organized macroscopic structures. In photocatalytic water oxidation on cationic silver over silver chloride photoanodes, zeolite is not essential when using visible light. However, it can significantly increase the active surface area [210].

Using zeolites as host materials have also shown a method for modulating the photophysics of adsorbed guest species. As a result, the photoelectrochemistry community will continue to gain significantly from interacting with zeolites. Despite its growing popularity, transient spectroscopy using a diffuse reflectance detection approach still has experimental constraints and technological challenges to address to provide experimental data with the same level of dependability as transmittance mode spectroscopy. Furthermore, it is critical to establish theoretical treatments that characterize the complicated kinetic behavior of excited species inside zeolites using a more superficial image. Given the efforts being made from both an experimental and theoretical viewpoint, we should expect further progress in this area in the following years.

Agro-waste-photocatalytic composites

Recently, the use of agro-industrial wastes as support for photocatalytic nanoparticles has been extensively reported to reduce the cost of photoactive materials and improve their performance. In general, the conversion of wastes into high values products, e.g., activated carbon, biochar [211,212]of gas/liquid products [213], is considered a sustainable approach that fits the circular economy. This approach encourages the reduction of agro-industrial wastes in the environment and a significant enhancement in the photocatalytic and adsorptive efficiencies of photocatalysts reported compared to naked photocatalytic materials. In fact, the fixation of nano-sized photocatalytic materials on lignocellulosic biomass fibers leads to generate so-called Adsorb & Shuttle process-based materials wherein the sorbing area works continuously to concentrate the chemical species nearby the photoactive area. As a result, both the photocatalytic kinetics and the ultimate performance are highly boosted. More discussion regarding the Adsorb & Shuttle process is reported elsewhere [214–216]. It is essential to mention that photocatalysis as a single process suffers from very low kinetics, which limits its competition with co-existing technologies, as critically discussed by Djellabi et al. [217]. On top of that, the hybridization of photocatalytic nanoparticles with biomass waste boosts the visible light response of the whole composite. Also, it improves the transfer of charges, reducing the recombination of charges. Djellabi et al. [218] studied the hybridization of TiO_2 nanoparticles with lignocellulosic biomass wastes. They found that an interface bridge between biomass and TiO2 created a so-called Ti–O–C bridge, as shown in Fig. 24 (a). Photoelectrochemical studies showed that the hybridization of biomass waste with TiO_2 led to excellent photocurrent activity under visible light as compared to bare TiO_2 (Fig. 24 (b)) [219]. Despite numerous studies investigating the use of agro-industrial waste in combination with photocatalytic materials, further research is needed to examine the hydrogen generation potential via photoelectrochemical processes. Carbon materials derived from various agro-wastes can act as a photosensitizer for photocatalytic materials, offering a more comprehensive approach for implementing this technology under natural solar light. Different mechanistic pathways of carbon materials for enhanced photoelectrochemical H_2 production were discussed previously [220]. Therefore, agroindustrial waste has the potential to be a highly advantageous natural support due to its affordability, ecological friendliness, and ability to form more photostable semiconducting nanostructures. By manipulating the origin of the waste, one can obtain waste with diverse morphologies and sizes, which can be integrated with other semiconducting materials to fabricate composites to develop novel photocatalysts and treat actual industrial samples.

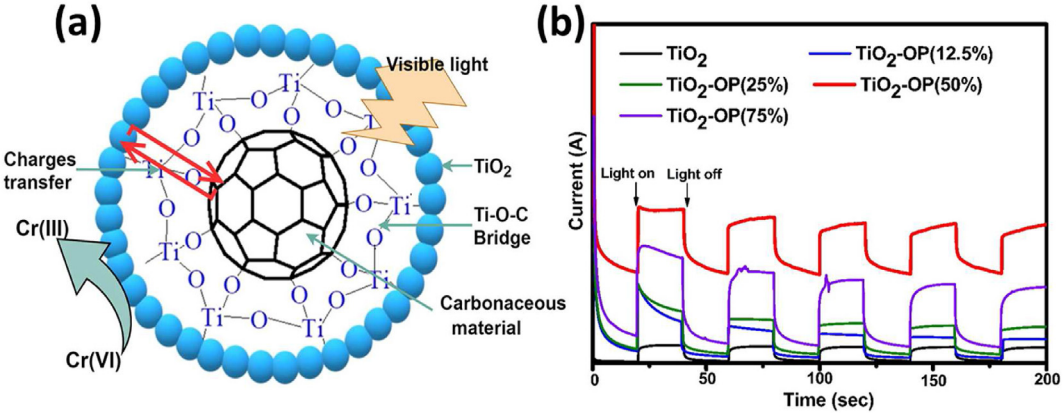

Fig. 24 – (a) Formation of Ti–O–C bridge between TiO_2 and biomass waste, reproduced with permission from Ref. [218], (b) Photocurrent of TiO_2@Biomass compared to bare TiO_2 under visible light, OP: olive biomass waste. The OP ratio increase further boosts the photocurrent activity due to the enhanced e^-/h^+ separation, reproduced with permission from Ref. [219].

Challenges and future prospects

One of the most significant bibliometric restrictions is that the Web of Science only contains articles (along with a few chapters and conference proceedings cited online), leaving out monographs and edited volumes. The analysis is somewhat skewed as a result of this. However, if you use CitNetExplorer's 'include non-matching references' option, the network will still contain large books (or chapters) mentioned in Web of Science articles but aren't in the database (and thus not displaying cross-references). A second drawback is that new articles are often absent from the graphs due to their low citation scores.

Although recent advances have been made, it is still difficult to establish a practical, unassisted photoelectrochemical water-splitting system. This technology for producing hydrogen using semiconductor photoelectrodes is still in its infancy and requires significant advances in materials, material systems, and reactor development. Dual tandem photoelectric systems are suitable for this application to achieve zero bias and decouple photoelectrochemical hydrogen production from conventional resources. It is anticipated that photoanodes and photocathodes tailored for absorption of the visible light spectrum will be used. In addition to having high band gaps, low absorption coefficients, poor electrical conductivity, short charge carrier lifetimes, and long diffusion lengths, metal oxides have limited performance due to their nanostructure. By fabricating nanostructures such as nanowires, nanotubes, and nanopores, nanostructuring can address this problem by lowering the carrier diffusion distance towards the electrolyte solution. To build a successful solar water splitting system for more sustainable solar energy utilization, a solid understanding of unassisted photoelectrochemical water splitting mechanisms and methods to optimize charge transfer and separation for redox reactions.

Using a nanoporous photoanode in actual wastewater samples should be investigated further to determine the semiconductor's durability. Furthermore, since nanoporous materials absorb the most visible light, it would be more meaningful and beneficial if future research concentrated on using direct sunlight instead of commercially available simulated solar light. Most investigations on the use of nanoporous materials for photoelectrocatalytic degradation of organics have shown that little is known about how the technique of manufacture and structural characteristic of those materials impact the process' effectiveness. As a result, future research should focus on how these variables influence photoanode performance.

Conclusions

This review presents an overview of photoelectrochemical systems for nanoporous material-based solar water splitting, drawing on bibliometric analysis and literature review. According to the bibliometric analysis, research on photoelectrochemical and hydrogen is most prevalent in China, the US, Canada, the UK, Germany, South Korea, and Australia. China is a crucial node connecting the US, Canada, the UK, Australia, Sweden, Taiwan, and India. The co-occurrence network plot indicated certain keywords, such as cadmium sulfide, photosensitization, layers, photocatalyst, anodic growth, hematite, graphene oxide, nanoporous titania, and tungsten trioxide, were infrequently used, indicating a research gap in those areas. This work also aims to provide knowledge for developing effective and sustainable photoelectrochemical water-splitting methods based on aided nanoporous materials. Solar water splitting is a promising avenue for sustainable, clean fuel due to its high efficiency in converting solar energy into a virulent chemical form. Still, long-term stability remains a significant challenge due to catalyst and electrolyte degradation. We explore how photoelectrochemical device design and operation can affect degradation processes and emphasize the importance of material design and configuration integration for effective photoelectrochemical strategies. Despite recent advancements in transition-metal-based electrocatalysts for hydrogen and oxygen evolution reactions, their impact on diverse photoelectrodes for photoelectrochemical performance remains limited. The use of nanoporous materials holds promise for enhancing the performance of photoelectrochemical water-splitting systems, with the potential for cheap and high-activity energy devices. Innovative techniques for building heterostructures of nanomaterials show particular potential for increasing photocatalytic efficiency. While current nanotechnological techniques have improved our understanding of photocatalytic mechanisms, developing new heterostructure photocatalysts, particularly those utilizing two-dimensional nanostructures, remains an important area for future research.

Declaration of competing interests

The authors declare that they have no known competing financial interests or personal relationships that could have appeared to influence the work reported in this paper.

Acknowledgments

The principal author, Walid Nabgan, is thankful for the support from Universitat Rovira i Virgili under the Maria Zambrano Programme (Reference number: 2021URV-MZ-10), Proyectos de Generación de Conocimiento AEI/MCIN (PID2021-123665OB-I00), and the project reference number of TED2021-129343B-I00. The authors would like to express their gratitude for the financial support provided by Grant PID2021-123665OB-I00 and TED2021-129343B-I00, which were funded by MCIN/AEI/10.13039/501100011033. Additionally, where applicable, support was received from "ERDF A way of making Europe," the "European Union," or the "European Union NextGenerationEU/PRTR."

REFERENCES

[1] Hou J, Wei B, Du Q, Wang J, Wang Q, Zhang G. Production prediction of cyclic multi-thermal fluid stimulation in a horizontal well. J Petrol Sci Eng 2016;146:949–58.

[2] Kumar A, Kumar K, Kaushik N, Sharma S, Mishra S. Renewable energy in India: current status and future potentials. Renew Sustain Energy Rev 2010;14:2434–42.
[3] Tahir F, Saeed MA, Ali U. Biomass energy perspective in Pakistan based on chemical looping gasification for hydrogen production and power generation. Int J Hydrogen Energy 5 June 2023;48(48):18211–32.
[4] Rahman A, Farrok O, Haque MM. Environmental impact of renewable energy source based electrical power plants: solar, wind, hydroelectric, biomass, geothermal, tidal, ocean, and osmotic. Renew Sustain Energy Rev 2022;161:112279.
[5] Contreras-Lisperguer R, de Cuba K. The potential impact of climate change on the energy sector in the Caribbean region. Washington DC: Organization of American States; 2008.
[6] Agrawala S, Raksakulthai V, van Aalst M, Larsen P, Smith J, Reynolds J. Development and climate change in Nepal: focus on water resources and hydropower. Citeseer; 2003.
[7] Hunt JD, Stilpen D, de Freitas MAV. A review of the causes, impacts and solutions for electricity supply crises in Brazil. Renew Sustain Energy Rev 2018;88:208–22.
[8] Nieto M. Whatever it takes to reach net zero emissions around 2050 and limit global warming to 1.5 c: the cases of United States, China, European Union and Japan. BAFFI CAREFIN Centre Research Paper; 2022.
[9] Macedo MS, Soria MA, Madeira LM. Process intensification for hydrogen production through glycerol steam reforming. Renew Sustain Energy Rev 2021;146:111151.
[10] Gong Y, Yao J, Wang P, Li Z, Zhou H, Xu C. Perspective of hydrogen energy and recent progress in electrocatalytic water splitting. Chin J Chem Eng 2022;43:282–96.
[11] Tang D, Tan G-L, Li G-W, Liang J-G, Ahmad SM, Bahadur A, et al. State-of-the-art hydrogen generation techniques and storage methods: a critical review. J Energy Storage 2023;64:107196.
[12] Megía PJ, Vizcaíno AJ, Calles JA, Carrero A. Hydrogen production technologies: from fossil fuels toward renewable sources. A mini review. Energy Fuel 2021;35:16403–15.
[13] Bethoux O. Hydrogen fuel cell road vehicles and their infrastructure: an option towards an environmentally friendly energy transition. Energies 2020;13:6132.
[14] Kumar S, Arzaghi E, Baalisampang T, Garaniya V, Abbassi R. Insights into decision-making for offshore green hydrogen infrastructure developments. Process Saf Environ Protect 2023;174:805–17.
[15] Dash SK, Chakraborty S, Elangovan D. A brief review of hydrogen production methods and their challenges. Energies; 2023.
[16] Pei H, Zhang L, Zhi G, Kong D, Wang Y, Huang S, et al. Rational construction of hierarchical porous FeP nanorod arrays encapsulated in polypyrrole for efficient and durable hydrogen evolution reaction. Chem Eng J 2022;433:133643.
[17] Alraeesi A, Gardner T. Assessment of sieverts law assumptions and 'n' values in palladium membranes: experimental and theoretical analyses. Membranes 2021;11:778.
[18] Mishra P, Krishnan S, Rana S, Singh L, Sakinah M, Ab Wahid Z. Outlook of fermentative hydrogen production techniques: an overview of dark, photo and integrated dark-photo fermentative approach to biomass. Energy Strategy Rev 2019;24:27–37.
[19] Armaroli N, Balzani V. The hydrogen issue. ChemSusChem 2011;4:21–36.
[20] Iea I. The future of hydrogen. June. The Future of Hydrogen; 2019.
[21] Hoffert MI, Caldeira K, Jain AK, Haites EF, Harvey LDD, Potter SD, et al. Energy implications of future stabilization of atmospheric CO2 content. Nature 1998;395:881–4.
[22] Heidrich ES, Curtis TP, Dolfing J. Determination of the internal chemical energy of wastewater. Environ Sci Technol 2011;45:827–32.
[23] Mahmoud M. Electricity-driven microbial factory for value-added resources recovery from waste streams. In: Kumar P, Kuppam C, editors. Bioelectrochemical systems: vol1 principles and processes. Singapore: Springer Singapore; 2020. p. 119–38.
[24] Wang C, Lan F, He Z, Xie X, Zhao Y, Hou H, et al. Iridium-based catalysts for solid polymer electrolyte electrocatalytic water splitting. ChemSusChem 2019;12:1576–90.
[25] Ng B-J, Putri LK, Kong XY, Teh YW, Pasbakhsh P, Chai S-P. Z-scheme photocatalytic systems for solar water splitting. Adv Sci 2020;7:1903171.
[26] Li J, Li H, Zhan G, Zhang L. Solar water splitting and nitrogen fixation with layered bismuth oxyhalides. Acc Chem Res 2017;50:112–21.
[27] Grätzel M. Photoelectrochemical cells. Nature 2001;414:338–44.
[28] Hisatomi T, Kubota J, Domen K. Recent advances in semiconductors for photocatalytic and photoelectrochemical water splitting. Chem Soc Rev 2014;43:7520–35.
[29] Ager JW, Shaner MR, Walczak KA, Sharp ID, Ardo S. Experimental demonstrations of spontaneous, solar-driven photoelectrochemical water splitting. Energy Environ Sci 2015;8:2811–24.
[30] Callejas JF, Read CG, Roske CW, Lewis NS, Schaak RE. Synthesis, characterization, and properties of metal phosphide catalysts for the hydrogen-evolution reaction. Chem Mater 2016;28:6017–44.
[31] Horiuchi Y, Toyao T, Takeuchi M, Matsuoka M, Anpo M. Recent advances in visible-light-responsive photocatalysts for hydrogen production and solar energy conversion – from semiconducting TiO2 to MOF/PCP photocatalysts. Phys Chem Chem Phys 2013;15:13243–53.
[32] Huang Q, Ye Z, Xiao X. Recent progress in photocathodes for hydrogen evolution. J Mater Chem 2015;3:15824–37.
[33] Jiang C, Moniz SJA, Wang A, Zhang T, Tang J. Photoelectrochemical devices for solar water splitting – materials and challenges. Chem Soc Rev 2017;46:4645–60.
[34] Abdi FF, Berglund SP, van de Krol R. Multinary metal oxide photoelectrodes. In: Giménez S, Bisquert J, editors. Photoelectrochemical solar fuel production: from basic principles to advanced devices. Cham: Springer International Publishing; 2016. p. 355–91.
[35] Chandrasekaran S, Yao L, Deng L, Bowen C, Zhang Y, Chen S, et al. Recent advances in metal sulfides: from controlled fabrication to electrocatalytic, photocatalytic and photoelectrochemical water splitting and beyond. Chem Soc Rev 2019;48:4178–280.
[36] Zhang Y, Xiao J, Lv Q, Wang S. Self-supported transition metal phosphide based electrodes as high-efficient water splitting cathodes. Front Chem Sci Eng 2018;12:494–508.
[37] Li X, Zhang J, Huo Y, Dai K, Li S, Chen S. Two-dimensional sulfur- and chlorine-codoped g-C3N4/CdSe-amine heterostructures nanocomposite with effective interfacial charge transfer and mechanism insight. Appl Catal B Environ 2021;280:119452.
[38] Ansari SA, Cho MH. Growth of three-dimensional flower-like SnS2 on g-C3N4 sheets as an efficient visible-light photocatalyst, photoelectrode, and electrochemical supercapacitance material. Sustain Energy Fuels 2017;1:510–9.

[39] Li C, Sun T, Zhang D, Zhang X, Qian Y, Zhang Y, et al. Fabrication of ternary Ag/La-black TiO2−x photocatalyst with enhanced visible-light photocatalytic activity for tetracycline degradation. J Alloys Compd 2022;891:161960.
[40] Rabha S, Dobbidi P. Structural, electrical properties and stability in microwave dielectric properties of (1−x) MgTiO3-x SrTiO3 composite ceramics. J Alloys Compd 2021;872:159726.
[41] Liu X, Shen X, Sa B, Zhang Y, Li X, Xue H. Piezotronic-enhanced photocatalytic performance of heterostructured BaTiO3/SrTiO3 nanofibers. Nano Energy 2021;89:106391.
[42] Pham DP, Lee S, Le AHT, Cho E-C, Hyun Cho Y, Yi J. Monocrystalline silicon-based tandem configuration for solar-to-hydrogen conversion. Inorg Chem Commun 2020;116:107926.
[43] Li H, Xu W, Qu Y, Wang M, Liu G, Qiao G. Enhanced photoelectrochemical performance of In2O3 nanocubes with oxygen vacancies via hydrogenation. Inorg Chem Commun 2019;102:70–4.
[44] Zhou L, Wu Y, Wang L, Yang Y, Na Y. Excellent performance of water oxidation at low bias potential achieved by transparent WO3/BiVO4 photoanode integrated with molecular nickel porphyrin. Inorg Chem Commun 2019;107:107480.
[45] Jeon TH, Moon G-h, Park H, Choi W. Ultra-efficient and durable photoelectrochemical water oxidation using elaborately designed hematite nanorod arrays. Nano Energy 2017;39:211–8.
[46] Liu Z, Ma C, Cai Q, Hong T, Guo K, Yan L. Promising cobalt oxide and cobalt oxide/silver photocathodes for photoelectrochemical water splitting. Sol Energy Mater Sol Cell 2017;161:46–51.
[47] Guo X, Diao P, Xu D, Huang S, Yang Y, Jin T, et al. CuO/Pd composite photocathodes for photoelectrochemical hydrogen evolution reaction. Int J Hydrogen Energy 2014;39:7686–96.
[48] Wannapop S, Somdee A. Effect of citric acid on the synthesis of ZnWO4/ZnO nanorods for photoelectrochemical water splitting. Inorg Chem Commun 2020;115:107857.
[49] Desai MA, Vyas AN, Saratale GD, Sartale SD. Zinc oxide superstructures: recent synthesis approaches and application for hydrogen production via photoelectrochemical water splitting. Int J Hydrogen Energy 2019;44:2091–127.
[50] Salomão PEA, Gomes DS, Ferreira EJC, Moura F, Nascimento LL, Patrocínio AOT, et al. Photoelectrochemical hydrogen production from water splitting using heterostructured nanowire arrays of Bi2O3/BiAl oxides as a photocathode. Sol Energy Mater Sol Cell 2019;194:276–84.
[51] Yousefzadeh S, Faraji M, Moshfegh AZ. Constructing BiVO4/Graphene/TiO2 nanocomposite photoanode for photoelectrochemical conversion applications. J Electroanal Chem 2016;763:1–9.
[52] Luo Z, Wang T, Gong J. Single-crystal silicon-based electrodes for unbiased solar water splitting: current status and prospects. Chem Soc Rev 2019;48:2158–81.
[53] Salomão PEA, de Souza Barbosa LR, Andrade TS, Junio da Cruz Ferreira E, Pereira MC. ZnBi38O60/Bi2O3 photocathode for hydrogen production from water splitting. Int J Hydrogen Energy 2019;44:28603–12.
[54] Kaur G, Divya Satsangi VR, Dass S, Shrivastav R. 3D-nano-hetero-structured n/n junction, CuO/Ru−ZnO thin films, for hydrogen generation with enhanced photoelectrochemical performances. Int J Hydrogen Energy 2020;45:21051–67.
[55] Li M, Tian X, Zou X, Han X, Du C, Shan B. Promoting photoelectrochemical hydrogen evolution activity of CuBi2O4 photocathode through ramping rate control. Int J Hydrogen Energy 2020;45:15121–8.
[56] Patil RP, Mahadik MA, Chae W-S, Choi SH, Jang JS. Self-templated fabrication of 2-D dual nanoarchitecture Zn1-xCdxS porous nanosheet and ZnO nanorod for photoelectrochemical hydrogen production. Appl Surf Sci 2021;539:148267.
[57] Angelomé PC, Andrini L, Calvo ME, Requejo FG, Bilmes SA, Soler-Illia GJAA. Mesoporous anatase TiO2 films: use of Ti K XANES for the quantification of the nanocrystalline character and substrate effects in the photocatalysis behavior. J Phys Chem C 2007;111:10886–93.
[58] Yu H, Chen S, Quan X, Zhao H, Zhang Y. Silicon nanowire/TiO2 heterojunction arrays for effective photoelectrocatalysis under simulated solar light irradiation. Appl Catal B Environ 2009;90:242–8.
[59] Peng K, Wang X, Lee S-T. Silicon nanowire array photoelectrochemical solar cells. Appl Phys Lett 2008;92:163103.
[60] Sahai S, Ikram A, Rai S, Dass S, Shrivastav R, Satsangi VR. CdSe quantum dots sensitized nanoporous hematite for photoelectrochemical generation of hydrogen. Int J Hydrogen Energy 2014;39:11860–6.
[61] Chen H, Chen K-F, Lai S-W, Dang Z, Peng Y-P. Photoelectrochemical oxidation of azo dye and generation of hydrogen via CN co-doped TiO2 nanotube arrays. Sep Purif Technol 2015;146:143–53.
[62] Gan J, Lu X, Rajeeva BB, Menz R, Tong Y, Zheng Y. Efficient photoelectrochemical water oxidation over hydrogen-reduced nanoporous BiVO4 with Ni−Bi electrocatalyst. Chemelectrochem 2015;2:1385–95.
[63] Gu T-T, Wu X-M, Dong Y-M, Wang G-L. Novel photoelectrochemical hydrogen peroxide sensor based on hemin sensitized nanoporous NiO based photocathode. J Electroanal Chem 2015;759:27–31.
[64] Li Q, Zheng M, Zhang B, Zhu C, Wang F, Song J, et al. InP nanopore arrays for photoelectrochemical hydrogen generation. Nanotechnology 2016;27:075704.
[65] Anderson N, Neale N. Nanoporous black silicon as a platform for photoelectrochemical hydrogen production: exciting catalysts and nailing down the flatband potential. Abstr Pap Am Chem Soc 2016:251.
[66] Zhang Y, Wang D, Zhang X, Chen Y, Kong L, Chen P, et al. Enhanced photoelectrochemical performance of nanoporous BiVO4 photoanode by combining surface deposited cobalt-phosphate with hydrogenation treatment. Electrochim Acta 2016;195:51–8.
[67] Li Q, Zheng M, Ma L, Zhong M, Zhu C, Zhang B, et al. Unique three-dimensional InP nanopore arrays for improved photoelectrochemical hydrogen production. ACS Appl Mater Interfaces 2016;8:22493–500.
[68] Liu M, Yu Y-X, Zhang W-D. A non-enzymatic hydrogen peroxide photoelectrochemical sensor based on a BiVO4 electrode. Electroanalysis 2017;29:305–11.
[69] Sápi A, Varga A, Samu GF, Dobó D, Juhász KL, Takács B, et al. Photoelectrochemistry by design: tailoring the nanoscale structure of Pt/NiO composites leads to enhanced photoelectrochemical hydrogen evolution performance. J Phys Chem C 2017;121:12148–58.
[70] Almohammedi A, Shaban M, Mostafa H, Rabia M. Nanoporous TiN/TiO2/alumina membrane for photoelectrochemical hydrogen production from sewage water. Nanomaterials 2021:11.
[71] Griffiths S, Sovacool BK, Kim J, Bazilian M, Uratani JM. Industrial decarbonization via hydrogen: a critical and systematic review of developments, socio-technical

systems and policy options. Energy Res Social Sci 2021;80:102208.
[72] Sathish S, Aravind kumar J, Prabu D, Annam Renita A, Murugesan K, Rajasimman M, et al. Latest avenues on solar light-driven photocatalytic hydrogen generation using surface modified nanomaterials towards sustainable environment and circular bioeconomy. Fuel 2023;340:127398.
[73] Dincer I, Acar C. Smart energy solutions with hydrogen options. Int J Hydrogen Energy 2018;43:8579–99.
[74] Hu S, Xiang C, Haussener S, Berger AD, Lewis NS. An analysis of the optimal band gaps of light absorbers in integrated tandem photoelectrochemical water-splitting systems. Energy Environ Sci 2013;6:2984–93.
[75] Greenblatt JB, Miller DJ, Ager JW, Houle FA, Sharp ID. The technical and energetic challenges of separating (photo) electrochemical carbon dioxide reduction products. Joule 2018;2:381–420.
[76] Aydin MI, Karaca AE, Qureshy AMMI, Dincer I. A comparative review on clean hydrogen production from wastewaters. J Environ Manag 2021;279:111793.
[77] Pinaud BA, Benck JD, Seitz LC, Forman AJ, Chen Z, Deutsch TG, et al. Technical and economic feasibility of centralized facilities for solar hydrogen production via photocatalysis and photoelectrochemistry. Energy Environ Sci 2013;6:1983–2002.
[78] Fragiacomo P, Genovese M. Technical-economic analysis of a hydrogen production facility for power-to-gas and hydrogen mobility under different renewable sources in Southern Italy. Energy Convers Manag 2020;223:113332.
[79] Ahmed SF, Mofijur M, Nuzhat S, Rafa N, Musharrat A, Lam SS, et al. Sustainable hydrogen production: technological advancements and economic analysis. Int J Hydrogen Energy 2022;47:37227–55.
[80] Pritchard A. Statistical bibliography or bibliometrics. J Doc 1969;25:348.
[81] Calabuig-Moreno F, González-Serrano MH, Fombona J, García-Tascón M. The emergence of technology in physical education: a general bibliometric analysis with a focus on virtual and augmented reality. Sustainability 2020.
[82] Bartolacci F, Caputo A, Soverchia M. Sustainability and financial performance of small and medium sized enterprises: a bibliometric and systematic literature review. Bus Strat Environ 2020;29:1297–309.
[83] Vidal-Vilaplana A, Valantine I, Staskeviciute-Butiene I, González-Serrano MH, Capranica L, Calabuig F. Combining sport and academic career: exploring the current state of student-athletes' dual career research field. J Hospit Leisure Sports Tourism Educ 2022;31:100399.
[84] S. Adriaanse L, Rensleigh C. Web of science, Scopus and google scholar. Electron Libr 2013;31:727–44.
[85] ScientificPublications. Scopus or Web of Science: how to choose a journal for publication? Which one is better? Scientific Publications; 2022.
[86] Falagas ME, Pitsouni EI, Malietzis GA, Pappas G. Comparison of PubMed, Scopus, web of science, and Google scholar: strengths and weaknesses. Faseb J 2008;22:338–42.
[87] Salisbury L. Web of Science and Scopus: a comparative review of content and searching capabilities. Charlest Advis 2009;11:5–18.
[88] Levine Clark M, Gil E. A comparative analysis of social sciences citation tools. Online information review; 2009.
[89] Decker F, Cattarin S. PHOTOELECTROCHEMICAL CELLS | overview. In: Garche J, editor. Encyclopedia of electrochemical power sources. Amsterdam: Elsevier; 2009. p. 1–9.
[90] Schwarz-Schampera U, Herzig PM. Indium: geology, mineralogy, and economics. Springer Berlin Heidelberg; 2013.
[91] Schwarz-Schampera U, Herzig PM. Indium: geology, mineralogy, and economics. Springer Science & Business Media; 2002.
[92] Felix N. Indium and indium compounds. Ullmann's Encyclopedia of Industrial Chemistry; 2000.
[93] Alfantazi AM, Moskalyk RR. Processing of indium: a review. Miner Eng 2003;16:687–94.
[94] Chung Y-H, Lee C-W. Electrochemical behaviors of indium. J Electrochem Sci Technol 2012;3:1–13.
[95] Yi S-S, Wang Z-Y, Li H-M, Zafar Z, Zhang Z-T, Zhang L-Y, et al. Coupling effects of indium oxide layer on hematite enabling efficient photoelectrochemical water splitting. Appl Catal B Environ 2021;283:119649.
[96] Kim YB, Jung SH, Kim DS, Deshpande NG, Lee HS, Cho HK. Interleaved biphasic p–n blended copper indium selenide photoelectrode and its application in pulse-driven photoelectrochemical water splitting. Appl Catal B Environ 2021;285:119839.
[97] Kim JS, Baek SK, Kim YB, Do HW, Kwon YH, Cho SW, et al. Copper indium selenide water splitting photoanodes with artificially designed heterophasic blended structure and their high photoelectrochemical performances. Nano Energy 2018;46:1–10.
[98] Piercy R, Hampson NA. The indium electrode in perchlorate electrolytes: a rotating disc and impedance study. J Electroanal Chem Interfacial Electrochem 1974;57:297–308.
[99] Yang Y. Recent advances in the electrochemical oxidation water treatment: spotlight on byproduct control. Front Environ Sci Eng 2020;14:85.
[100] Martínez-Huitle CA, Rodrigo MA, Sirés I, Scialdone O. Single and coupled electrochemical processes and reactors for the abatement of organic water pollutants: a critical review. Chem Rev 2015;115:13362–407.
[101] Bonomo M, Dini D, Decker F. Electrochemical and photoelectrochemical properties of nickel oxide (NiO) with nanostructured morphology for photoconversion applications. Front Chem 2018;6.
[102] Yang Q, Lv C, Huang Z, Zhang C. Amorphous film of ternary NiCoP alloy on Ni foam for efficient hydrogen evolution by electroless deposition. Int J Hydrogen Energy 2018;43:7872–80.
[103] Wu Y, Zhang Z, Xu K, Lu J, Wang A, Dai X, et al. A study on the formation conditions of amorphous nickel-phosphorus (Ni-P) alloy by laser-assisted electrodeposition. Appl Surf Sci 2021;535:147707.
[104] Huang S-C, Cheng C-C, Lai Y-H, Lin C-Y. Sustainable and selective formic acid production from photoelectrochemical methanol reforming at near-neutral pH using nanoporous nickel-iron oxyhydroxide-borate as the electrocatalyst. Chem Eng J 2020;395:125176.
[105] Beluomini MA, Stradiotto NR, Boldrin MV. Electrosynthesis of three-dimensional nanoporous nickel on screen-printed electrode used for the determination of narirutin in citrus wastewater. Food Chem 2021;353:129427.
[106] Bachmeier A, Hall S, Ragsdale SW, Armstrong FA. Selective visible-light-driven CO2 reduction on a p-type dye-sensitized NiO photocathode. J Am Chem Soc 2014;136:13518–21.
[107] Yu JM, Lee J, Kim YS, Song J, Oh J, Lee SM, et al. High-performance and stable photoelectrochemical water splitting cell with organic-photoactive-layer-based photoanode. Nat Commun 2020;11:5509.
[108] Zhang J, Djellabi R, Zhao S, Qiao M, Jiang F, Yan M, et al. Recovery of phosphorus and metallic nickel along with HCl production from electroless nickel plating effluents: the key role of three-compartment photoelectrocatalytic cell system. J Hazard Mater 2020;394:122559.

[109] Ding Y, Chen M, Erlebacher J. Metallic mesoporous nanocomposites for electrocatalysis. J Am Chem Soc 2004;126:6876–7.
[110] Tian M, Shi S, Shen Y, Yin H. PtRu alloy nanoparticles supported on nanoporous gold as an efficient anode catalyst for direct methanol fuel cell. Electrochim Acta 2019;293:390–8.
[111] Pröschel A, Chacko J, Whitaker R, Chen MAU, Detsi E. Visible light plasmonic heating-enhanced electrochemical current in nanoporous gold cathodes. J Electrochem Soc 2019;166:H146–50.
[112] Shi L, Li Z, Dao TD, Nagao T, Yang Y. A synergistic interaction between isolated Au nanoparticles and oxygen vacancies in an amorphous black TiO2 nanoporous film: toward enhanced photoelectrochemical water splitting. J Mater Chem 2018;6:12978–84.
[113] Sarfraz N, Khan I. Plasmonic gold nanoparticles (AuNPs): properties, synthesis and their advanced energy, environmental and biomedical applications. Chem Asian J 2021;16:720–42.
[114] Kushwaha A, Aslam M. Defect controlled water splitting characteristics of gold nanoparticle functionalized ZnO nanowire films. RSC Adv 2014;4:20955–63.
[115] Inyang AO, Chowdhury M. Photoactive and self-cleaning properties of copper oxide thin film non-enzymatic glucose biosensor. Mater Today Proc 2021;38:903–6.
[116] Xu Y, Jian G, Zachariah MR, Wang C. Nano-structured carbon-coated CuO hollow spheres as stable and high rate anodes for lithium-ion batteries. J Mater Chem 2013;1:15486–90.
[117] Ko S, Lee J-I, Yang HS, Park S, Jeong U. Mesoporous CuO particles threaded with CNTs for high-performance lithium-ion battery anodes. Adv Mater 2012;24:4451–6.
[118] Wang L, Cheng W, Gong H, Wang C, Wang D, Tang K, et al. Facile synthesis of nanocrystalline-assembled bundle-like CuO nanostructure with high rate capacities and enhanced cycling stability as an anode material for lithium-ion batteries. J Mater Chem 2012;22:11297–302.
[119] Lee J-I, Choi S, Park S. A simple fabrication of interconnected CuO nanotube electrodes for high-performance lithium-ion batteries. Chem Asian J 2013;8:1377–80.
[120] Tang B, Zhou M, Zhou R, Bai PF, Zhou GF. Well-ordered nanoporous copper fabricated by dealloying Cu-Mn and its characterizations. Key Eng Mater 2016;693:662–8.
[121] Zhao M, Shadman F, Keswani M. Gradient filling of copper in porous silicon using a non-contact electrochemical method. Appl Surf Sci 2018;445:505–11.
[122] Shi H, Zhou Y-T, Yao R-Q, Wan W-B, Ge X, Zhang W, et al. Spontaneously separated intermetallic Co3Mo from nanoporous copper as versatile electrocatalysts for highly efficient water splitting. Nat Commun 2020;11:2940.
[123] Li Z, Zhang Z. Tetrafunctional Cu2S thin layers on Cu2O nanowires for efficient photoelectrochemical water splitting. Nano Res 2018;11:1530–40.
[124] Kurniawan M, Stich M, Marimon M, Camargo M, Peipmann R, Hannappel T, et al. Electrodeposition of cuprous oxide on a porous copper framework for an improved photoelectrochemical performance. J Mater Sci 2021;56:11866–80.
[125] Sun J, Maimaiti H, Xu B, Feng L, Bao J, Zhao X. Photoelectrocatalytic degradation of wastewater and simultaneous hydrogen production on copper nanorod-supported coal-based N-carbon dot composite nanocatalysts. Appl Surf Sci 2022;585:152701.
[126] Maksymiuk K, Stroka J, Galus Z. CHEMISTRY, electrochemistry, and electrochemical applications | lead. In: Garche J, editor. Encyclopedia of electrochemical power sources. Amsterdam: Elsevier; 2009. p. 762–71.
[127] Stroka J, Maksymiuk K, Galus Z. Electrochemistry of Lead. In: Bard AJ, editor. In Encyclopedia of Electrochemistry; 2007. https://doi.org/10.1002/9783527610426.bard072403.
[128] Kurt Urhan B, Çepni E, Temur E, Öztürk Doğan H, Demir Ü. Electrochemical fabrication of lead oxide-electrochemically reduced graphene oxide nanocomposites (PbO-ERGO) and their photoelectrochemical properties. Mater Today Proc 2021;46:6895–8.
[129] Negishi R, Naya S-i, Kobayashi H, Tada H. Gold(Core)–Lead(Shell) nanoparticle-loaded titanium(IV) oxide prepared by underpotential photodeposition: plasmonic water oxidation. Angew Chem Int Ed 2017;56:10347–51.
[130] Tan C, Wang J, Zhong X, Jiang J, Zhang X, Ding Y. Switchable photoelectrochemical response controlled by ferroelectric polarization in (101)-oriented Pb(Zr0.2Ti0.8)O3 thin film. Mater Des 2017;129:186–91.
[131] Romero N, Castro GR, Gagneten AM. Chapter 28 - ecotoxicologic effects of silver nanoparticles on freshwater nontarget species. In: Shah MP, Rodriguez Couto S, Kumar V, editors. New trends in removal of heavy metals from industrial wastewater. Elsevier; 2021. p. 705–33.
[132] Lu Q, Rosen J, Zhou Y, Hutchings GS, Kimmel YC, Chen JG, et al. A selective and efficient electrocatalyst for carbon dioxide reduction. Nat Commun 2014;5:3242.
[133] Wang X, Liu Q, Shu J, Ouyang D, Zhang X, Chen J, et al. The preparation and electrochemical performance analysis of different porous silicon composites. Silicon 2021.
[134] Zhao X, Deng Z, Zhao W, Feng B, Wang M, Huang M, et al. Nanoporous silver using pulsed laser deposition for high-performance oxygen reduction reaction and hydrogen peroxide sensing. Nanoscale 2020;12:19413–9.
[135] Ali W, Zhang X, Zhang X, Ali S, Zhao L, Shaheen S, et al. Improved visible-light activities of g-C3N4 nanosheets by co-modifying nano-sized SnO2 and Ag for CO2 reduction and 2,4-dichlorophenol degradation. Mater Res Bull 2020;122:110676.
[136] Luo J, Han P, Dan Z, Qin F, Tang T, Dong Y. Bimodal nanoporous silver fabricated from dual-phase Ag10Zn90 precursor via electrochemical dealloying for direct ammonia-borane electrooxidation. Microporous Mesoporous Mater 2020;308:110532.
[137] Wang M, Guo L, Sun H. Manufacture of biomaterials. In: Narayan R, editor. Encyclopedia of biomedical engineering. Oxford: Elsevier; 2019. p. 116–34.
[138] Smith AJ, Trimm DL. The preparation of skeletal catalysts. Annu Rev Mater Res 2005;35:127–42.
[139] Yang W, Zheng X-G, Wang S-G, Jin H-J. Nanoporous aluminum by galvanic replacement: dealloying and inward-growth plating. J Electrochem Soc 2018;165:C492–6.
[140] Suárez OM, Estremera EG, Soler R, Declet A, Hernández-Maldonado AJ. Fabrication of porous and nanoporous aluminum via selective dissolution of Al-Zn alloys. Adv Mater Sci Eng 2014;2014:963042.
[141] Dvorak F, Zazpe R, Krbal M, Sopha H, Prikryl J, Ng S, et al. One-dimensional anodic TiO2 nanotubes coated by atomic layer deposition: towards advanced applications. Appl Mater Today 2019;14:1–20.
[142] Md Jani AM, Losic D, Voelcker NH. Nanoporous anodic aluminium oxide: advances in surface engineering and emerging applications. Prog Mater Sci 2013;58:636–704.
[143] Hernández-Eguía LP, Ferré-Borrull J, Macias G, Pallarès J, Marsal LF. Engineering optical properties of gold-coated nanoporous anodic alumina for biosensing. Nanoscale Res Lett 2014;9:414.
[144] Kapruwan P, Ferré-Borrull J, Marsal LF. Nanoporous anodic alumina platforms for drug delivery applications: recent advances and perspective. Adv Mater Interfac 2020;7:2001133.

[145] Canham LT. Silicon quantum wire array fabrication by electrochemical and chemical dissolution of wafers. Appl Phys Lett 1990;57:1046–8.
[146] Brinker M, Dittrich G, Richert C, Lakner P, Krekeler T, Keller TF, et al. Giant electrochemical actuation in a nanoporous silicon-polypyrrole hybrid material. Sci Adv 2020;6:eaba1483.
[147] Zhao Y, Anderson NC, Zhu K, Aguiar JA, Seabold JA, Jvd Lagemaat, et al. Oxidatively stable nanoporous silicon photocathodes with enhanced onset voltage for photoelectrochemical proton reduction. Nano Lett 2015;15:2517–25.
[148] Vijselaar WJC, Perez-Rodriguez P, Westerik PJ, Tiggelaar RM, Smets AHM, Gardeniers H, et al. A stand-alone Si-based porous photoelectrochemical cell. Adv Energy Mater 2019;9:1803548.
[149] Perez-Rodriguez P, Digdaya I, Raventos AM, Falkenberg M, Vasudevan R, Zeman M, et al. Solar fuel production by using PV/PEC junctions based on earth-abundant materials. In: 2016 IEEE 43rd photovoltaic specialists conference (PVSC); 2016. p. 3620–4.
[150] Chandrasekaran S, McInnes SJP, Macdonald TJ, Nann T, Voelcker NH. Porous silicon nanoparticles as a nanophotocathode for photoelectrochemical water splitting. RSC Adv 2015;5:85978–82.
[151] Batzill M, Diebold U. The surface and materials science of tin oxide. Prog Surf Sci 2005;79:47–154.
[152] Varley JB, Janotti A, Singh AK, Van de Walle CG. Hydrogen interactions with acceptor impurities in SnO2: first-principles calculations. Phys Rev B 2009;79:245206.
[153] Akgul FA, Gumus C, Er AO, Farha AH, Akgul G, Ufuktepe Y, et al. Structural and electronic properties of SnO2. J Alloys Compd 2013;579:50–6.
[154] Schleife A, Varley JB, Fuchs F, Rödl C, Bechstedt F, Rinke P, et al. Tin dioxide from first principles: quasiparticle electronic states and optical properties. Phys Rev B 2011;83:035116.
[155] Park N-G, Kang MG, Ryu KS, Kim KM, Chang SH. Photovoltaic characteristics of dye-sensitized surface-modified nanocrystalline SnO2 solar cells. J Photochem Photobiol Chem 2004;161:105–10.
[156] Zhang Z, Gao C, Wu Z, Han W, Wang Y, Fu W, et al. Toward efficient photoelectrochemical water-splitting by using screw-like SnO2 nanostructures as photoanode after being decorated with CdS quantum dots. Nano Energy 2016;19:318–27.
[157] Faramarzi MS, Abnavi A, Ghasemi S, Sanaee Z. Nanoribbons of SnO2 as a high performance Li-ion battery anode material. Mater Res Express 2018;5:065040.
[158] Ma D, Li Y, Zhang P, Lin Z. Oxygen vacancy engineering in tin(IV) oxide based anode materials toward advanced sodium-ion batteries. ChemSusChem 2018;11:3693–703.
[159] Mohanta D, Ahmaruzzaman M. Tin oxide nanostructured materials: an overview of recent developments in synthesis, modifications and potential applications. RSC Adv 2016;6:110996–1015.
[160] Cao L, Liu J, Xu S, Xia Y, Huang W, Li Z. Inherent superhydrophobicity of Sn/SnOx films prepared by surface self-passivation of electrodeposited porous dendritic Sn. Mater Res Bull 2013;48:4804–10.
[161] Yao X, Song Y, Jiang L. Applications of bio-inspired special wettable surfaces. Adv Mater 2011;23:719–34.
[162] Zhang Y-P, Yang J-H, Li L-L, Cui C-X, Li Y, Liu S-Q, et al. Facile fabrication of superhydrophobic copper- foam and electrospinning polystyrene fiber for combinational oil–water separation. Polymers 2019;11.
[163] Gurgul M, Lytvynenko AS, Jarosz M, Gawlak K, Sulka GD, Zaraska L. Hierarchical nanoporous Sn/SnOx systems obtained by anodic oxidation of electrochemically deposited Sn nanofoams. Nanomaterials 2020;10:410.
[164] Liu H, Miao B, Chuai H, Chen X, Zhang S, Ma X. Nanoporous tin oxides for efficient electrochemical CO2 reduction to formate. Green Chem Eng 2021.
[165] Bury NR, Boyle D, Cooper CA. 4 - iron. In: Wood CM, Farrell AP, Brauner CJ, editors. Fish physiology. Academic Press; 2011. p. 201–51.
[166] Liu G, Li Y, Xiao Y, Jia D, Li C, Zheng J, et al. Nanoporous Fe-doped BiVO4 modified with MIL-53 (Fe) for enhanced photoelectrochemical stability and water splitting perfromances. Catal Lett 2019;149:870–5.
[167] Peerakiatkhajohn P, Yun J-H, Chen H, Lyu M, Butburee T, Wang L. Stable hematite nanosheet photoanodes for enhanced photoelectrochemical water splitting. Adv Mater 2016;28:6405–10.
[168] Wang Q, Zhu N, Liu E, Zhang C, Crittenden JC, Zhang Y, et al. Fabrication of visible-light active Fe2O3-GQDs/NF-TiO2 composite film with highly enhanced photoelectrocatalytic performance. Appl Catal B Environ 2017;205:347–56.
[169] Nosaka Y, Nosaka AY. Reconsideration of intrinsic band alignments within anatase and rutile TiO2. J Phys Chem Lett 2016;7:431–4.
[170] Ju M-G, Sun G, Wang J, Meng Q, Liang W. Origin of high photocatalytic properties in the mixed-phase TiO2: a first-principles theoretical study. ACS Appl Mater Interfaces 2014;6:12885–92.
[171] An D, Li Y, Lian X, Zou Y, Deng G. Synthesis of porous ZnO structure for gas sensor and photocatalytic applications. Colloids Surf A Physicochem Eng Asp 2014;447:81–7.
[172] Wang C, Zhu G, Liu P, Chen Q. Monolithic nanoporous Zn anode for rechargeable alkaline batteries. ACS Nano 2020;14:2404–11.
[173] Cai Y, Li X, Sun P, Wang B, Liu F, Cheng P, et al. Ordered ZnO nanorod array film driven by ultrasonic spray pyrolysis and its optical properties. Mater Lett 2013;112:36–8.
[174] Su X, Gao L, Zhou F, Cai W, Duan G. "Close network" effect of a ZnO micro/nanoporous array allows high UV-irradiated NO2 sensing performance. RSC Adv 2017;7:21054–60.
[175] Yang X, Wolcott A, Wang G, Sobo A, Fitzmorris RC, Qian F, et al. Nitrogen-doped ZnO nanowire arrays for photoelectrochemical water splitting. Nano Lett 2009;9:2331–6.
[176] Wang Y, Wang Q, Zhan X, Wang F, Safdar M, He J. Visible light driven type II heterostructures and their enhanced photocatalysis properties: a review. Nanoscale 2013;5:8326–39.
[177] Rasouli F, Rouhollahi A, Ghahramanifard F. Fabrication of silver nanoparticles decorated zinc oxide nanotubes by electrodeposition technique for photoelectrochemical water splitting. Mater Sci Semicond Process 2019;93:371–8.
[178] Chatterjee S, Bhanja P, Ghosh D, Kumar P, Kanti Das S, Dalapati S, et al. Metformin-templated nanoporous ZnO and covalent organic framework heterojunction photoanode for photoelectrochemical water oxidation. ChemSusChem 2021;14:408–16.
[179] Serre C, Taulelle F, Ferey G. Rational design of porous titanophosphates. Chem Commun 2003:2755–65.
[180] Serre C, Groves JA, Lightfoot P, Slawin AMZ, Wright PA, Stock N, et al. Synthesis, structure and properties of related microporous N,N'-Piperazinebismethylenephosphonates of aluminum and titanium. Chem Mater 2006;18:1451–7.
[181] Jang JS, Ahn CW, Won SS, Kim JH, Choi W, Lee B-S, et al. Vertically aligned core–shell PbTiO3@TiO2 heterojunction nanotube array for photoelectrochemical and photocatalytic applications. J Phys Chem C 2017;121:15063–70.

[182] Xue J, Gao C, Zhang L, Cui K, He W, Yu J. A single-interface photoelectrochemical sensor based on branched TiO2 nanorods@strontium titanate for the detection of two biomarkers. J Mater Chem B 2018;6:4697–703.
[183] Shu J, Qiu Z, Lv S, Zhang K, Tang D. Plasmonic enhancement coupling with defect-engineered TiO2–x: a mode for sensitive photoelectrochemical biosensing. Anal Chem 2018;90:2425–9.
[184] Wang Z, Yin H, Tang Y, Hou Q, He C, Yuan H. Reinforced photoelectrochemical properties of nanostructural TiO2/C/SiO2 integrated on conductive Ti3SiC2. Ceram Int 2019;45:7253–61.
[185] Feng G, Hu M, Yuan S, Nan J, Zeng H. Hydrogenated amorphous TiO2–x and its high visible light photoactivity. Nanomaterials 2021:11.
[186] Peng Y, Ruan Q, Lam CH, Meng F, Guan C-Y, Santoso SP, et al. Plasma-implanted Ti-doped hematite photoanodes with enhanced photoelectrochemical water oxidation performance. J Alloys Compd 2021;870:159376.
[187] Kim TW, Choi K-S. Nanoporous BiVO4 photoanodes with dual-layer oxygen evolution catalysts for solar water splitting. Science 2014;343:990–4.
[188] Liu H, Hou H, Gao F, Yao X, Yang W. Tailored fabrication of thoroughly mesoporous BiVO4 nanofibers and their visible-light photocatalytic activities. ACS Appl Mater Interfaces 2016;8:1929–36.
[189] Das T, Rocquefelte X, Laskowski R, Lajaunie L, Jobic S, Blaha P, et al. Investigation of the optical and excitonic properties of the visible light-driven photocatalytic BiVO4 material. Chem Mater 2017;29:3380–6.
[190] Mao J, Wu Q, Tao F, Xu W, Hong T, Dong Y. Facile fabrication of porous BiVO4 hollow spheres with improved visible-light photocatalytic properties. RSC Adv 2020;10:6395–404.
[191] Kim TW, Ping Y, Galli GA, Choi K-S. Simultaneous enhancements in photon absorption and charge transport of bismuth vanadate photoanodes for solar water splitting. Nat Commun 2015;6:8769.
[192] Hirakawa H, Shiota S, Shiraishi Y, Sakamoto H, Ichikawa S, Hirai T. Au nanoparticles supported on BiVO4: effective inorganic photocatalysts for H2O2 production from water and O2 under visible light. ACS Catal 2016;6:4976–82.
[193] Hong SJ, Lee S, Jang JS, Lee JS. Heterojunction BiVO4/WO3 electrodes for enhanced photoactivity of water oxidation. Energy Environ Sci 2011;4:1781–7.
[194] Jo WJ, Jang JW, Kong Kj, Kang HJ, Kim JY, Jun H, et al. Phosphate doping into monoclinic BiVO4 for enhanced photoelectrochemical water oxidation activity. Angew Chem 2012;124:3201–5.
[195] Murphy AB, Barnes PRF, Randeniya LK, Plumb IC, Grey IE, Horne MD, et al. Efficiency of solar water splitting using semiconductor electrodes. Int J Hydrogen Energy 2006;31:1999–2017.
[196] Liu C, Yang Y, Li W, Li J, Li Y, Chen Q. A novel Bi2S3 nanowire @ TiO2 nanorod heterogeneous nanostructure for photoelectrochemical hydrogen generation. Chem Eng J 2016;302:717–24.
[197] Chen J, Tao HB, Liu B. Unraveling the intrinsic structures that influence the transport of charges in TiO2 electrodes. Adv Energy Mater 2017;7:1700886.
[198] Wang T, Wei Y, Chang X, Li C, Li A, Liu S, et al. Homogeneous Cu2O p-n junction photocathodes for solar water splitting. Appl Catal B Environ 2018;226:31–7.
[199] Rassoolkhani AM, Cheng W, Lee J, McKee A, Koonce J, Coffel J, et al. Nanostructured bismuth vanadate/tungsten oxide photoanode for chlorine production with hydrogen generation at the dark cathode. Commun Chem 2019;2:57.
[200] Zong L, Cui P, Qin F, Zhao K, Wang Z, Yu R. Heterostructured bismuth vanadate multi-shell hollow spheres with high visible-light-driven photocatalytic activity. Mater Res Bull 2017;86:44–50.
[201] Orimolade BO, Arotiba OA. Bismuth vanadate in photoelectrocatalytic water treatment systems for the degradation of organics: a review on recent trends. J Electroanal Chem 2020;878:114724.
[202] Ioannidou E, Kyzas GZ. Chapter 35 - nanotitanium photocatalytic technology in wastewater treatment. In: Shah M, Rodriguez-Couto S, Mehta K, editors. The future of effluent treatment plants. Elsevier; 2021. p. 739–58.
[203] Hu W, Quang ND, Majumder S, Jeong MJ, Park JH, Cho YJ, et al. Three-dimensional nanoporous SnO2/CdS heterojunction for high-performance photoelectrochemical water splitting. Appl Surf Sci 2021;560:149904.
[204] Shaban M, Mustafa M, Khan AAP. Hexagonal diameter in cadmium sulfide/anodic alumina nanoporous bi-layer membrane by a sol–gel spin coating and their sensing application. Appl Phys A 2020;126:268.
[205] Kandy MM, Gaikar VG. Continuous photocatalytic reduction of CO2 using nanoporous reduced graphene oxide (RGO)/Cadmium sulfide (CdS) as catalyst on porous anodic alumina (PAA)/Aluminum support. J Nanosci Nanotechnol 2019;19:5323–31.
[206] Shen L, Bao N, Prevelige PE, Gupta A. Escherichia coli bacteria-templated synthesis of nanoporous cadmium sulfide hollow microrods for efficient photocatalytic hydrogen production. J Phys Chem C 2010;114:2551–9.
[207] Auerbach SM, Carrado KA, Dutta PK. Handbook of zeolite science and technology. CRC press; 2003.
[208] Sadeghbeigi R. Chapter 4 - FCC catalysts. In: Sadeghbeigi R, editor. Fluid catalytic cracking handbook. 3rd ed. Oxford: Butterworth-Heinemann; 2012. p. 87–115.
[209] Lin J, Dong Y, Zhang Q, Hu D, Li N, Wang L, et al. Interrupted chalcogenide-based zeolite-analogue semiconductor: atomically precise doping for tunable electro-/photoelectrochemical properties. Angew Chem Int Ed 2015;54:5103–7.
[210] Calzaferri G, Leiggener C, Glaus S, Schürch D, Kuge Ki. The electronic structure of Cu+, Ag+, and Au+ zeolites. Chem Soc Rev 2003;32:29–37.
[211] Abderrahim N, Mergbi M, Ben Amor H, Djellabi R. Optimization of microwave assisted synthesis of activated carbon from biomass waste for sustainable industrial crude wet-phosphoric acid purification. J Clean Prod 2023;394:136326.
[212] Coker EN, Lujan-Flores X, Donaldson B, Yilmaz N, Atmanli A. An assessment of the conversion of biomass and industrial waste products to activated carbon. Energies; 2023.
[213] Djellabi R, Aboagye D, Greta Galloni M, Vilas Andhalkar V, Nouacer S, Nabgan W, et al. Combined conversion of lignocellulosic biomass into high-value products with ultrasonic cavitation and photocatalytic produced reactive oxygen species - a review. Bioresour Technol 2023;368:128333.
[214] Saber AN, Djellabi R, Fellah I, Abderrahim N, Bianchi CL. Synergistic sorption/photo-Fenton removal of typical substituted and parent polycyclic aromatic hydrocarbons from coking wastewater over CuO-Montmorillonite. J Water Proc Eng 2021;44:102377.
[215] Abderrahim N, Djellabi R, Amor HB, Fellah I, Giordana A, Cerrato G, et al. Sustainable purification of phosphoric acid contaminated with Cr(VI) by Ag/Ag3PO4 coated activated carbon/montmorillonite under UV and solar light: materials design and photocatalytic mechanism. J Environ Chem Eng 2022;10:107870.
[216] Fellah I, Djellabi R, Amor HB, Abderrahim N, Bianchi CL, Giordana A, et al. Visible light responsive heterostructure HTDMA-BiPO4 modified clays for effective diclofenac sodium

oxidation: role of interface interactions and basal spacing. J Water Proc Eng 2022;48:102788.
[217] Djellabi R, Giannantonio R, Falletta E, Bianchi CL. SWOT analysis of photocatalytic materials towards large scale environmental remediation. Curr Opin Chem Eng 2021;33:100696.
[218] Djellabi R, Yang B, Wang Y, Cui X, Zhao X. Carbonaceous biomass-titania composites with TiOC bonding bridge for efficient photocatalytic reduction of Cr(VI) under narrow visible light. Chem Eng J 2019;366:172–80.
[219] Djellabi R, Yang B, Xiao K, Gong Y, Cao D, Sharif HMA, et al. Unravelling the mechanistic role of TiOC bonding bridge at titania/lignocellulosic biomass interface for Cr(VI) photoreduction under visible light. J Colloid Interface Sci 2019;553:409–17.
[220] Bellani S, Antognazza MR, Bonaccorso F. Carbon-based photocathode materials for solar hydrogen production. Adv Mater 2019;31:1801446.